Disinfection by Pulsed Power Discharges

Thesis by

Weng Ki Ching

In Partial Fulfillment of the Requirements
for the Degree of
Doctor of Philosophy

California Institute of Technology
Pasadena, California

2001

(Submitted May 3, 2001)

© 2001

Weng Ki Ching

All Rights Reserved

to my family

Acknowledgments

I am most indebted to my advisor, Michael Hoffmann, for his faith and trust in my abilities as a scientist. I am truly grateful for his support, guidance and patience throughout my graduate tenure. Particularly, I am thankful for his disinterested concern and thoughtfulness during those anxious months of my cancer treatments, without which my recovery would have been much more difficult.

I would like to acknowledge A. J. Colussi for his mentorship and invaluable help and expertise in chemical kinetics as well as my thesis committee: Ken Nealson, Dianne Newman and Jared Leadbetter for their help on different portions of this work. Also I would like to give thanks to Henry Sun for teaching me how to think like a microbiologist and wander about the incredible world within.

I will surely miss being greeted by the big smile that is Linda Scott. I truly enjoyed our conversations and mutual ramblings on the wonderful worlds of architecture and travel mishaps. Among these illustrious personalities, I acknowledge Fran Matzen who appears to be the only person who can tackle the Purchasing Department head-on, and Rich Eastvedt and Mike Vondrus in the machine shop who were always glad to make those last minute rush jobs seem like a walk in the park. They certainly made my stay at Keck Labs possible and more enjoyable.

A big thanks to my officemate and friend John A. Moss, who has shown me that you can be a chemist and still run marathons in 2 ½ hours, and my girl Sue Friedman who never seems to give up on me.

I am grateful to Kim, Sue C., and the entire staff at the Residence Life Office in my other life as an RA at Avery House. The tools I learned from them surely will go a long way.

I would also like to acknowledge my bud Mark Duttweiler, Parandeh Kia, Cindy Quezada, Nathan Dalleska, Kim West, Mckell Carter, Jennie Stephens, and Kitty Erkkila who tirelessly drove me to and from UCLA for my radiation treatments last Fall.

Last but not least, I would like to thank my parents, Koon Ying Ching, Sich Guil Ching, and my sister Joting, Peter, and Zelan vonKaenel for all their sacrifices and their continual search for a better life that enabled me to be who I am today.

This work was partially supported by the Defense Advanced Research Projects Agency (DARPA Grant NAV5HFMN N0001492J1901), the Office of Naval Research (ONR), the Electric Power Institute (EPRI Grant RP 8003-37) and the Northrup-Grumman Corporation, whose financial support is gratefully appreciated.

Abstract

We study the disinfection of *Escherichia coli* in a pulsed power discharge reactor. The pulsed power discharge process is an electrohydraulic phenomenon characterized by a rapid release of electrical energy across a submerged electrode pair.

The survival kinetics of pure strains of *E. coli* suspensions exposed to 5.5 kV, 90 kA electrohydraulic discharges (EHD) is investigated. The probability of survival P_n of a 2×10^7 *E. coli* CFU mL^{-1} population after 50 consecutive EHD's follows a log*it* distribution that corresponds to lethal doses of LD_{50} = 2.2 and LD_{90} = 10.8 EHDs. Variation of the initial cell concentration produced nearly constant values of $LD_{50} = 0.9 \pm 0.1$ in the range $2 \times 10^3 \leq$ *E. coli*/CFU $mL^{-1} \leq 3 \times 10^6$. Beyond 10^6 CFU mL^{-1}, the LD_{50} values increase exponentially due to nonlinear light absorbance with increasing *E. coli* concentrations. Qualitatively similar initial cell concentration dependence is observed for survival under low intensity 254 nm irradiation, in contrast with lower values of LD_{50} obtained in denser colonies to 20 kHz power ultrasound exposure.

The high intensity (3.3×10^{10} W m^{-2}) ultraviolet radiation emitted by the electrohydraulic discharge is completely suppressed in the presence of less than 100 mg L^{-1} 2,2'-dihydroxy-4,4'-dimethoxybenzophenone-5,5'-disulfonic acid (BP9), a well-known sunscreen agent. Concentrations of BP9, in the range (0 – 100) mg L^{-1}, are varied to measure the sterilization kinetics of ~ 3×10^7 CFU mL^{-1} suspensions to varying degrees of high intensity UV exposure. The slope of the logit plots of *E. coli* as function of BP9 concentration is consistent with the screening of radiation as the sole lethal agent. Computed values of biologically available light fluences are 5.0×10^{11} photons CFU^{-1} for

high intensity, high power, pulsed EHD experiments and 6.6 x 10^8 photons CFU^{-1} for separate low power continuous UV experiments. The net availability of 3 orders of magnitude more photons during high intensity UV exposure suggests the possibility of a multiphotonic disinfection mechanism at play in the EHD process relative to low intensity case.

The overall resistance to long term exposure to EHD is also investigated. Selective pressure experiments with *E. coli* exposed to 11 cycles of 50 consecutive EHDs each show a weak kinetic change in the dose-response curves reflected in the nearly constant values of $LD_{50} = 0.24 \pm 0.03$. A greater than 98 % metabolic similarity in carbon source consumption between initial and final *E. coli* populations are enzymatically related. In addition, the results indicate that no bacterial contaminants are propagated throughout the experiment.

Table of Contents

	Acknowledgments	iv
	Abstract	vi
	Table of contents	viii
	List of figures	xii
	List of tables	xviii
Chapter I.	**Introduction**	
	General disinfection methods	I - 2
	Disinfection by electrohydraulic discharges	I - 4
	The pulsed plasma discharge reactor	I - 5
	Chemical effects	I – 6
	High intensity UV emission	I – 7
	Shockwave effects	I – 8
	Motivation	I – 9
	Thesis purpose and overview	I – 10
	References cited	I – 12
Chapter II.	**Experimental section**	
	Electronics	II – 2
	Reactor mixing conditions	II – 6

Escherichia coli II – 7

Substrate sensitivity experiments II – 8

Statistical analyses II – 9

References cited II – 11

Chapter III. Kinetics of *Escherichia coli* disinfection by electrohydraulic discharges

Abstract III – 3

Introduction III – 4

Experimental methods III – 6

Sterilization devices III – 6

Bacterial cultures and procedures III – 7

β-D-galactosidase assay III – 8

Results and discussion III – 10

Disinfection kinetics and mechanism III – 10

Lethal agent characterization III – 12

Conclusions III – 14

References cited III – 15

Chapter IV. Soluble sunscreens fully inhibit *E. coli* disinfection by high intensity UV irradiation in electrohydraulic discharges

Abstract IV – 3

Introduction IV – 4

High intensity UV irradiation IV – 6

Experimental methods IV – 8

The pulsed power plasma reactor system IV – 8

Bacterial cultures and procedures IV – 10

Benzophenone-9 IV – 11

Statistical analyses IV – 11

Results and discussion IV – 13

Dose-response curves IV – 13

Modeling the experiments IV – 14

Discussion IV – 16

Conclusions IV – 19

References cited IV – 20

Chapter V. EHD selective pressure experiments

Introduction V – 2

Method of approach V – 4

GN2 MicroPlate™ assay V – 4

Results and discussion V – 6

Mutagenicity V – 7

Conclusion V – 8

References cited V – 9

Chapter VI. Discussion and conclusions

Disinfection kinetics VI – 2

High intensity UV disinfection VI – 3

Vitalism vs. mechanism VI – 4

Background VI – 4

Recommendations for Future Research VI – 6

Combined ozone/EHD disinfection experiments VI – 6

Ozone dissolution experiment VI – 9

Ozone disinfection rate constant VI – 10

Hydroxyl radical production in the EHD VI – 11

Combined peroxydisulfate/EHD disinfection experiments VI – 12

References cited VI – 14

A Appendix A – 1

List of Figures

Chapter I

Figure 1. Schematic diagram of the EHD reactor and the corresponding electronic circuit. I – 19

Figure 2. Description of main events during a typical electrohydraulic discharge event. I – 20

Figure 3. Blackbody spectrum at 15 000 K. Maximum emission occurs at λ = 300 nm. At higher temperatures (EHD is 50 000 K), the maximum emission shifts to the left (lower wavelengths). I – 21

Figure 4. Normalized spectrum of a 50 000 K blackbody (solid circles) at λ_{max} = 100 nm and measured absorbance of *E. coli* (solid triangles) with $\varepsilon_{254\,nm} = 1.13 \times 10^{9}$ mL CFU^{-1} cm^{-1}. I – 22

Figure 5. Electronic levels of DNA thymine. S_0, ground state; S_1, lowest singlet excited state; S_N, higher singlet excited state; T_1, lowest triplet excited state; T_N, higher triplet excited state; $h\nu_1$, first photon absorbed; $h\nu_2$, second photon absorbed by either S_1 or T_1; *isc*, intersystem crossing; t_1^S, lifetime of S_1; t_1^T, lifetime of T_1. I – 23

Figure 6. Schematic diagram of a typical municipal water treatment facility. Boxed area is the result of the 1992 Surface Water Treatment Rule (SWTR) required by the U. S. EPA. I – 24

Chapter II

Figure 1. Photograph of the Caltech electrohydraulic discharge reactor. The reactor outer diameter is 16 inches. II – 12

Figure 2. Detail of EHD reactor chamber (cover opened). For scaling purposes, the reactor outer diameter is 16 inches. II – 13

Figure 3. Sample preparation protocols and viability measurement. II – 14

Chapter III

Figure 1. See Fig. 1, Chap. I. I – 19

Figure 2. Schematic diagram of the combined UV and ultrasound reactor system. III – 18

Figure 3a. Disinfection of 3 L of a 2.0×10^7 CFU mL^{-1} *E. coli* suspension in 0.01 M PBS at pH = 7.4 by 50 consecutive electrohydraulic discharges. Discharges are characterized by E_{CB} = 7 kJ, spark gap = 4 mm, and pulse rate = 0.1 Hz. The solid line is a bi-exponential fit to the data. III – 19

Figure 3b. A logit plot of the data of Fig. 3. The solid line is calculated from Eq. 1 (see text). P_n is the percentual survival probability of the colonies after n discharges. III – 20

Figure 4. The number of EHD required to inactivate 50 % of the initial population LD_{50} vs. initial *E. coli* cell concentration, as obtained from initial disinfection rates. The solid line is an empirical 3-parameter exponential growth fit to the data. III – 21

Figure 5. LD_{50} values (in min of UV exposure) for *E. coli* disinfection by 254 nm light vs. initial cell concentrations. Conditions: 100-mL of *E. coli* suspensions in 0.01 M PBS at pH = 7.4. III – 22

Figure 6. LD_{50} values (in min of ultrasound exposure) for *E. coli* disinfection by 20 kHz ultrasound vs. initial cell concentrations. Conditions: 100-mL of *E. coli* suspensions in 0.01 M PBS at pH = 7.4. III – 23

Figure 7. β-D-galactosidase activity of *E. coli* vs. the number of electrohydraulic discharges. ▼: in the cell lysate. ▲: in the supernatant. III – 24

Chapter IV

Figure 1. See Fig. 1, Chap. I. I –19

Figure 2. Total viable E. coli concentration, expressed as % viability at seven different concentrations of sunscreen BP9 added (0, 1, 5, 20, 40, 60, 100 mg/L). Each case was subject to 50 consecutive electrohydraulic discharges. Discharges are characterized by E_{CB} = 7 kJ, spark gap = 4 mm, and pulse rate = 0.1 Hz. IV – 24

Figure 3. BP9 sunscreen concentration dependence on slope of rectified disinfection curve. Solid line represents single-photon model fit to data (Equation 6). IV – 25

Figure 4. Normalized spectrum of 50 000 K blackbody (solid circles) at λ_{max} = 100 nm. Measured absorbance of *E. coli* (solid triangles) $\varepsilon_{254\ nm} = 1.13 \times 10^9$ mL CFU^{-1} cm^{-1}, and BP9 sunscreen (solid squares) $\langle\varepsilon\rangle_{180\text{-}300} = 0.06$ L mg^{-1} cm^{-1}. IV – 26

Chapter V

Figure 1. EHD selective pressure experiments of E. coli suspensions in 0.01 M PBS at pH = 7.4, subject to 50 EHDs per cycle for a total of 11 cycles. Discharges are characterized by E_{CB} = 7 kJ, spark gap = 4 mm. Cycle 0 represents the kinetics of *E. coli* subject to 50 EHDs. Cycle 6 represents the kinetics after a total of 6 cycles each of 50 EHDs (= 300 EHDs total). Cycle 11 represents the kinetics after a total of 11 cycles each of 50 EHDs (= 550 EHDs total). V – 12

Figure 2. Rectified log*it* plot of the data in Fig. 1. Cycle 0 represents the kinetics of *E. coli* subject to 50 EHDs. Cycle 6 represents the kinetics after a total of 6 cycles each of 50 EHDs (= 300 EHDs total). Cycle 11 represents the kinetics after a total of 11 cycles each of 50 EHDs (= 550 EHDs total). The plotted lines are regression fits to the data. V – 13

Figure 3. Image of metabolic fingerprint results for *E. coli* at cycle 0 using Biolog GN2 MicroPlate™ test panel. Absorbance of blank slot A1 = 0.865 measured at 490 nm. V – 15

Figure 4. Image of metabolic fingerprint results for *E. coli* at cycle 8 (= 400 EHDs) using Biolog GN2 MicroPlate™ test panel. Absorbance of blank slot A1 = 0.667 measured at 490 nm. V – 16

Chapter VI

Figure 1. Absorbance measurements of 1/100th dilutions of EHD generated samples with *E. coli* in 0.01M PBS at 0 EHDs (solid line), 60 EHDs (dotted line), and 100 EHDs (dashed line). VI – 16

Figure 2. Full-scale EHD disinfection experiments of *E. coli* suspensions of 3 x 10^7 CFU mL^{-1} (solid circles) and 2 x 10^3 CFU mL^{-1} (solid triangles) in 0.01 M PBS at pH = 7.4. Discharges are characterized by: E_{CB} = 7 kJ, spark gap = 4 mm, and pulse rate = 0.1 Hz. VI – 17

Figure 3. Absorbance measurements of *E. coli* concentrations at 600 nm (OD_{600}). VI – 18

Figure 4. Kinetic simulation of ozone and hydroxyl radical concentrations in a combined EHD/Ozone experiment. VI – 19

Figure 5. Kinetic simulation of cell viability in a combined EHD/ozone reactor. VI – 20

Figure 6. *E. coli* sensitivity experiments with sulfite, sulfate, thiosulfate and benzophenone-9 in 0.01 M PBS at 25 °C over a 42-hour time period. Initial cell concentration was 4 x 10^9 CFU mL^{-1}. All experiments and incubations were done in the dark. VI - 21

List of Tables

Chapter IV

Table 1. Initial conditions and regression results of rectified dose-response curves for *Escherichia coli* disinfection by 50 consecutive EHDs with varying concentrations of added BP9 sunscreen. E_{CB} = 7 kJ, spark gap = 4 mm, pH = 7.4, and pulse rate = 0.1 Hz. IV – 23

Chapter V

Table 1. Biolog GN2 MicroPlate™ test panel. All carbon sources contain tetrazolium violet used as a redox dye for colorimetric identification at 490 nm. Each bacterial sample was suspended in GN/GP-IF medium. V – 11

Table 2. Linear regression results of cycles 0, 6, and 11 of rectified data for EHD selective pressure experiments. Cycle 0 represents the kinetics of *E. coli* subject to 50 EHDs. Cycle 6 represents the kinetics after a total of 6 cycles each of 50 EHDs (= 300 EHDs total). Cycle 11 represents the kinetics after a total of 11 cycles each of 50 EHDs (= 550 EHDs total). The plotted lines are regression fits to the data. V – 14

Table 3. Metabolic fingerprint results for *E. coli* at cycle 0 using Biolog GN2 MicroPlate™ test panel. Absorbance of blank slot A1 = 0.865 measured at 490 nm. Grey boxes indicate positive (+) measurement of metabolic function, using Δ $OD_{490} > 0.100$. V – 17

Table 4. Metabolic fingerprint results for *E. coli* at cycle 4 (= 200 total EHDs) using Biolog GN2 MicroPlate™ test panel. Absorbance of blank slot A1 = 1.217 measured at 490 nm. Grey boxes indicate positive (+) measurement of metabolic function, using Δ $OD_{490} > 0.100$. V – 18

Table 5. Metabolic fingerprint results for *E. coli* at cycle 8 (= 400 total EHDs) using Biolog GN2 MicroPlate™ test panel. Absorbance of blank slot A1 = 0.667 measured at 490 nm. Grey boxes indicate positive (+) measurement of metabolic function, using Δ $OD_{490} > 0.100$. V – 19

Table 6. Metabolic fingerprint results for *E. coli* at cycle 11 (= 550 total EHDs) using Biolog GN2 MicroPlate™ test panel. Absorbance of blank slot A1 = 1.056 measured at 490 nm. Grey boxes indicate positive (+) measurement of metabolic function, using Δ $OD_{490} > 0.100$. V – 20

Chapter VI

Table 1. Rates of ozone decomposition. VI - 8

Appendix

Table A1. Raw data for EHD disinfection experiments on 11/98, 12/99, and 3/29/00. Disinfection of *E. coli* suspensions (3 L) in 0.01 M PBS at pH = 7.4 by 50 consecutive electrohydraulic discharges. E_{CB} = 7 kJ, spark gap = 4 mm, and pulse rate = 0.1 Hz. A – 2

Table A2. Raw data for EHD disinfection experiments on 7/98 and 10/98. Disinfection of *E. coli* suspensions (3 L) in 0.01 M PBS at pH = 7.4 by 50 consecutive electrohydraulic discharges. E_{CB} = 7 kJ, spark gap = 4 mm, and pulse rate = 0.1 Hz. A – 3

Table A3. Raw data of EHD disinfection rate dependence on initial cell concentration of 3.0-L volumes of *E. coli* subject to 2 consecutive discharges. E_{CB} = 7 kJ, pH = 7.4 in 0.01 M PBS. $C_1 = 1.7 \times 10^7$ CFU mL^{-1}; $C_2 = 9.4 \times 10^6$ CFU mL^{-1}; $C_3 = 5.5 \times 10^6$ CFU mL^{-1}. A – 4

Table A4. Raw data of EHD disinfection rate dependence on initial cell concentration of 3.0-L volumes of *E. coli* subject to 2 consecutive discharges. E_{CB} = 7 kJ, pH = 7.4 in 0.01 M PBS. $C_4 = 1.3 \times 10^6$ CFU mL^{-1}; $C_5 = 6.6 \times 10^5$ CFU mL^{-1}; $C_6 = 9.4 \times 10^4$ CFU mL^{-1}. A – 5

Table A5. Raw data of US disinfection rate dependence on initial cell concentration of 100-mL volumes of *E. coli* subject to 5 minutes of ultrasonic irradiation (C_1 was subject to 10 minutes) at pH = 7.4 in 0.01M PBS. $C_1 = 1.8 \times 10^{10}$ CFU mL^{-1}; $C_2 = 4.7 \times 10^9$ CFU mL^{-1}. A – 6

Table A6. Raw data of US disinfection rate dependence on initial cell concentration of 100-mL volumes of *E. coli* subject to 5 minutes of ultrasonic irradiation at pH = 7.4 in 0.01M PBS. $C_3 = 1.6 \times 10^8$ CFU mL^{-1}; $C_4 = 1.1 \times 10^8$ CFU mL^{-1}. A – 7

Table A7. Raw data of US disinfection rate dependence on initial cell concentration of 100-mL volumes of *E. coli* subject to 5 minutes of ultrasonic irradiation at pH = 7.4 in 0.01M PBS. $C_5 = 1.2 \times 10^7$ CFU mL^{-1}; $C_6 = 1.1 \times 10^6$ CFU mL^{-1}. A – 8

Table A8. Raw data of UV disinfection rate dependence on initial cell concentration of 100-mL volumes of *E. coli* subject to 1 minute of ultraviolet irradiation at pH = 7.4 in 0.01M PBS. $C_1 = 2.2 \times 10^9$ CFU mL^{-1}; $C_2 = 1.1 \times 10^9$ CFU mL^{-1}. A – 9

Table A9. Raw data of UV disinfection rate dependence on initial cell concentration of 100-mL volumes of *E. coli* subject to 1 minute of ultraviolet irradiation at pH = 7.4 in 0.01M PBS. $C_3 = 2.3 \times 10^7$ CFU mL^{-1}; $C_4 = 6.4 \times 10^5$ CFU mL^{-1}. A – 10

Table A10. Raw data of UV disinfection rate dependence on initial cell concentration of 100-mL volumes of *E. coli* subject to 1 minute of ultraviolet irradiation at pH = 7.4 in 0.01M PBS. $C_5 = 2.5 \times 10^5$ CFU mL^{-1}; $C_6 = 3.2 \times 10^4$ CFU mL^{-1}. A – 11

Table A11. Raw data for LD_{50} dependence on initial cell concentration on electrohydraulic discharge process (EHD), ultraviolet irradiation (UV), and ultrasonic irradiation (US). Units of LD_{50}(EHD) are in number of EHDs, LD_{50}(UV) are in minutes of UV exposure, and LD_{50}(US) are in minutes of US irradiation. A – 12

Table A12. Raw data for β-D-galactosidase experiments on 8/26/98. *E. coli* suspension (3 L) in 0.01 M PBS at pH = 7.4 subject to 30 consecutive electrohydraulic discharges. E_{CB} = 7 kJ, spark gap = 4 mm, and pulse rate = 0.1 Hz. A – 13

Table B1. Raw data for sunscreen experiments. [BP9] = 0 mg/L. A – 14

Table B2. Raw data for sunscreen experiments. [BP9] = 1 mg/L. A – 15

Table B3. Raw data for sunscreen experiments. [BP9] = 5 mg/L. A – 16

Table B4. Raw data for sunscreen experiments. [BP9] = 20 mg/L. A – 17

Table B5. Raw data for sunscreen experiments. [BP9] = 40 mg/L. A – 18

Table B6. Raw data for sunscreen experiments. [BP9] = 60 mg/L. A – 19

Table B7. Raw data for sunscreen experiments. [BP9] = 100 mg/L. A – 20

Table C1. Raw data from 1/1/2001 for EHD selective pressure experiments in Ch. 5. A - 21

Chapter I

Introduction

Chapter I. Introduction

General Disinfection Methods

Many strategies for the management and reduction of microorganisms in water for human consumption have been devised (*1,2*). Examples of these strategies include water filtration by screens and osmosis (*3*), flocculation and aggregation (*4*), and UV light irradiation (*5*). By far, the most common treatment technique used is disinfection by chlorine (*6*).

Recent studies have recognized new or emerging pathogens that survive and proliferate in the drinking water treatment and distribution systems (*7*). Among these are newly identified fecal pathogens like enterohemorrhagic *Escherichia coli* (*8,9*), *Campylobacter jejuni* (*10*), enteric viruses like rotavirus, calicivirus, astrovirus (*11-13*), and the parasites *Cryptosporidium parvum*, *Giardia lamblia* and microsporidia (*14,15*). Also, environmental pathogenic bacteria such as *Pseudomonas aeruginosa*, *Legionella* spp., *Mycobacterium* spp., and *Aeromonas* spp. have been identified to grow in treatment facilities in both planktonic and biofilm environments (*16-18*).

Advanced disinfection techniques make use of ozone (*19-21*), hydrogen peroxide (*22*), ultrasonic irradiation (*23-28*), gamma irradiation (*29-33*), semiconductor photocatalysis (*34-40*), flash photolysis (*41*), biocidal polymers (*42,43*), high intensity laser photolysis (*44-47*), and high-voltage pulses (*48-50*) as possible water treatment processes. But as with any emerging technology, cost and treatment volume limit their

range of applicability. The continual search for a more general and cost effective technique for water disinfection is the motivation for this work.

Disinfection by Electrohydraulic Discharges

Pulsed-power plasma or electrohydraulic discharge reactors have been used effectively in the past for the treatment of environmentally recalcitrant pollutants offering rapid mineralization rates of chemicals like 2,4,6-trinitrotoluene, 4-chlorophenol, and 3,4-dichloroaniline (*51-54*). Other applications include simulation of underwater explosions (*55*), metal forming (*56*), rock fragmentation (*56*), and shockwave lithotripsy (*56-58*).

Disinfection by electrohydraulic discharge (EHD) reactors is a novelty motivated by previous work done at Caltech (*57,59,60*). In addition, EHD generated UV radiation and shockwave effects on bacteria have been studied previously but in the context of food science and protection (*61-63*). The electrohydraulic discharge process can be an effective technique for water disinfection for the following reasons: EHDs generate hot, localized plasmas strongly emitting high intensity UV light; they also produce shockwaves and generate hydroxyl radicals during water photodissociation. UV light in the range of 200 to 400 nm is a known mutagen to cells (*64*), shockwaves are known to produce mechanical ruptures to cell membranes (*59*), and hydroxyl radical attack is a pathway for oxidative cell damage (*23*). The purpose of this thesis is to study the disinfection process by electrohydraulic discharges and investigate the relative importance of each component of disinfection for optimization of the technique.

The Pulsed Plasma Discharge Reactor

The Caltech electrohydraulic discharge (EHD) reactor consists of two electrodes submerged in a 4-liter reaction vessel to which a 135 μF capacitor bank is discharged across the spark gap (*51,52,54*). A 300 ns rise time semiconductor switch is used to trigger the discharge and it is capable of generating a 20 μs pulse with a total energy of 25 kJ and 1 GW peak power. Figure 1 shows the schematic of the EHD reactor system.

Under normal experimental conditions, measurements of the voltage across the electrodes can be as high as 5 kV with peak currents of 90 kA. The system is electrically analogous to an underdamped LRC circuit with a period of 50 μs. Following the rapid discharge of the capacitor bank, a fraction of the current leaks into the spark gap and heats the water surrounding the electrodes forming gas bubbles (Fig. 2). These bubbles enable the formation of a plasma channel across the liquid medium. The plasma channel can reach temperatures in the range of 14 000 - 50 000 K and functions as a blackbody radiation source with a maximum emittance in the VUV spectrum (λ = 75 - 185 nm). The plasma channel consists of a highly ionized, high-pressure and high-temperature fluid. Once formed, the plasma channel tends to expand. The mechanical inertia of the surrounding water resists this expansion resulting in the development of very high pressures. The energy stored in the plasma channel is slowly dissipated (slow relative to the plasma formation process) as thermal radiation and mechanical work. At the detonation front, the high-pressure build up in the plasma is transmitted into the water interface and an intense compression wave (shockwave) is formed that travels ahead of the expanding gas bubble at a speed several times faster than the speed of sound. Pressure

jumps across the shock can be as high as ~ 5-20 kbars. When the shockwave reaches a free surface, the stress-free condition at the interface instantly transforms the compression wave into a tension (or rarefaction) wave and it is reflected back into the liquid medium. This rarefaction wave induces cavitation as it travels back through the water. The shockwaves, rarefaction waves, and gas bubble expansion sustain a highly turbulent mixing environment until all pressures are equalized.

Chemical Effects

The simultaneous occurrence of multiple processes makes the chemistry and physics of the EHD process quite complicated. In an attempt to differentiate between the different physicochemical processes, we shall group them into *localized* and *extended* effects. We define oxidative degradation that occurs within the plasma channel and within the immediate vicinity as a localized effect. This includes pyrolysis within the high-temperature plasma, oxidation due to direct and indirect VUV photolysis, and supercritical water oxidation. Mechanical damage resulting from shockwaves and UV radiation in the bulk aqueous solution are defined as extended effects. In the context of biological disinfection, the localized effects lead to zero-order kinetics. We have focused, therefore, on the study of the kinetics of disinfection by mechanical and UV radiation damage to *E. coli*. In the EHD process, chemical degradation can occur within the plasma channel directly due to pyrolysis and free radical reactions. However, the small volume of the plasma channel (1-3 mL) limits the amount of solution that can be directly exposed to high-temperature pyrolytic processes.

High Intensity UV Emission

The plasma channel formed during an electrohydraulic discharge can reach temperatures of 14 000 - 50 000 K and thus functions as a blackbody radiation source with a maximum emittance in the vacuum ultraviolet VUV region of the spectrum (λ = 75-185 nm (*65*)). Figure 3 shows a typical blackbody spectrum at 15 000 K. The VUV light emitted from the hot plasma is absorbed by the water layer immediately surrounding the plasma channel (*66*), and the UV light with $\lambda > 184$ nm penetrates into the bulk of the solution. An additional component due to absorption of light by *E. coli* was measured using direct reflectance UV absorption spectroscopy with a Shimadzu UV-2101 PC UV-Vis Scanning Spectrophotometer outfitted with an integrating sphere. Figure 4 shows the blackbody spectrum at 50 000 K and the measured absorbance spectrum of *E. coli*.

In principle, all wavelengths below 200 nm are absorbed by water. DNA thymidine dimerization is known to occur only at wavelengths below 400 nm so the range of interest for biological disinfection is 200 nm $< \lambda <$ 400 nm.

The high intensity of the UV light emission in the EHD reactor further complicates matters. Stepwise multiphoton absorption at UV light intensities higher than 10^6 W/cm^2 generated by picosecond and nanosecond laser irradiation is known to produce nonlinear photoprocesses in nucleic acids (*44,67,68*). In our experiments the EHD reaches intensities as high as 3 x 10^6 W/cm^2, which leads us clear into the multiphotonic photochemistry regime.

In low-intensity, UV irradiation of nucleic acids, absorption to the first excited singlet and triplet states (S_1 and T_1 respectively) leads to formation of C_5-C_6 cyclobutyl dimers between neighboring pyridines weakening and distorting DNA strands, ultimately blocking DNA replication. Figure 5 shows the thymine electronic level diagram.

Non-conventional high-lying quasi-Rydberg S_N and T_N state photochemical processes in thymine can occur with high intensity UV irradiation due to two photon absorption mechanisms that lead to the formation of DNA-base radicals, ejection of a hydrated electron e^-_{aq}, or direct ionization (*69-71*). Oxidative damage incurred by the subsequent reactions between these highly energetic moeties and the cellular material produces DNA single and double strand breaks (*44,72-74*).

The inactivation process displays similar kinetics to disinfection by pulsed radiolysis and ionizing radiation (*45,75*) and additional pathways of action have been verified, i.e., formation of single and double strand DNA breaks (ssb, dsb), interstrand crosslinking, and protection by the cytoplasm (*72,74,76*).

Shockwave Effects

Experiments with exploding wires have shown that electrohydraulic discharges induce extreme electromagnetic and mechanical conditions in the bulk solutions outside of the plasma channel region that may affect the inactivation of microorganisms in solution (*55,65,77,78*).

During the formation of the plasma channel (1-2 μs), an intense 5-20 kbar shockwave is generated due to the rapidly expanding plasma channel (*77*). The resulting

shockwave can induce pyrolytic and free radical reactions indirectly via electrohydraulic cavitation (*79*). As the plasma channel cools over 1-3 ms, thermal energy is transferred to the surrounding water, resulting in the formation of a steam bubble (*55*). Within the steam bubble, the temperatures and pressures are high enough for the formation of transient supercritical water (*78*). However, the overall temperatures after 50 EHDs is less than 35 °C, confirming that most of the bactericidal effects are due to other nonthermal mechanisms.

Motivation

In the United States, the Environmental Protection Agency (USEPA) enacted the 1992 Surface Water Treatment Rule (SWTR, Fig. 6) requiring all community water treatment systems, in addition to the usual Total Coliform Rule (TCR) with a maximum concentration level goal (MCLG) of zero, to disinfect surface waters before distribution and filtering (*80*). Specifically, all surface water systems must filter and disinfect 99.9 % removal and inactivation of *Giardia*, and 99.99 % removal and inactivation of viruses. These stringent requirements were established as a result of common and novel pathogens that survive the standard chlorination technique (*7*). The need for new and broader techniques for treatment of municipal water systems is the main motivation for this work.

Thesis Purpose and Overview

The purpose of this thesis is to study the feasibility of the pulsed power discharge reactor for the treatment of municipal waters. This work is divided into three major areas of interest: first, an investigation on the rates of disinfection of *E. coli* by EHD (Chapter 3); second, a determination of the main component of disinfection (Chapter 4); and third, the implications of long-term EHD exposure on mutation rates of *E. coli* survivors (Chapter 5).

The first portion of this research will be directed towards determining the net rate of EHD disinfection given an initial concentration of *E. coli*. The kinetics of the disinfection process will be discussed and compared with two well-known systems: low intensity UV lamp disinfection and low power ultrasonic irradiation. Values of LD_{50} will be computed for the EHD disinfection technique, followed by a general discussion on efficiency regimes.

The second portion of this research will attempt to ascertain the main mechanism of disinfection during an EHD event. In particular, an assessment of the degree of disinfection by high intensity UV emission will be performed, enabled by the use of a chemical sunscreen. The relative effectiveness of the UV component of the EHD will be discussed in the context of the overall process optimization.

The final portion of this research will be directed at determining the possible emergence of mutants that can survive exposure to long-term EHD treatment. The study will focus on EHD selective pressure experiments subject to 11 growth and death cycles. The net kinetic change in the dose-response curves and the net metabolic activity

between initial and final populations will be discussed and compared. The conclusions regarding the outcome of these experiments will indicate the degree of mutagenicity generated by EHD.

References Cited

(1) Letterman, R. D. *Water quality and treatment*; 5th ed.; Letterman, R. D., Ed.; McGraw-Hill: New York, 1999.

(2) Clesceri, L. S.; Greenberg, A. E.; Trussell, R. R. *Standard Methods for the Examination of Water and Wastewater*; 17th ed.; Clesceri, L. S.; Greenberg, A. E.; Trussell, R. R., Ed.; APHA, AWWA, and WPCF: Washington, D.C., 1989.

(3) Eisenberg, T. N.; Middlebrooks, E. J. *Removal of microorganisms by reverse osmosis*. In: *Reverse osmosis treatment of drinking water*; Butterworth Publishers: Stoneham, MA, 1986, pp 133.

(4) Treweek, G. P. The flocculation of E. coli with polyethyleneimene. Ph.D. Thesis, California Institute of Technology, 1975.

(5) Scheible, O. K.; Forndran, A. *Ultraviolet Disinfection of Wastewaters from Secondary Effluent and Combined Sewer Overflows*, Report EPA-600/2-86/005; U.S. EPA, 1986.

(6) White, G. C. *Handbook of chlorination and alternative disinfectants*; 4th ed.; Wiley: New York, 1999.

(7) Szewzyk, U.; Szewzyk, R.; Manz, W.; Schleifer, K.-H. *Ann. Rev. Microbiol.* **2000**, *54*, 81.

(8) Goosney, D. L.; Gruenheid, S.; Finley, B. B. *Ann. Rev. Cell Dev. Biol.* **2000**, *16*, 173.

(9) Bieber, D.; Ramer, S. W.; Wu, C. Y.; Murray, W. J.; Tobe, T.; Fernandez, R.; Schoolnik, G. K. *Science* **1998**, *280*, 2114.

(10) Obiri-Danso, K.; Paul, N.; Jones, K. *J. Appl. Microbiol.* **2001**, *90*, 256.

(11) Soule, H.; Genoulaz, O.; Gratacap-Cavallier, B.; Chevallier, P.; Liu, J. X.; Seigneurin, J. M. *Wat. Res.* **2000**, *34*, 1063.

(12) Pinto, R. M.; Gajardo, R.; Abad, F. X.; Bosch, A. *Environ. Sci. Technol.* **1995**, *29*, 2636.

(13) Abad, F. X.; Pinto, R. M.; Diez, J. M.; Bosch, A. *Appl. Environ. Microbiol.* **1994**, *60*, 2377.

(14) Fayer, R. *Cryptosporidium and Cryptosporidiosis*; Fayer, R., Ed.; CRC Press: Boca Raton, FL, 1997.

(15) Slifko, T. R.; Smith, H. V.; Rose, J. B. *Int. J. Parasitology* **2000**, *30*, 1379.

(16) Lin, Y. E.; Vidic, R. D.; Stout, J. E.; Yu, V. L. *J. Am. Wat. Works Assoc.* **1998**, *90*, 112.

(17) Bert, F.; Maubec, E.; Bruneau, B.; Berry, P.; Lambert-Zechovsky, N. *J. Hosp. Infect.* **1998**, *39*, 53.

(18) Nguyen, L.; Pron, B.; Quesne, G.; Brusset, M. C.; Berche, P. *J. Hosp. Infec.* **1998**, *39*, 301.

(19) Hunt, N.; Marinas, B. *Wat. Res.* **1997**, *31*, 1355.

(20) Hunt, N. K.; Marinas, B. J. *Wat. Res.* **1999**, *33*, 2633.

(21) Zhou, H.; Smith, D. *J. Environ. Eng.* **1992**, *120*, 841.

(22) White, G. C. *Ozone, Peroxone, and AOxPs.* In: *Handbook of chlorination and alternative disinfectants*; Wiley: New York, 1999.

(23) Hua, I.; Thompson, J. E. *Wat. Res.* **2000**, *34*, 3888.

(24) Vollmer, A. C.; Kwakye, S.; Halpern, M.; Everbach, E. C. *Appl. Environ. Microbiol.* **1998**, *64*, 3927.

(25) Phull, S. S.; Newman, A. P.; Lorimer, J. P.; Pollet, B.; Mason, T. J. *Ultrason. Sonochem.* **1997**, *4*, 157.

(26) Allison, D. G.; D'Emanuele, A.; Eginton, P.; Williams, A. R. *J. Basic Microbiol.* **1996**, *36*, 3.

(27) Miller, D. L.; Thomas, R. M. *Ultrasound Med. Biol.* **1996**, *22*, 681.

(28) Miller, D. L.; Thomas, R. M.; Frazier, M. E. *Ultrasound Med. Biol.* **1991**, *17*.

(29) Bertinchamps, A. J.; Huttermann, J.; Kohnlein, W.; Teoule, R. *Effects of Ionizing Radiation on DNA*; Bertinchamps, A. J.; Huttermann, J.; Kohnlein, W.; Teoule, R., Ed.; Springer: Berlin, 1978.

(30) von Sonntag, C. *The Chemical Basis of Radiation Biology*; Taylor & Francis: London, 1987.

(31) Teebor, G. W.; Boorstein, R. J.; Cadet, J. *Int. J. Radiat. Biol.* **1988**, *54*, 131.

(32) Steenken, S. *Chem. Rev.* **1989**, *89*, 503.

(33) Cadet, J.; Berger, M.; Mouret, J.-F.; Odin, F.; Polverelli, M.; Ravanat, J.-L. . In: *Early Effects of Radiation on DNA*; Fielden, E. M. and O'Neill, P., Ed.; NATO ASI Series, 1990.

(34) Matsunaga, T.; Okochi, M.; Takahashi, M.; Nakayama, T.; Wake, H.; Nakamura, N. *Wat. Res.* **2000**, *34*, 3117.

(35) Maness, P.-C.; Smolinski, S.; Blake, D. M.; Huang, Z.; Wolfrum, E. J.; Jacoby, W. A. *Appl. Environ. Microbiol.* **1999**, *65*, 4094.

(36) Sunada, K.; Kikuchi, Y.; Hashimoto, K.; Fujushima, A. *Environ. Sci. Technol.* **1998**, *32*, 726.

(37) Block, S. S.; Seng, V. P.; Goswami, D. W. *ASME J. Solar Energy Eng.* **1997**, *119*, 85.

(38) Horie, Y.; David, D. A.; Taya, M.; Tone, S. *Ind. Eng. Chem. Res.* **1996**, *35*, 3920.

(39) Ireland, J. C.; Klostermann, P.; Rice, E. W.; Clark, R. M. *Appl. Environ. Microbiol.* **1993**, *59*, 1668.

(40) Saito, T.; Iwase, T.; Horie, J.; Morioka, T. *J. Photochem. Photobiol. B: Biol.* **1992**, *14*, 369.

(41) Oldham, T. C.; Phillips, D. *J. Phys. Chem. B* **1999**, *103*, 9333.

(42) Sun, G.; Wheatley, W. B.; Worley, S. D. *Ind. Eng. Chem. Res.* **1994**, *33*, 168.

(43) Sun, G.; Allen, L. C.; Luckie, E. P.; Wheatley, W. B.; Worley, S. D. *Ind. Eng. Chem. Res.* **1995**, *34*, 4106.

(44) Gorner, H. *J. Photochem. Photobiol. B: Biology* **1994**, *26*, 117.

(45) Angelov, D.; Berger, M.; Cadet, J.; Getoff, N.; Keskinova, E.; Solar, S. *Radiat. Phys. Chem.* **1991**, *37*, 717.

(46) Masnyk, T. W.; Nguyen, H. T.; Minton, K. W. *J. Biol. Chem.* **1989**, *264*, 2482.

(47) Nikogosyan, D. N.; Oraevsky, A. A.; Zavilgelsky, G. B. *Photobiochem. Photobiophys.* **1986**, *10*, 189.

(48) van Heesch, E. J. M.; Pemen, A. J. M.; Huijbrechts, P. A. H. J.; van der Laan, P. C. T.; Ptasinski, K. J.; Zanstra, G. J.; de Jong, P. *IEEE Trans. Plasma Sci.* **2000**, *28*, 137.

(49) Jayaram, S.; Castle, G. S. P.; Margaritis, A. *Biotechnol. Bioeng.* **1992**, *40*, 1412.

(50) Mizuno, A. *IEEE Trans. Ind. Appl.* **1988**, *24*, 387.

(51) Willberg, D. M.; Lang, P. S.; Hochemer, R. H.; Kratel, A.; Hoffmann, M. R. *Environ. Sci. Technol.* **1996**, *30*, 2526.

(52) Willberg, D. M.; Lang, P. S.; Hochemer, R. H.; Kratel, A.; Hoffmann, M. R. *Chemtech* **1996**, *26(4)*, 53.

(53) Hochemer, R. Degradation of organic compounds by acoustic cavitation and pulsed-power discharges. Ph.D. Thesis, California Institute of Technology, 1996.

(54) Lang, P. S.; Ching, W.-K.; Willberg, D. M.; Hoffmann, M. R. *Environ. Sci. Technol.* **1998**, *32*, 3142.

(55) Buntzen, R. R. *The Use of Exploding Wires in the Study of Small-Scale Underwater Explosions*. In: *Exploding Wires, Vol 2*; Chace, W. G. and Moore, H. K., Ed.; Plenum Press: New York, NY, 1962, pp 195.

(56) Smith, K. F. *Electro-Hydraulic Forming*. In: *High-Velocity Forming of Metals*; Wilson, F. W., Ed.; Prentice Hall: Englewood Cliffs, NJ, 1964, pp 77.

(57) Howard, D. D. Part I. Mechanisms of injury associated with extracorporeal shock wave lithotripsy ; Part II. Exsolution of volatiles. Ph.D. Thesis, California Institute of Technology, 1996.

(58) Lokhanwalla, M.; Sturtevant, B. *Physics in Medicine and Biology* **2000**, *45*, 1923.

(59) Howard, D.; Sturtevant, B. *Ultrasound Med. Biol.* **1997**, *23*, 1107.

(60) Kratel, A. W. H. Pulsed power discharges in water. Ph.D. Thesis, California Institute of Technology, 1996.

(61) Edebo, L.; Selin, I. *J. Gen. Microbiol.* **1968**, *50*, 253.

(62) Gilliland, S. E.; Speck, M. L. *Appl. Microbiol.* **1967**, *15*, 1031.

(63) Gilliland, S. E.; Speck, M. L. *Appl. Microbiol.* **1967**, *15*, 1038.

(64) Matsunaga, T.; Hieda, K.; Nikaido, O. *Photochem. Photobiol.* **1991**, *54*, 403.

(65) Robinson, J. W.; Ham, M.; Balaster, A. N. *J. Appl. Phys.* **1973**, *44*, 72.

(66) Jakob, L.; Hashem, T. M.; Burki, S.; Guindy, N. M.; Braun, A. M. *J. Photochem. Photobiol. A* **1993**, *7*, 97.

(67) Nikogosyan, D. N.; Letokhov, V. S. *Riv. Nuovo Cimento* **1983**, *6*, 1.

(68) Nikogosyan, D. N.; Angelov, D. A.; Oraevsky, A. A. *Photochem. Photobiol.* **1982**, *35*, 627.

(69) Goez, M.; Zubarev, V. *Chem. Phys.* **2000**, *256*, 107.

(70) Reuther, A.; Nikogosyan, D. N.; Laubereau, A. *J. Phys. Chem.* **1996**, *100*, 5570.

(71) Oraevsky, A. A.; Nikogosyan, D. N. *Chem. Phys.* **1985**, *100*, 429.

(72) Schulte-Frohlinde, D.; Simic, M. G.; Gorner, H. *Photochem. Photobiol.* **1990**, *52*, 1137.

(73) Bothe, E.; Gorner, H.; Opitz, J.; Schulte-Frohlinde, D.; Siddiqi, A.; Malgorzata, W. *Photochem. Photobiol.* **1990**, *52*, 949.

(74) Masnyk, T. W.; Minton, K. W. *Photochem. Photobiol.* **1991**, *54*, 99.

(75) Schulte-Frohlinde, D.; Bothe, E. *Pulse radiolysis of nucleic acids in aqueous solutions*; CRC Press: Boca Raton, FL, 1991.

(76) Kochevar, I. E.; Walsh, A. A.; Green, H. A.; Sherwood, M.; Shih, A. G.; Sutherland, B. M. *Cancer Res.* **1991**, *51*, 288.

(77) Martin, E. A. *J. Appl. Phys.* **1960**, *31*, 225.

(78) Ben'kovskii, V. G.; Golubnichii, P. I.; Maslennikov, S. I. *Sov. Phys. Acoust.* **1974**, *20*, 14.

(79) Coleman, A. J.; Saunders, J. E.; Crum, L. A.; Dyson, M. *Ultrasound Interact. Med. Biol.* **1987**, *13*, 69.

(80) *25 Years of Safe Drinking Water Act*, EPA 816-R-99-007; U. S. EPA, 1999.

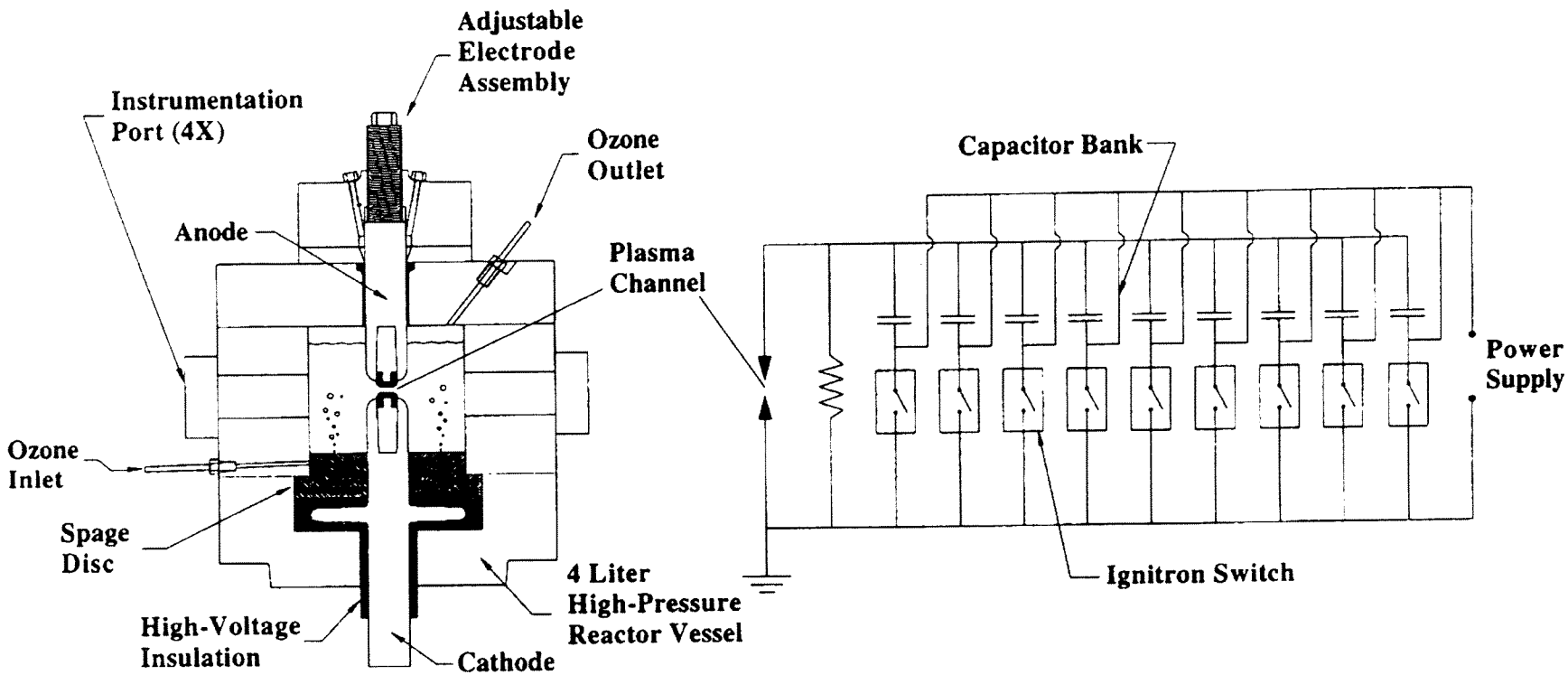

Figure 1. Schematic diagram of the EHD/O3 reactor and electronic circuit.

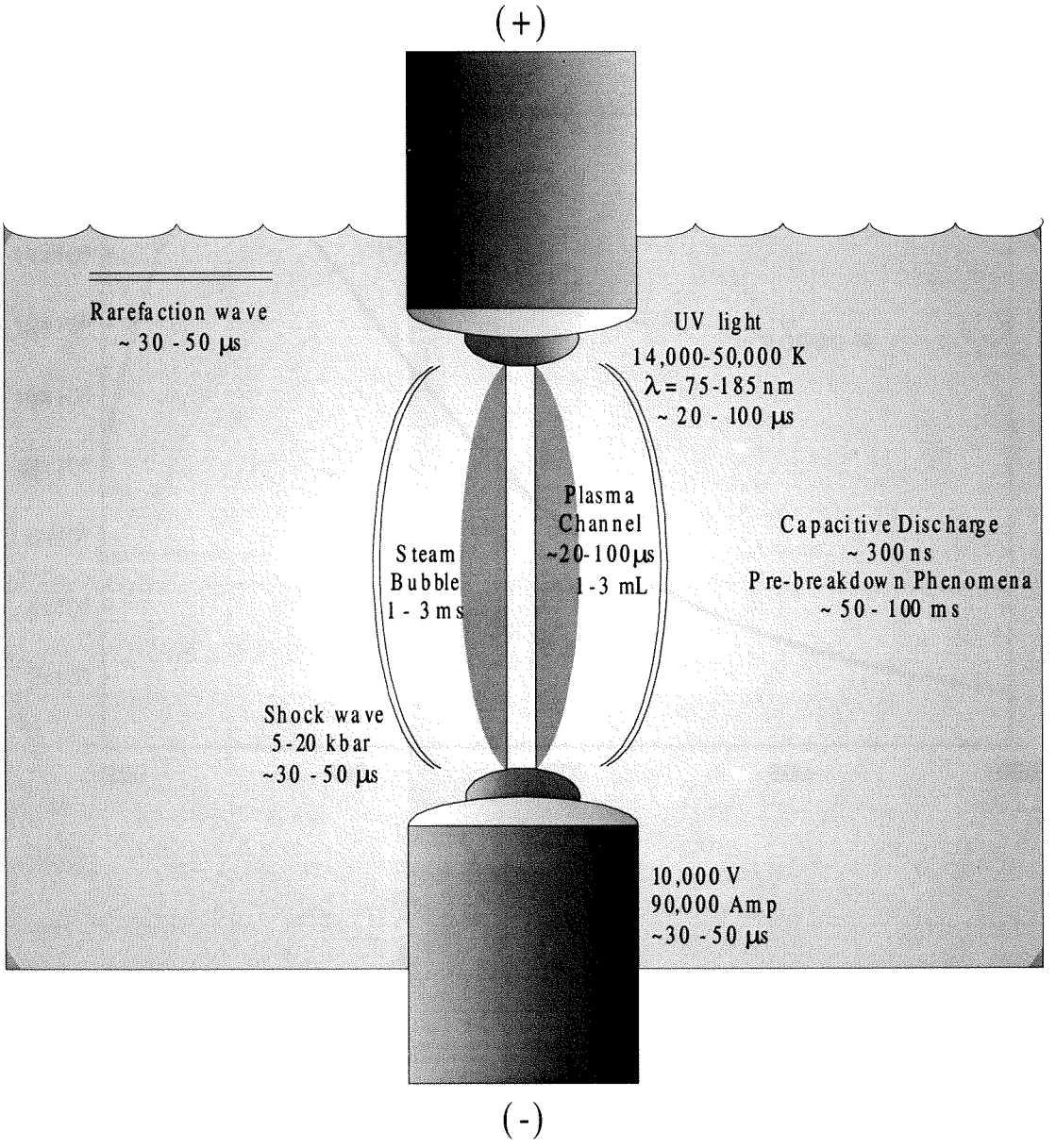

Figure 2. Description of main events during a typical electrohydraulic discharge event.

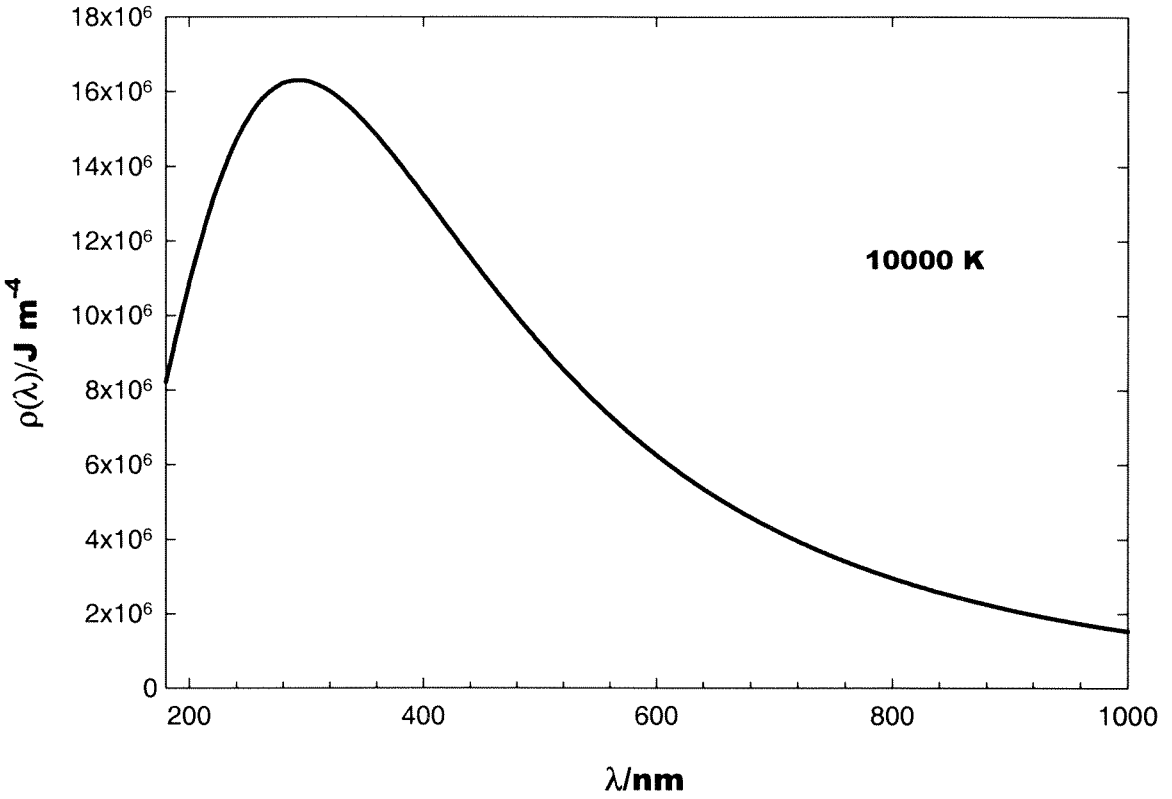

Figure 3. Blackbody spectrum at 15 000 K. Maximum emision occurs at λ = 300 nm. At higher temperatures (EHD is 50 000 K), the maximum emission shifts to the left (lower wavelengths).

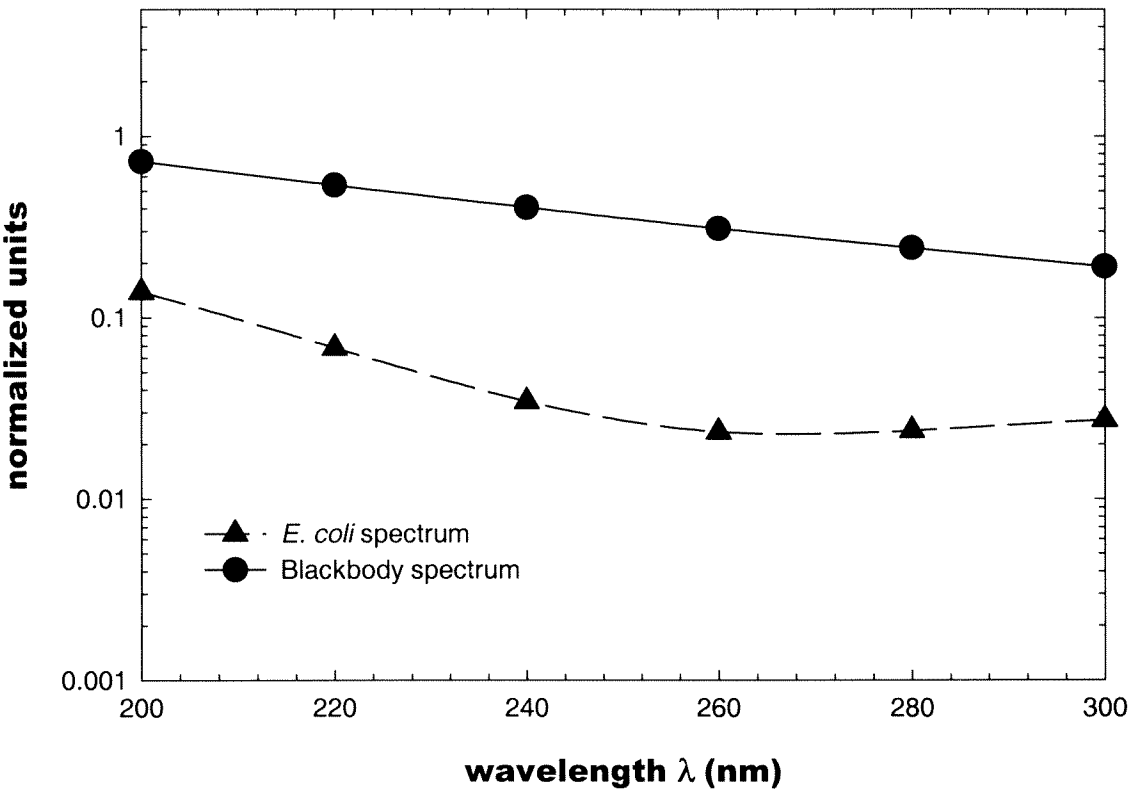

Figure 4. Normalized spectrum of a 50 000 K blackbody (solid circles) at λ_{max} = 100 nm and measured absorbance of *E. coli* (solid triangles) with $\varepsilon_{254\ nm} = 1.13 \times 10^{9}$ mL CFU^{-1} cm^{-1}.

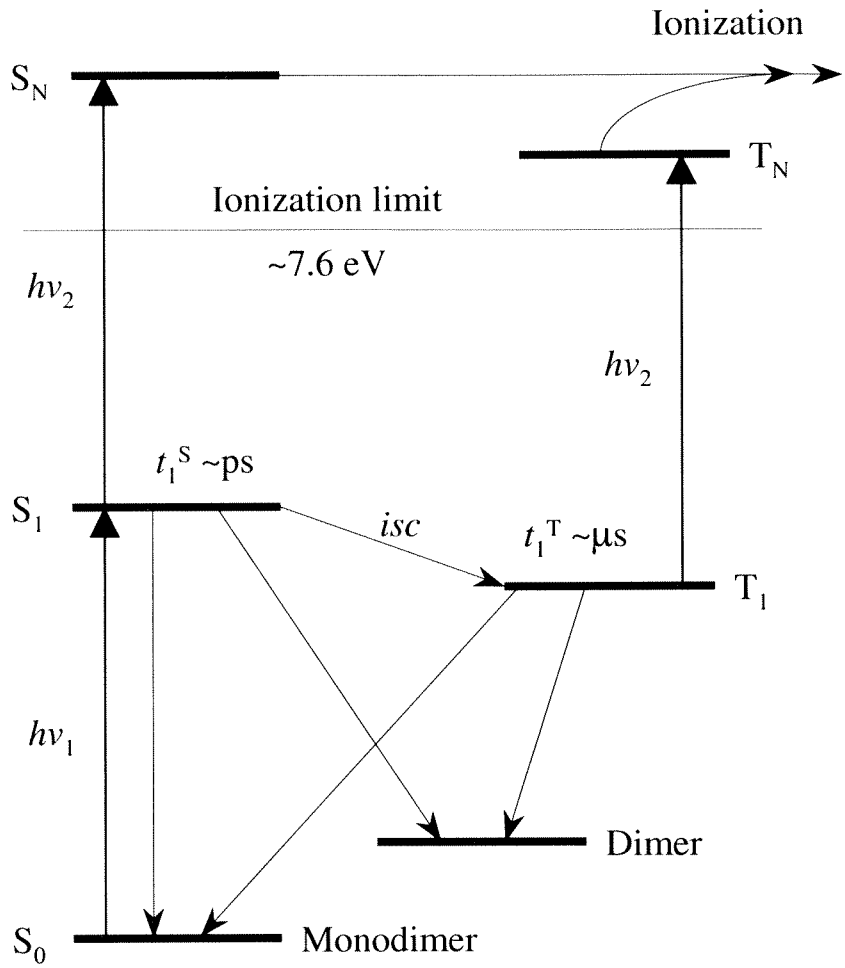

Figure 5. Electronic levels of DNA thymine. S_0, ground state; S_1, lowest singlet excited state; S_N, higher singlet excited state; T_1, lowest triplet excited state; T_N, higher triplet excited state; $h\nu_1$, first photon absorbed; $h\nu_2$, second photon absorbed by either S_1 or T_1; *isc*, intersystem crossing; t_1^S, lifetime of S_1; t_1^T, lifetime of T_1.

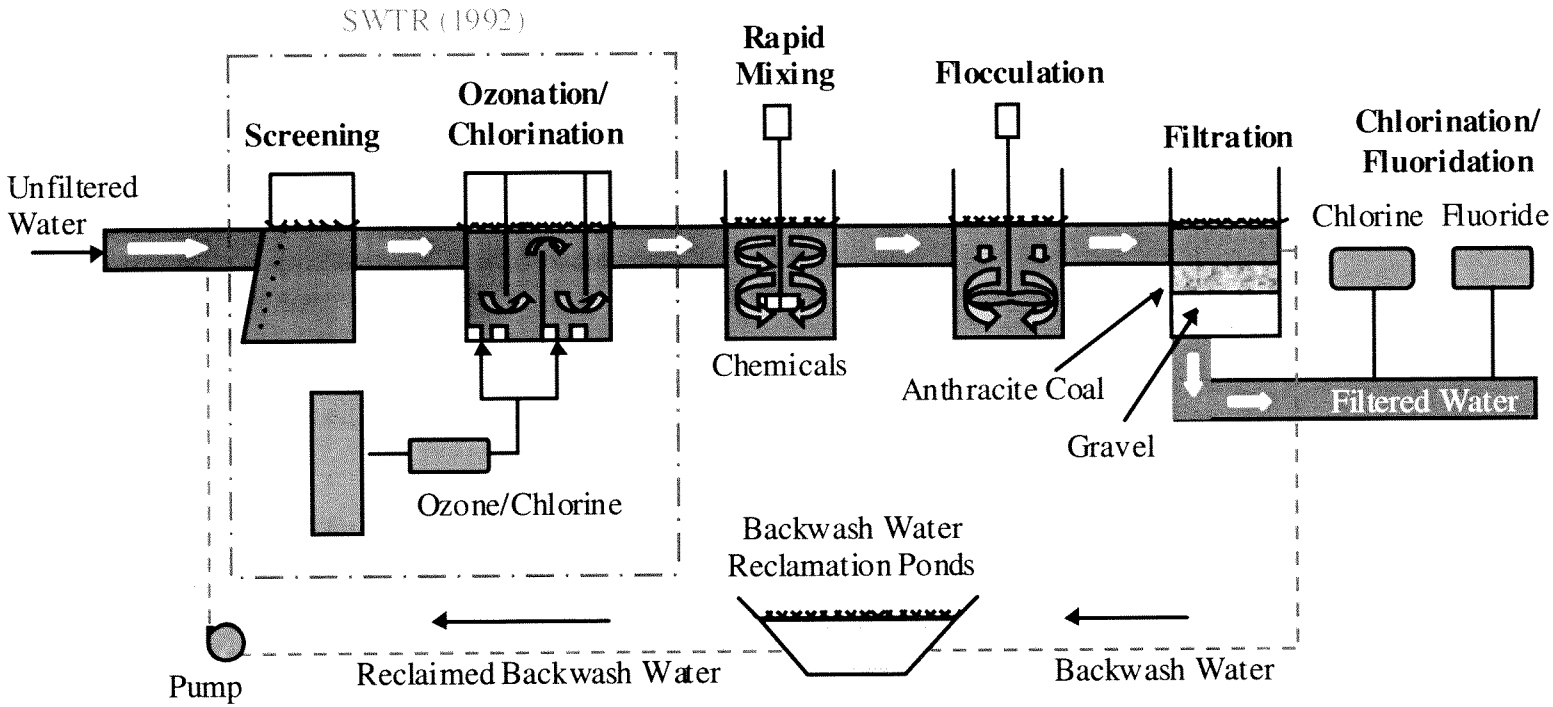

Figure 6. Schematic diagram of a typical municipal water treatment facility. Boxed area is the result of the 1992 Surface Water Treatment Rule (SWTR) required by the U. S. EPA.

Chapter II

Experimental Section

Chapter II. Experimental Section

Electronics

The Caltech EHD reactor has two principal components, which include a power supply that is connected to a 135 μF capacitor bank with control electronics, and a 4-L discharge chamber that contains the solution to be treated (*1*). Figure 1 shows a photograph of the facility. The capacitor bank can be charged with net energies ranging from 2 to 25 kJ and then discharged through fast (300 ns rise time) ignitron switches into the electrode gap in the discharge chamber. The electrode gap in the reaction chamber (see Fig. 2) is typically 4 mm and can be varied from 0 to 32 mm in length with an adjustable electrode assembly. The lifetime of the plasma channel under typical experimental conditions ranges from 20 to 100 μs (*1*). The EHD reactor system can be represented as a large LRC circuit in which the discharge events often exhibit current reversal, and as a consequence, they are categorized as underdamped discharges. The reaction chamber has been designed to withstand the high-pressure shockwaves and the large electrical voltages and currents without electrical arcing or mechanical failure.

An opposing electrode design was selected for shock resistance and adjustability. The adjustable ground electrode assembly allows for the precise control (± 0.1 mm) of the spark-gap length within a range of 0-30 mm; it maintains the structural integrity of the chamber; and it provides a tight compression connection for the high current pulses. The ground electrode can be readjusted to maintain a constant spark-gap separation to offset any effect due to erosion of the electrode tips. Tantalum was selected for the

electrode tips because it is a refractory metal (mp = 2996 °C) that minimizes electrode erosion; tantalum and their oxides are relatively inert and do not interfere significantly with the disinfection process under investigation. The tantalum tips are joined to the steel electrodes by incorporating them into locking Morse taper assemblies. Flat cylindrical tips are used to minimize the effects of tip erosion during the lifetime of an experiment.

The electronics package that drives the pulsed discharge unit is an RLC circuit designed and built by Pulsed Power Technologies Inc. (PPTI, San Diego). It has been specifically designed with a low inductance (250 – 300 nH) and a relatively large capacitance (135 μF) to generate short but high-energy pulses. It is capable of delivering a 20 μs pulse with a total energy of 25 kJ and a peak power of up to 1 GW. Fast ignitron switches with a 300 ns rise time are used to trigger the discharge.

Electrical current was measured on the hot electrode bus (cathode) using a Rogowski coil that has been calibrated against a 123.3 μΩ current viewing resistor (T&M Research). Voltages were measured on the cathode bus bar using a high-voltage probe (North Star Research). Triggering of the circuit and collection of the current and voltage traces was done remotely using a PC computer that was controlled with LabView software (National Instruments).

A single electrical discharge in the chamber can be described by the governing differential equation:

$$L\frac{d^2q}{dt^2} + R(t)\frac{dq}{dt} + \frac{q}{C} = 0 \qquad (1)$$

where L is the inductance of the circuit, C is the capacitance, and q is the stored charge. R(t) is the resistance of the plasma channel. Depending on the specific values of R, L, and C, there are three regimes of discharge operation, underdamped $R < 2(L/C)^{1/2}$, critically damped $R = 2(L/C)^{1/2}$, and overdamped $R > 2(L/C)^{1/2}$. All discharges in our experiments were either underdamped or critically damped (i.e., most discharges exhibit current reversal).

In a typical EHD experiment, the large capacitor bank was charged to V_{CB} = 10.2 kV, which yielded the total stored energy of E_{CB} = 7kJ. After complete charging, the capacitor bank was discharged very rapidly using the fast ignitron switches in order to charge the submerged electrodes. As a voltage of 10.2 kV, the electric field is insufficient to cause the formation of a plasma channel directly through liquid water. In this case, the resulting ionic current heats the water in the spark-gap, forming gas bubbles through which the discharge occurs (*2*). The pre-discharge current leakage significantly reduces the energy available for the discharge from an initial value of E_{CB} = 7 kJ to E_D = 2 kJ. After a plasma channel is formed, a current pulse arcs across the underwater spark-gap (0.4 cm). Since the plasma channel is the major resistive element in the circuit, most of the energy in the current pulse is deposited into the solution in the reactor chamber (*3*).

Exposure of Cells to EHD

For experiments with *E. coli* a fluid volume of 3.0 L was loaded into the reactor chamber with the total energy of the capacitor bank set to E_{CB} = 7 kJ. The measured voltage on the cathode at the time of discharge was V_D = 5.5 ± 0.3 kV, and the energy

delivered in the EHD pulse was $E_D = 2.0 \pm 0.2$ kJ. The peak current of these pulses was typically 90 kA. The value of E_{CB} rather than E_D was used for all efficiency calculations, since it includes all of the energy losses due to the preliminary plasma-channel breakdown phenomenon. However, it is possible that some thermal disinfection of microbes could occur during the preliminary breakdown phase.

We define the lifetime of an EHD pulse as the period of time between the first and last time the current pulse reaches 10% of its peak value. The duration of the pulse can be directly related to the voltage at the initiation of the plasma channel. In these experiments, the average current pulse lasted 41 ± 4 μs.

The survival kinetics of *E. coli* were investigated using several fixed parameters. In all of the experiments, the solution volume was maintained at 3.0 L. Since the total volume of the reactor chamber is 4.0 L, a head space of 1.0 L was maintained in the chamber to facilitate mixing due to reflected shockwaves (negative-pressure rarefaction waves) that produced a "depth charge" effect.

A 0.01 M phosphate buffered-saline, pH = 7.4 (PBS) solution was used as an electrolyte to increase conductivity and to ensure rapid formation of the plasma channel across the underwater electrode gap. In addition, PBS is used as wash and resuspension medium for *E. coli* to ensure that cells remain in stasis throughout the duration of the experiment.

After placement of the bacterial sample in the reaction chamber, it was allowed to equilibrate for 5 min prior to the first sampling point. During the course of the EHD treatment, sample aliquots were extracted with sterile Pasteur pipettes. The extracted

samples were held temporarily in a constant temperature ice bath. Given the repetition (pulse) rate of the charging circuit of 0.1 Hz, the total experimental run times were approximately 1 hour for a 50 consecutive discharge experiment. However, the total plasma exposure time over such an experiment was 2 ms (assuming 50 EHDs at 40 μs per EHD gives 2 ms).

Reactor Mixing Conditions

We tested mixing conditions in the reactor during and between pulses by following the dispersal of small volumes of colored solutions (1 mL 0.01 M MnO_4K) injected in the gap region. Without pulsing, the colored solute is slowly homogenized by diffusion/convection throughout the reactor in about 2 hours. In contrast, a single pulse suffices to produce a uniformly colored solution. Assuming that in the latter case mixing is driven by pressure waves generated by the discharge, that these waves travel at the speed of sound (1500 m/s), and that they travel back and forth across the reactor 10 times before dissipating, we estimate that mixing takes about 0.6 ms. Since the shortest time interval between consecutive discharges is 10 seconds, the reaction chamber can be assumed to be thoroughly mixed before each discharge. At typical pulse repetition and sampling rates, a 50 consecutive discharge experiment amounts to 2 ms plasma exposure time, but takes 1 hour to complete.

Escherichia coli

E. coli is a gram-negative bacterium whose presence in water is often used as an indicator for fecal coliforms (*4*). *E. coli* is a well known organism (*5*) with well developed techniques for study (*6*). In pure cultures, it requires simple growth conditions and handling that facilitate measurement and detection.

Escherichia coli type-strain ATCC 25922 was used throughout this work. Stock cultures were maintained on Luria-Bertani (LB) agar slants in the dark at 5 °C, and at -20 °C in LB broth with 60 % glycerol added as cryoprotectant. Prior to each experiment, *E. coli* stock was inoculated into sterilized LB broth (1 % tryptone, 0.5 % yeast extract, and 1 % salt), and grown in the dark for 12 hours at 37 °C, while shaken at 225 rpm. Cells from the exponential growth-phase were separated by centrifugation, washed once and resuspended in 0.01 M PBS (10X: 24.72 g Na_2HPO_4, 3.60 g $NaH_2PO_4 \cdot H_2O$, 170.0 g NaCl, pH = 7.4). Resuspended samples were appropriately diluted, then equilibrated in corresponding reactors for 5 min, and finally sterilized by EHD treatment. Sample aliquots, drawn at regular intervals, were held for less than 1 hour at room temperature, prior to incubation and counting. Sample preparation protocols and viability measurement details are shown in Figure 3.

Heterotrophic plate counts were performed to quantify the culturable bacteria present in each sample using Standard Method 9215C (*7*). The samples taken at known intervals during an EHD experiment were thoroughly mixed and diluted in sterile 0.01 M phosphate-buffered saline (PBS), and 0.1 mL of appropriate dilutions were spread onto

LB agar plates. The plates were counted following 12-15 hours incubation in the dark at 37 °C.

Most viability counting techniques rely on colorimetric assays based on cellular transport of fluorescent dye pairs (e.g., live/dead stains, DAPI stains, gram stains, etc.). In some cases, a live cell is shown in one color while a dead cell is shown in another. However, the drawback occurs when cells possess an intermediate coloration, in which case, it becomes difficult to distinguish.

By viability, we mean cells that are active and capable of reproduction and form visible colonies on solid medium. In doing so, we are discarding cells that have been completely destroyed as well as cells that may have sustained minor damage but cannot undergo cellular division.

Other techniques rely on statistical averages of positive dilution tubes, like the standard most probable number (MPN) test 9221C (*4*). But in practice, it was unreliable and difficult to use for the large amounts of viability counts required.

In our experience, we found that agar plate counts were the simplest and most direct method for viability measurement. Although the inherent error of the technique (~10%) left much to be desired, the reproducibility and the stability of the results far outweighed its drawbacks.

Substrate Sensitivity Experiments

Figure 6 (Chap. 6) shows the results of *E. coli* sensitivity experiments using background concentrations of 0.01 M PBS, 100 mM thiosulfate, 100 mM sulfate, 100

mM sulfite, and 5 g/L BP9 over a 42 hour time period in the dark at pH 7.0 and 25 °C. Triplicate viability measurements were performed at 0, 16, and 42 hours and each sample was plated in LB-agar dishes. The results suggest that these substrates at the given concentrations have no effect on *E. coli* viability over the time period indicated and 0.01 M PBS ensures cell stasis over a 2-day period.

Statistical Analyses

Plotted data that have error bars associated with them are shown as the mean ± the largest variance of triplicate samples. The relationships between the sunscreen concentrations and inactivation percentages by the electrohydraulic discharge process were determined using SigmaPlot (version 5.0) and Microsoft Excel (version 5.0). Data used for the slopes of the rectified disinfection curves were computed by transforming the abscissa into logarithmic base 10 units and the ordinate into log*it* units using the mapping,

$$\log it(y_i) = \log_{10}\left(\frac{y_i}{100 - y_i}\right) \qquad (2)$$

The resulting linearized data sets were analyzed using SigmaPlot by the least-squares fit method of linear regression with associated standard errors for both, y-intercepts and slopes. The relationships between the sunscreen concentrations and the slopes of each inactivation curve were then obtained from the regression analysis via the appropriate inverse transformations.

The values of lethal dosages for 50 % viability reduction, denoted by LD_{50}, were obtained by setting P_n to 0.5 and solving Eqn. 2 for n given y_o and m for each sunscreen concentration.

References Cited

(1) Willberg, D. M.; Lang, P. S.; Hochemer, R. H.; Kratel, A.; Hoffmann, M. R. *Environ. Sci. Technol.* **1996**, *30*, 2526.

(2) Naugolnykh, K. A.; Roy, N. A. *Electrical Discharges in Water. A Hydrodynamic Description*, Technical Report FTD-HC-2049-74; Foreign Technology Division, Wright-Patterson Air Force Base, 1974.

(3) Kratel, A. W. H. Pulsed power discharges in water. Ph. D. Thesis, California Institute of Technology, 1996.

(4) Clesceri, L. S.; Greenberg, A. E.; Trussell, R. R. *Standard Methods for the Examination of Water and Wastewater Part 9000: Microbiological Examination of Water*; 17th Edition ed.; Clesceri, L. S.; Greenberg, A. E.; Trussell, R. R., Ed.; APHA-AWWA-WPCF: Maryland, 1989.

(5) Neidhardt, F. C.; Ingraham, J. L.; Low, L. B.; Magasanik, B.; Schaechter, M.; Umbarger, H. E. *Escherichia coli and Salmonella typhimurium*; Neidhardt, F. C.; Ingraham, J. L.; Low, L. B.; Magasanik, B.; Schaechter, M.; Umbarger, H. E., Ed.; American Society for Microbiology: Washington D. C., 1987; Vol. 1-2.

(6) Sambrook, J.; Fritsch, E. F.; Maniatis, T. *Molecular cloning : a laboratory manual*; 2nd ed.; Cold Spring Harbor Laboratory: Cold Spring Harbor, NY, 1989; Vol. 1-3.

(7) Clesceri, L. S.; Greenberg, A. E.; Trussell, R. R. *Standard Methods for the Examination of Water and Wastewater*; 17th ed.; Clesceri, L. S.; Greenberg, A. E.; Trussell, R. R., Ed.; APHA, AWWA, and WPCF: Washington, D.C., 1989.

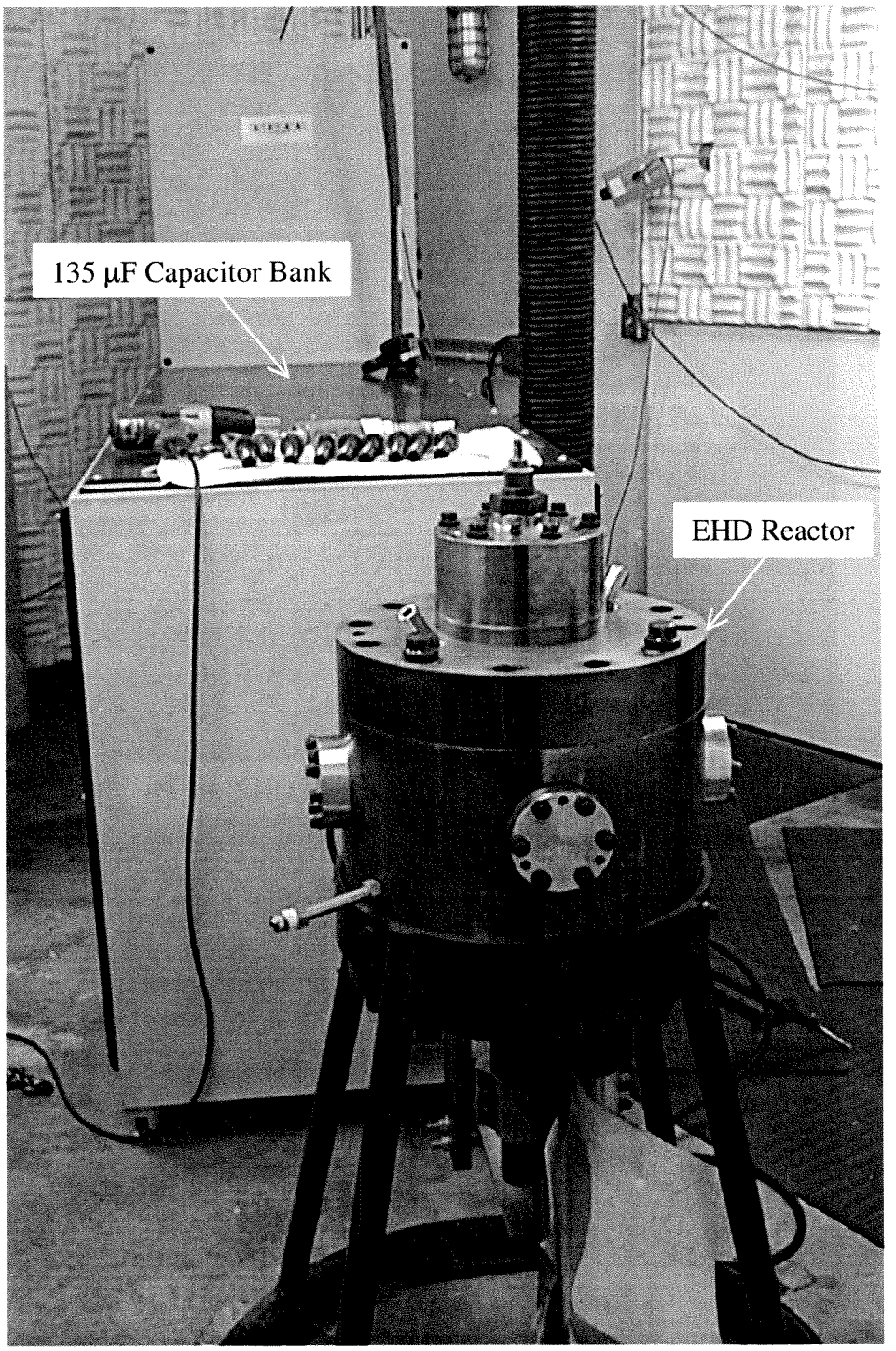

Figure 1. Photograph of the Caltech Electrohydraulic Discharge Reactor.

The reactor outer diameter is 16 inches.

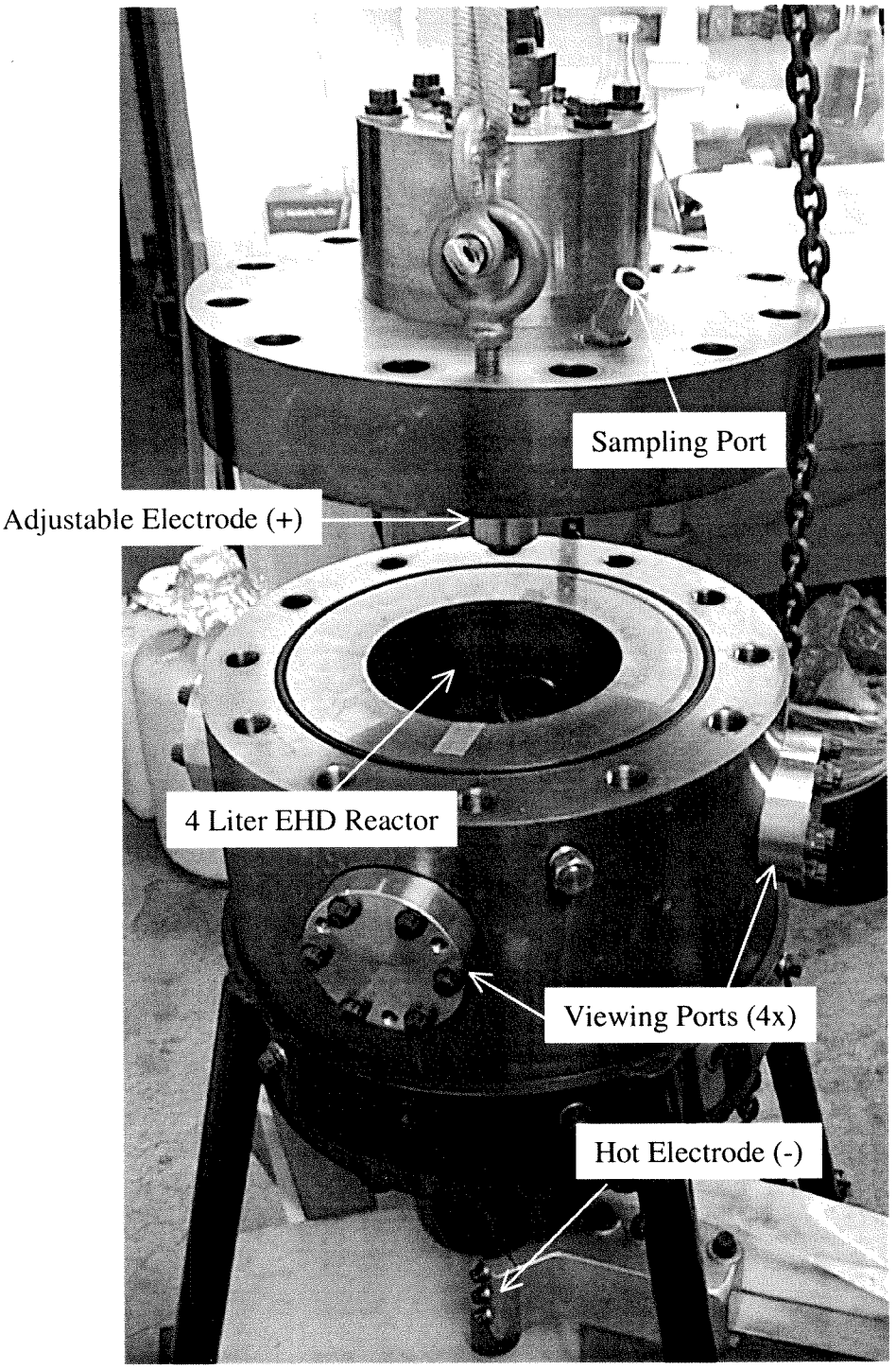

Figure 2. Detail of EHD reactor chamber (cover opened).

For scaling purposes, the reactor outer diameter is 16 inches.

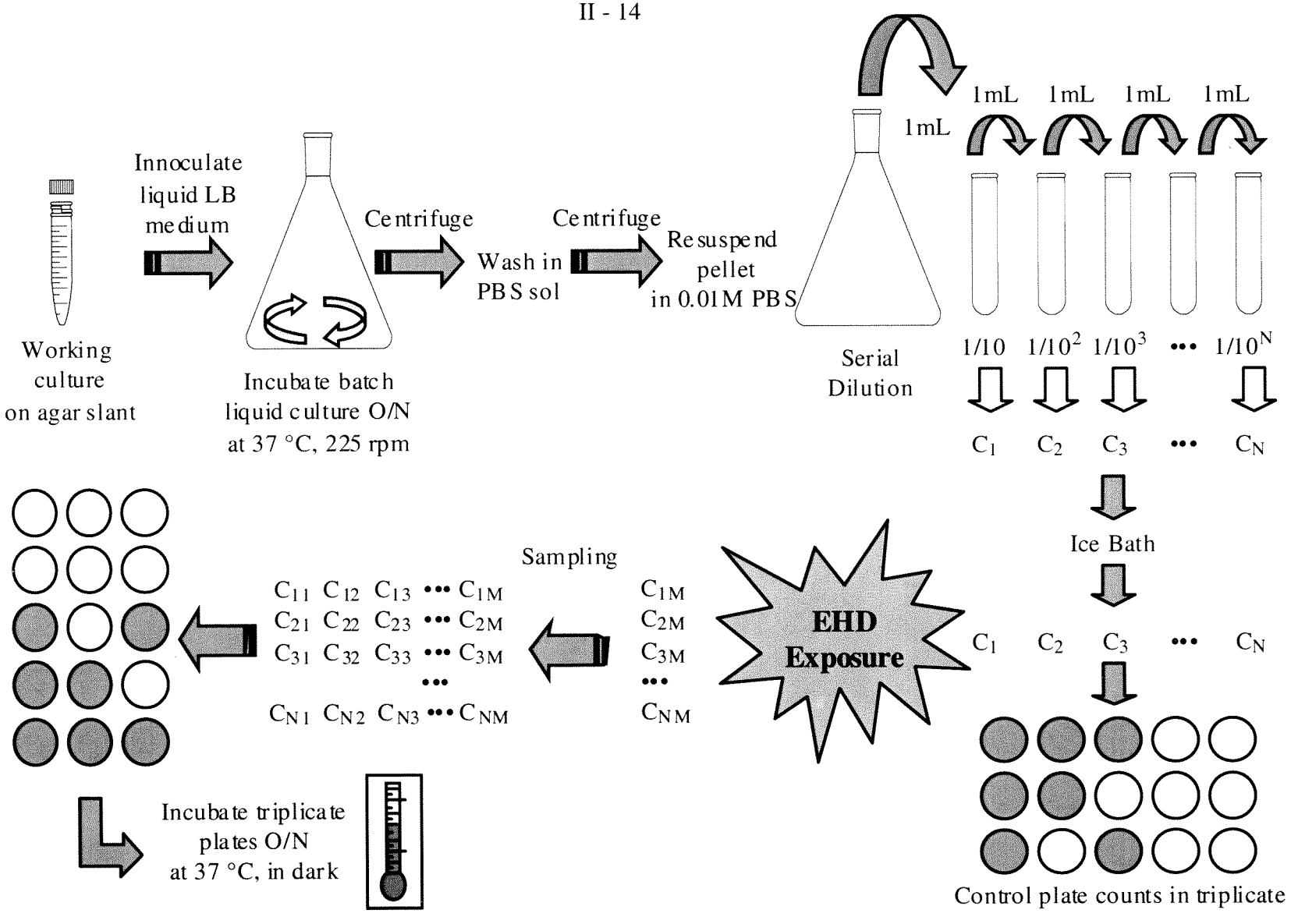

Figure 3. Sample Preparation Protocols and Viability Measurement.

Chapter III

Kinetics of *Escherichia coli* Disinfection by Electrohydraulic Discharges

Kinetics of *Escherichia coli* Disinfection by Electrohydraulic Discharges

by

W.-K. Ching, A. J. Colussi, H. J. Sun[†], K. H. Nealson[†] and M. R. Hoffmann*

W. M. Keck Laboratories
California Institute of Technology
Pasadena, CA 91125

submitted to

Environmental Science and Technology
February, 2001

[†] Jet Propulsion Laboratory, California Institute of Technology, Pasadena, CA 91109

Chapter III. Kinetics of *Escherichia coli* Disinfection by Electrohydraulic Discharges

Abstract

We study the survival of single-strain *Escherichia coli* colonies in aqueous media exposed to 5.5 kV, 90 kA electrohydraulic discharges (EHD). The probability of survival P_n of a 2×10^7 *E. coli* CFU mL^{-1} population after n consecutive EHD's follows a logit distribution:

$$\ln\left(\frac{P_n}{100 - P_n}\right) = 1.0466 - 1.3632 \ln n, \qquad r^2 = 0.998 \tag{1}$$

that corresponds to lethal doses of LD_{50} = 2.2 and LD_{90} = 10.8 EHD's. Considering that the reactor is thoroughly mixed during each discharge, and that $LD_{50} = 0.9 \pm 0.1$ values are nearly independent of *E. coli* concentrations in the range $2 \times 10^3 \leq$ *E. coli*/CFU $mL^{-1} \leq 3 \times 10^6$, we ascribe the non-exponential P_n decay of single-strain *E. coli* colonies to an intrinsic resistance distribution towards the lethal agent. The bacteria become more resistant at slightly higher initial concentrations. The qualitatively similar concentration dependence observed for survival under 254 nm radiation, in contrast with the lower resistance of denser colonies to 20 kHz power ultrasound, and the delayed onset of extracellular β-D-galactosidase activity in bacterial populations already decimated by EHD's, support the view that UV radiation is the dominant disinfection agent generated by electrohydraulic discharges.

Introduction

Disinfection by chlorine is the standard method used for municipal water treatment plants in the United States and most of the world. There are, however, organisms that survive chlorination, a phenomenon attributed to short contact times or to resistance to chlorine (*1*). Ozone (*2*) and ultraviolet (UV) light (*3*) are also used in water treatment facilities with success, but the operation costs and the periodic replacement of flash lamps have limited the use of these technologies. New approaches are needed to circumvent the above limitations, and alternative methods of disinfection such as ultrasonic irradiation (*4*), TiO_2 photocatalysis (*5-7*), electrochemical oxidation (*8*), flash photolysis (*9*), high-voltage discharges (*10-13*), and pressure shocks (*14*) have been proposed.

The use of electric power pulses to generate electrohydraulic discharges (EHDs) has also received attention (*15-17*). Industrial applications of EHD's have included the simulation of underwater explosions (*18*), metal forming (*19*), rock fragmentation (*20*), and mineralization of hazardous waste (*21-23*). Electrohydraulic discharges are generated by the rapid discharge of stored electrical charge across submerged electrodes. The formation of an electrical arc across the spark gap produces a localized plasma region that emits UV and VUV radiation and creates pressure and thermal shocks. Measurements of the UV radiation from electrical discharges in water have been reported to be as high as 200 MW peak radiant power (*24*) and associated tissue damage has been observed in extracorporeal shock-wave lithotripsy (*25*). We demonstrate that by taking advantage of

the intense UV radiation and the mechanical cell damage produced by the discharges, the electrohydraulic discharge process can be used as an alternative method of municipal water disinfection.

In this paper we explore the capabilities of EHD's and report the results of a kinetic study on the disinfection of water contaminated by *Escherichia coli.* These experiments identify the dominant mechanism of sterilization, and establish the survival kinetics (*26,27*) of single-strain *E. coli* colonies subjected to EHD.

Experimental Methods

Sterilization Devices

The Caltech electrohydraulic discharge reactor (Fig. 1, Chap. 1) has been described in detail in previous publications (*21-23*). In a typical experiment, a 135 μF capacitor bank storing E_{CB} = 7 kJ at V_{CB} = 10.2 kV is discharged through a 8 mm electrode gap into 3.0 L of a 0.01 M phosphate-buffered (pH = 7.4) saline (PBS) solution within 40 μs. The peak current of these pulses is about 90 kA. The buffered solution has the proper electrical conductivity for the discharge to flow across the immersed electrodes, and provides a medium in which suspended *E. coli* colonies remain in stasis. Upon charging the electrodes, local ohmic heating creates vapor microbubbles within the gap through which the EHD's occur. The energy utilized for vaporization is estimated at 5 kJ/pulse. Therefore, the energy effectively delivered per pulse is about E_{CB} = 2 kJ. These discharges simultaneously generate a localized hot spot, traveling shock waves and UV-VUV emissions. Since water absorbs strongly below 185 nm, thermal and VUV effects are necessarily localized within a small volume (a few mL) about the electrode gap region. In contrast, mechanical and UV effects may extend further into the reaction volume.

We tested mixing conditions in the reactor during and between pulses by following the dispersal of small volumes of colored solutions (1 mL 0.01 M MnO_4K) injected in the gap region. Without pulsing, the colored solute is slowly homogeneized by diffusion/convection throughout the reactor in about 2 hours. In contrast, a single pulse

suffices to produce a uniformly colored solution. Assuming that in the latter case mixing is driven by pressure waves generated by the discharge, that these waves travel at the speed of sound (1500 m/s), and that they travel back and forth across the reactor 10 times before dying out, we estimate that mixing takes about 0.6 ms. Since that the shortest interval between consecutive discharges is 10 seconds, the reaction chamber is thoroughly mixed before each discharge. At typical pulse repetition and sampling rates, a 50 consecutive discharge experiment amounts to 2 ms exposure time, but takes about 1 hour.

Figure 2 shows the reactor employed for UV/US sterilization. UV-only experiments were carried out by irradiating *E. coli* suspensions (100 mL, contained in a bottle fitted with a 1-inch quartz side window) with 254 nm light emitted by a 15 W Sterilaire SW germicidal lamp. The O_3 generated by the UV lamp, itself a powerful sterilizing agent, was removed from the reactor zone by an exhaust fan. We measured a 4.5 mW/cm^2 light flux at 5 inches away from the lamp. Alternatively, suspensions could be sonicated at 20 kHz by means of a ½ inch diameter Ti immersible probe (VibraCell™ Model VCX400). The ultrasonic probe emitted 11.3 W/cm^2 while dipping 5 mm into the suspension.

Bacterial Cultures and Procedures

E. coli type-strain ATCC 25922 was used throughout. Stock cultures were deposited on LB agar slants in the dark at 5 °C, and maintained at –20 °C in LB broth with 60 % glycerol added as cryoprotectant. Prior to each experiment, the *E. coli* stock

was innoculated into sterilized LB broth (1 % tryptone, 0.5 % yeast extract, 1 % salt), and grown in the dark for 12 hours at 37°C, while shaken at 225 rpm. Cells from the exponential growth-phase were separated by centrifugation, washed once and resuspended in 0.01 M PBS (24.72 g Na_2HPO_4, 3.60 g $NaH_2PO_4 \cdot H_2O$, 170.0 g NaCl, pH = 7.4). Resuspended samples were appropriately diluted, then equilibrated in the corresponding reactors for 5 min, and finally sterilized by EHD, UV, or ultrasound treatment. Sample aliquots, drawn at regular intervals, were held for less than 2 hours at 0°C, prior to incubation and counting. Treated samples were diluted in PBS buffer, spread on Petri dishes covered with LB agar (LB broth with 1.5 % agar), and the number of colonies (CFUs) counted after incubation in the dark at 37°C for 16 hours. This procedure excludes all the cells that will not reproduce by incubation, regardless of the damage undergone during sterilization.

β-D-galactosidase Assay

Mechanical damage to *E. coli* membranes could be inferred from the leakage of cellular material during sterilization. Following Miller (*28*), *E. coli* cultures were grown (see above) in the presence of 1mM isopropyl-β-D-thiogalactopyranoside (IPTG) to induce the synthesis of β-D-galactosidase(*29*). Sterilization experiments were performed on 1.0×10^7 modified CFU mL^{-1} and assayed for leaked β-D-galactosidase within 30 min of sample collection. Every sample aliquot was divided into two portions. The first portion was centrifuged at 8000 rpm for 10 min; the resulting pellet was separated from the supernatant and lysed with $CHCl_3$ and 1 % sodium dodecyl sulfate (SDS). β-D-

galactosidase activity was determined in the lysate as well as in the supernatant. The entire second portion was lysed and analyzed for total β-D-galactosidase activity. The fraction of total enzyme activity in the supernatant of the first portion provides a measure of enzyme leakage as function of the number of EHDs.

Results and Discussion

Disinfection Kinetics and Mechanism

Fig. 3a shows the logarithm of the concentration of viable *E. coli* cells after *n* EHD's for a colony having an initial concentration of 2.0×10^7 CFU mL^{-1}, at an electrode gap of 0.8 cm, E_{CB} = 7 kJ, at pH = 7.4. The bimodal decay of the bacterial population can be realistically fit by a double exponential (the solid line in Fig. 3a) or, alternatively, rectified by casting the data into a logit plot (Fig. 3b). Let $P_n = 100 \times CFU_n/CFU_0$, the percentual survival probability of an *E. coli* colony after *n* EHD's (*30*). The expression:

$$\ln\left(\frac{P_n}{100 - P_n}\right) = 1.0466 - 1.3632 \ln n \qquad (1)$$

actually provides and excellent fit to the data (r^2 = 0.998). From Eq. 1 one can evaluate the lethal doses required to inactivate 50% and 90% of the initial population: LD_{50} = 2.15 and LD_{90} = 10.5, respectively. Thus, it becomes increasingly difficult to reduce pathogenic levels below about 5%. It has been argued that tailing in bacterial survival kinetics is actually associated to experimental artifacts, such as improper mixing, shielding, biocide quenching (*31,32*), etc. Since we verified that the reactor contents are thoroughly mixed by the mechanical perturbation created by EHD pulses, and taking into account that all pulses are in principle equally intense, one should consider the possibility that succeeding discharges might become less effective because the accumulated bacterial debris attenuates their lethality. This possibility must be discarded under present conditions. That the tailing behavior is not artifactual but intrinsic to this process can be

inferred from the fact that the same LD_{50} value is obtained over a 3-order of magnitude variation of *E. coli* initial concentrations (Fig. 4). The data shown in Fig. 4 were obtained by exposing colonies in the range 10^3 to 10^7 CFU mL^{-1} to less than 4 consecutive EHD's, a condition that minimizes turbidity effects from cellular debris and electrode tip erosion. Since we are dealing with single-strain *E. coli* colonies (pure cultures), we ascribe disinfection tailing to the peculiarities of the disinfection process. Further work is underway to confirm this assumption in the present system.

On the other hand, if the concentration threshold for LD_{50} at about 7×10^6 CFU mL^{-1} (Fig. 4) were the result of disinfection action being limited by the production of a finite amount of lethal agent, *E. coli* decay would follow zero order kinetics, at variance with the bi-exponential dependence observed in Fig. 3a. A similar argument rules out localized sterilization, such as that provided by VUV radiation and heat shock about the electrode gap (see above). Thus, the non-monotonic dependence of LD_{50} on bacterial density involves a different mechanism.

The abrupt decline of disinfection efficiency beyond a concentration threshold suggests a cooperative phenomenon. Since the *E. coli* sample suspensions used in these experiments were prepared by dilution of a single culture ($OD_{600\ nm} = 2.0$) into a medium which maintains cellular stasis, this phenomenon is not associated with the expression of different phenotypes but, presumably, with the disgregation of the multicellular conglomerates that develop in growing bacterial populations (*33,34*). The standard behavior for growing *E. coli* microcolonies is to maximize cell-to-cell contact, i.e., population density, rather than individual cell access to substrate (*35*). Our finding

suggests that these bacterial aggregates may persist to some extent after moderate dilution, allowing a larger fraction of bacteria to survive treatment at the same biocide dose. A similar phenomenon was reported for the chemical disinfection of *Staphylococcus aureus* at concentrations above 3×10^8 CFU mL^{-1} (*31*).

Lethal Agent Characterization

In order to establish the mechanisms contributing to EHD biocidal action (*36*), we performed sterilization experiments by means of UV or ultrasonic irradiation. The results of the UV treatment as a function of initial cell concentration are shown in Fig. 5, which qualitatively resembles the behavior observed in Fig. 4 for EHD disinfection. Dilute colonies are killed at constant and relatively rapid rates up to initial cell concentrations exceeding ~3×10^8 CFU mL^{-1}. Ultrasonic irradiation also has deleterious effects on *E. coli* colonies. However, in contrast with the inverse dependence of efficiency on cell population observed for UV disinfection, it is easier to inactivate the denser colonies (Fig. 6). Hydrodynamic shearing of large biological structures with a minimum of redox effects is the expected outcome of cavitation under 20 kHz ultrasound waves. Thus, for example, high molecular weight polymers are degraded by ultrasound down to a limiting chain length (*37,38*). Hence, we conclude that bacterial sterilization by ultrasound involves the mechanical disruption of cell aggregates, and is more efficient in the case of dense colonies.

The extent of mechanical damage undergone by cell membranes under EHD was probed by assaying β-D-galactosidase in treated *E. coli* samples. Fig. 7 shows that after

30 EHDs, about half of the total β-D-galactosidase is released from the bacteria. The presence of enzyme in the supernatant represent evidence that cell membranes became permeable to a ~ 540 kDa moiety. Since extracellular β-D-galactosidase activity develops after about 10 EHDs, i.e., when only 10% of the initial *E. coli* population remains viable (Fig. 3b), these experiments exclude mechanical damage as a major mechanism of inactivation.

Conclusions

Present data on the kinetics of *E. coli* disinfection by the EHD process are consistent with a logistic dose-response dependence. The evidence presented rules out damage mediated by mechanical or chemical means, and points to UV radiation as the dominant lethal agent. We find that bacterial colonies become markedly more resistant to EHD treatment at densities larger than about 7×10^6 CFU mL^{-1}, a phenomenon that we ascribe to the survival protection accruing to individual cells in larger aggregates.

Acknowledgments: Financial support for this project was provided by the following agencies: DARPA, ONR, and EPRI.

References Cited

(1) Szewzyk, U.; Szewzyk, R.; Manz, W.; Schleifer, K.-H. *Ann. Rev. Microbiol.* **2000**, *54*, 81.

(2) Hunt, N.; Marinas, B. *Wat. Res.* **1997**, *31*, 1355.

(3) Scheible, O. K.; Forndran, A. *Ultraviolet Disinfection of Wastewaters from Secondary Effluent and Combined Sewer Overflows*, Report EPA-600/2-86/005; U.S. EPA, 1986.

(4) Vollmer, A. C.; Kwakye, S.; Halpern, M.; Everbach, E. C. *Appl. Environ. Microbiol.* **1998**, *64*, 3927.

(5) Pham, N. H.; McDowell, T.; Wilkins, E. *J. Environ. Sci. Health* **1995**, *A30*, 627.

(6) Horie, Y.; Taya, M.; Tone, S. *J. Chem. Eng. Japan* **1998**, *31*, 577.

(7) Saito, T.; Iwase, T.; Horie, J.; Morioka, T. *J. Photochem. Photobiol. B: Biol.* **1992**, *14*, 369.

(8) Matsunaga, T.; Okochi, M.; Takahashi, M.; Nakayama, T.; Wake, H.; Nakamura, N. *Wat. Res.* **2000**, *34*, 3117.

(9) Oldham, T. C.; Phillips, D. *J. Phys. Chem. B* **1999**, *103*, 9333.

(10) Mizuno, A. *IEEE Trans. Ind. Appl.* **1988**, *24*, 387.

(11) Jayaram, S.; Castle, G. S. P.; Margaritis, A. *Biotechnol. Bioeng.* **1992**, *40*, 1412.

(12) van Heesch, E. J. M.; Pemen, A. J. M.; Huijbrechts, P. A. H. J.; van der Laan, P. C. T.; Ptasinski, K. J.; Zanstra, G. J.; de Jong, P. *IEEE Trans. Plasma Sci.* **2000**, *28*, 137.

(13) Peleg, M. *J. Sci. Food and Agriculture* **1995**, *67*, 93.

(14) Teshima, K.; Ohshima, T.; Tanaka, S.; Nagai, T. *Shock Waves* **1995**, *4*, 293.

(15) Martin, E. A. *J. Appl. Phys.* **1960**, *31*, 225.

(16) Robinson, J. W. *J. Appl. Phys.* **1967**, *38*, 210.

(17) Naugolnykh, K. A.; Roy, N. A. *Electrical Discharges in Water. A Hydrodynamic Description*, Technical Report FTD-HC-2049-74; Foreign Technology Division, Wright-Patterson Air Force Base, 1974.

(18) Buntzen, R. R. *The Use of Exploding Wires in the Study of Small-Scale Underwater Explosions*. In: *Exploding Wires, Vol 2*; Chace, W. G. and Moore, H. K., Ed.; Plenum Press: New York, NY, 1962, pp 195.

(19) Smith, K. F. *Electro-Hydraulic Forming*. In: *High-Velocity Forming of Metals*; Wilson, F. W., Ed.; Prentice Hall: Englewood Cliffs, NJ, 1964, pp 77.

(20) Wesley, R. H.; Ayres, R. A., U. S. Patent No. 4,479,680, 1984.

(21) Willberg, D. M.; Lang, P. S.; Hochemer, R. H.; Kratel, A.; Hoffmann, M. R. *Environ. Sci. Technol.* **1996**, *30*, 2526.

(22) Willberg, D. M.; Lang, P. S.; Hochemer, R. H.; Kratel, A.; Hoffmann, M. R. *Chemtech* **1996**, *26(4)*, 53.

(23) Lang, P. S.; Ching, W.-K.; Willberg, D. M.; Hoffmann, M. R. *Environ. Sci. Technol.* **1998**, *32*, 3142.

(24) Robinson, J. W.; Ham, M.; Balaster, A. N. *J. Appl. Phys.* **1973**, *44*, 72.

(25) Howard, D.; Sturtevant, B. *Ultrasound Med. Biol.* **1997**, *23*, 1107.

(26) Gyurek, L. L.; Finch, G. R. *J. Environ. Eng.* **1998**, *124*, 783.

(27) Hiatt, C. W. *Bacteriol. Rev.* **1964**, *28*, 150.

(28) Miller, J. H. *Experiments in Molecular Genetics*; 3rd Edition ed.; Cold Springs Harbor: New York, 1972.

(29) Pardee, A. B.; Jacob, F.; Monod, J. *J. Mol. Biol.* **1959**, *1*, 165.

(30) Cerf, O. *J. Appl. Bacteriol.* **1977**, *42*, 1.

(31) Johnston, M. D.; Simons, E. A.; Lambert, R. J. W. *J. Appl. Microbiol.* **2000**, *88*, 237.

(32) Lambert, R. J. W.; Johnston, M. D. *J. Appl. Microbiol.* **2000**, *88*, 907.

(33) Brenner, M. P.; Levitov, L. S.; Budrene, E. O. *Biophys. J,* **1998**, *74*, 1677.

(34) Joiner, M. C.; Lambin, P.; Marples, B. *Comptes Rendus de L'Academie des Sciences Serie III* **1999**, *322*, 167.

(35) Shapiro, J. A. *Ann. Rev. Microbiol.* **1998**, *52*, 81.

(36) Cerf, O.; Davey, K. R.; Sadoudi, A. K. *Food Res. Internat.* **1996**, *29*, 219.

(37) Henglein, A. *Contributions to Various Aspects of Cavitation Chemistry.* In: *Advances in Sonochemistry*; Mason, T. J., Ed.; JAI Press: Greenwich, CT, 1993, pp 17.

(38) Henglein, A.; Gutierrez, M. *J. Phys. Chem.* **1990**, *94*, 5169.

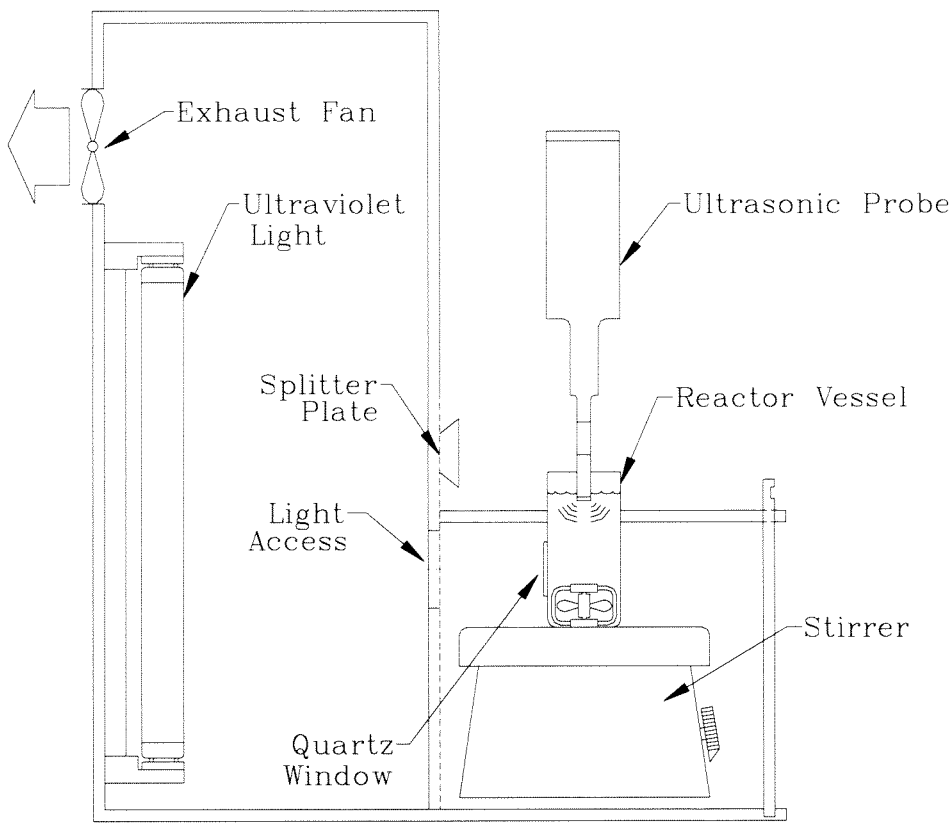

Figure 2. Schematic diagram of the UV/US reactor system.

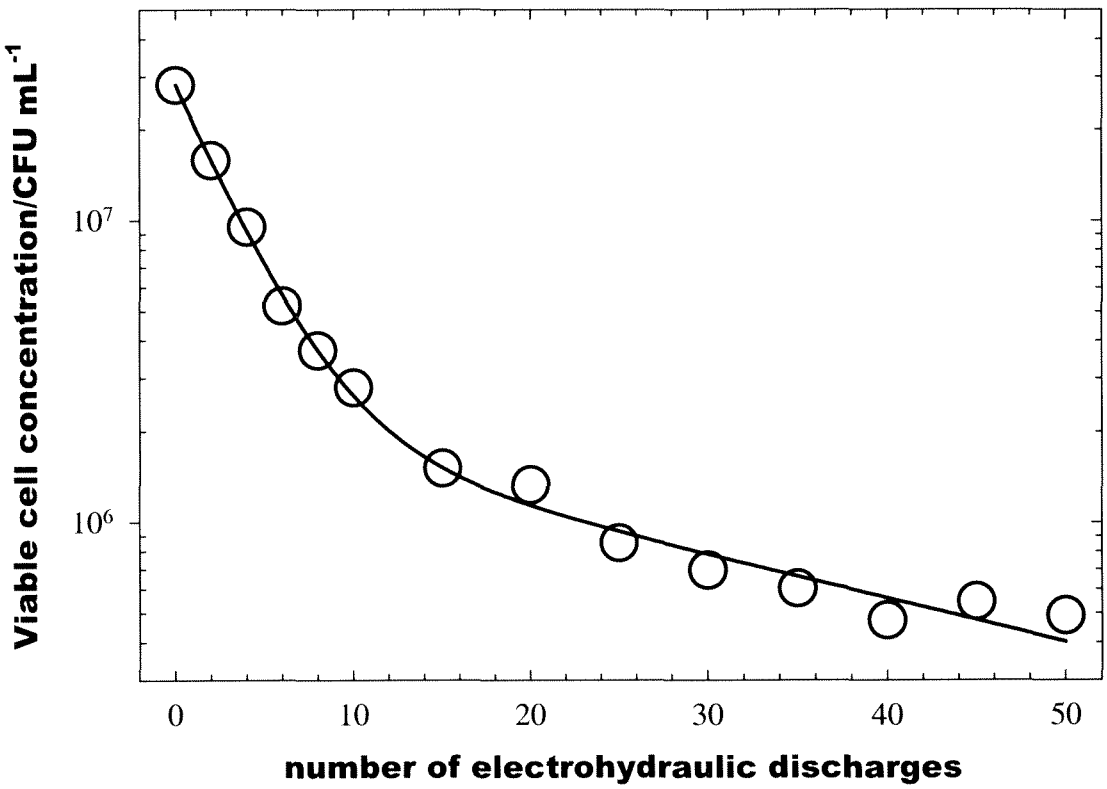

Figure 3a. Disinfection of 3 L of a 2.0 x 10^7 CFU mL^{-1} *E. coli* suspension in 0.01 M PBS at pH = 7.4 by 50 consecutive electrohydraulic discharges. Discharges are characterized by: E_{CB} = 7 kJ, spark gap = 4 mm, and pulse rate = 0.1 Hz. The solid line is a bi-exponential fit to the data.

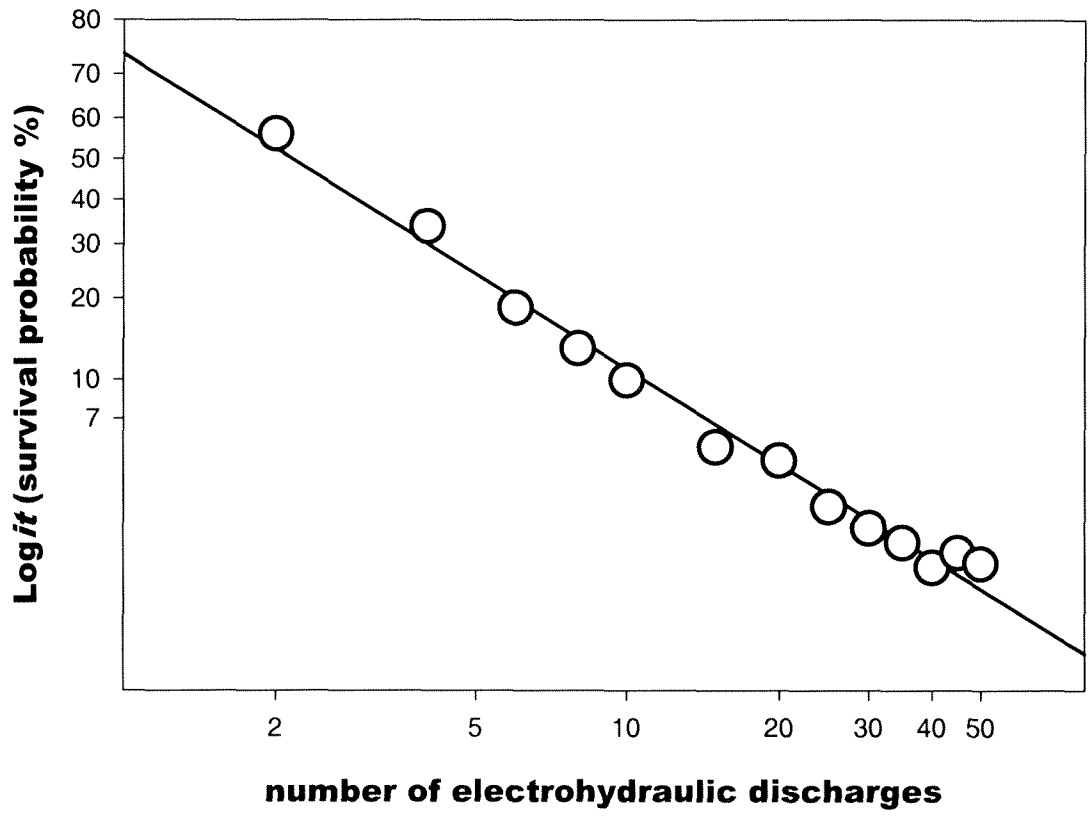

Figure 3b. A logit plot of the data of Fig. 3a. The solid line is calculated from Eq. 1 (see text). P_n is the percentual survival probability of the colonies after n discharges.

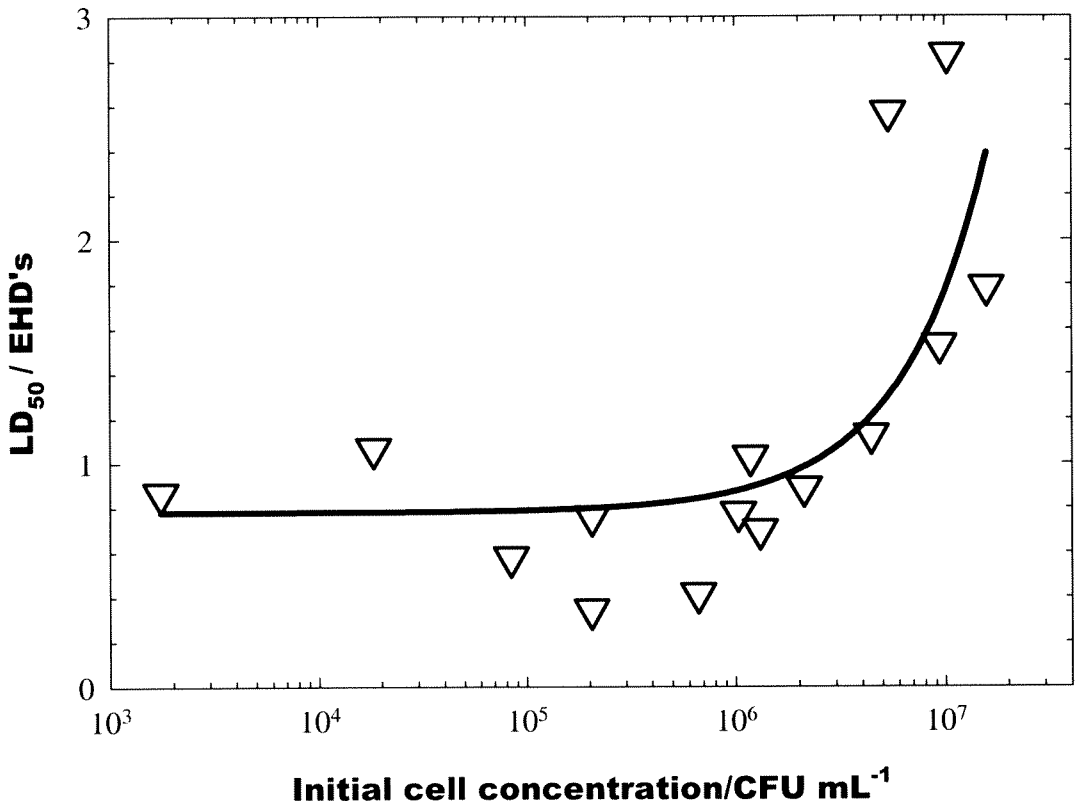

Figure 4. The number of EHD required to inactivate 50 % of the initial population LD_{50} vs. initial *E. coli* cell concentration, as obtained from initial disinfection rates. The solid line is an empirical 3-parameter exponential growth fit to the data.

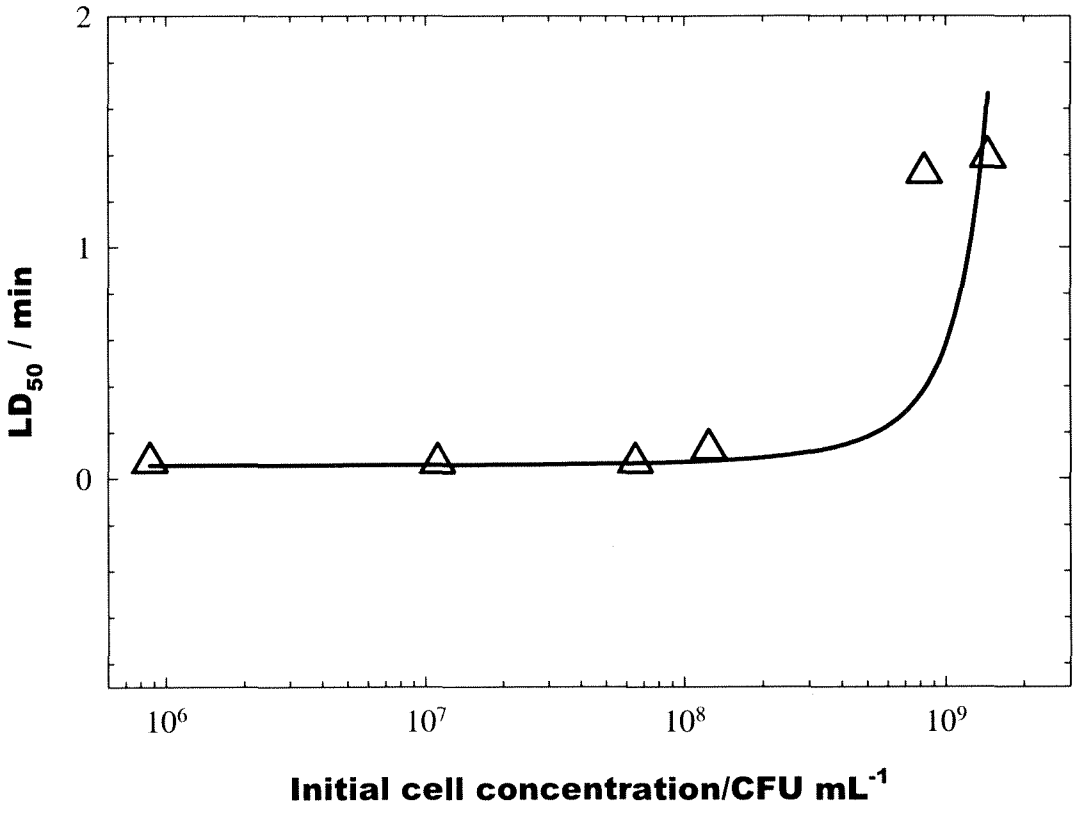

Figure 5. LD_{50} values (in min of UV exposure) for *E. coli* disinfection by 254 nm light vs. initial cell concentrations. Conditions: 100-mL of *E. coli* suspensions in 0.01 M PBS at pH = 7.4.

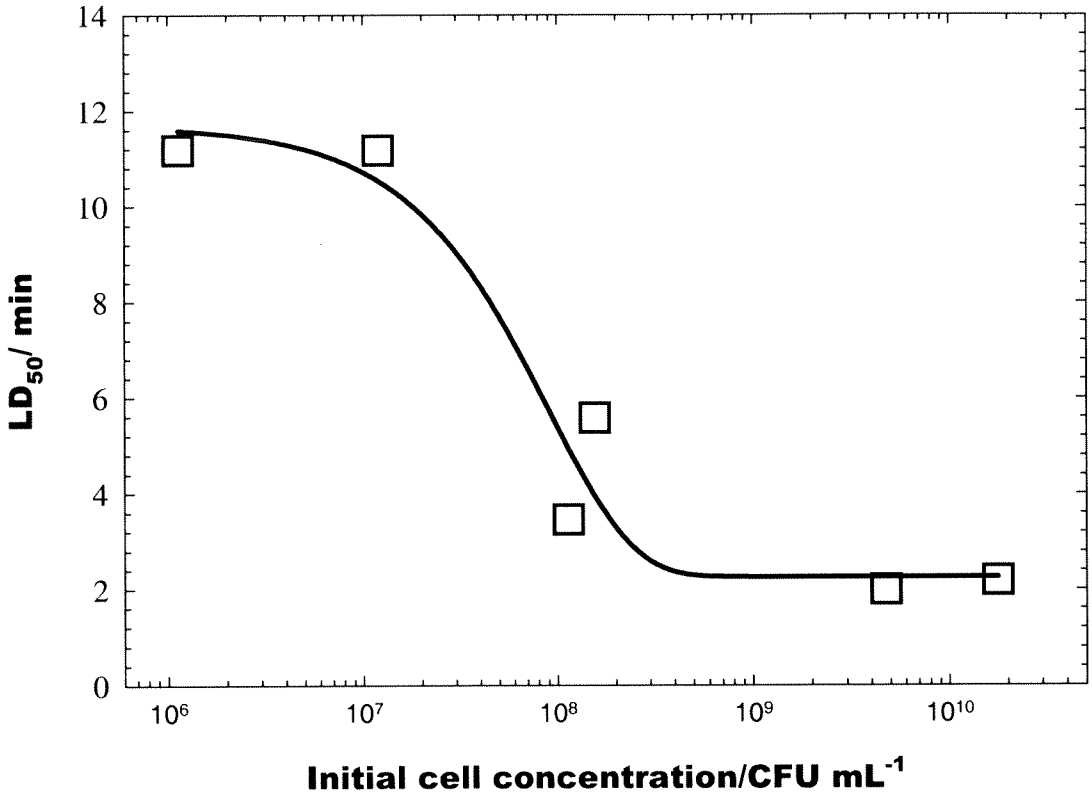

Figure 6. LD_{50} values (in min of ultrasound exposure) for *E. coli* disinfection by 20 kHz ultrasound vs. initial cell concentrations. Conditions: 100-mL of *E. coli* suspensions in 0.01 M PBS at pH = 7.4.

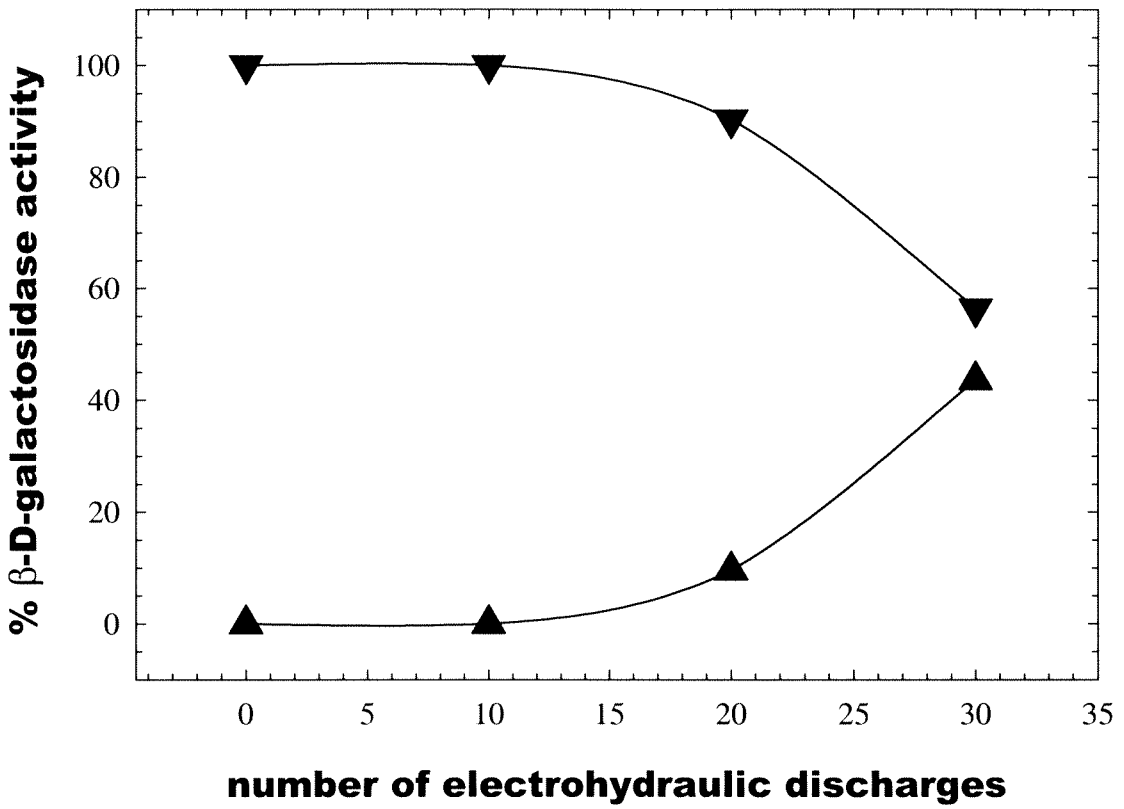

Figure 7. β-D-galactosidase activity of *E. coli* vs. the number of electrohydraulic discharges, in the cell lysate (inverted triangles) and in the supernatant (solid triangles).

Chapter IV

Soluble Sunscreens Fully Inhibit *E.coli* Disinfection by High Intensity UV Irradiation in Electrohydraulic Discharges.

Soluble Sunscreens Fully Inhibit *E.coli* Disinfection by High Intensity UV Irradiation in Electrohydraulic Discharges

by

W.-K. Ching, A. J. Colussi, and M. R. Hoffmann*

W. M. Keck Laboratories
California Institute of Technology
Pasadena, CA 91125

submitted to

Environmental Science and Technology
April 2001

* To whom correspondence should be addressed: California Institute of Technology, Phone (626)395-4391, FAX (626)395-2940, e-mail: mrh@its.caltech.edu

Chapter IV. Soluble Sunscreens Fully Inhibit *E.coli* Disinfection by High Intensity UV Irradiation in Electrohydraulic Discharges

Abstract

Electrohydraulic discharges sterilize *Escherichia coli* populations via the high intensity (3.3×10^{10} W m^{-2}) ultraviolet radiation emitted by underwater plasmas, rather than by mechanical damage or OH-radical attack, as disinfection can be completely suppressed in the presence of less than 100 mg L^{-1} *2,2'-dihydroxy-4,4'-dimethoxybenzophenone-5,5'-disulfonic acid* (BP9), a well-known sunscreen agent. Experiments involved measuring the sterilization kinetics of ~ 3×10^7 CFU mL^{-1} *E. coli* buffered suspensions in the presence BP9 in the range (0 – 100) mg L^{-1}. The slope of the log*it* plots of *E. coli* survival as function of the number of EHDs as function of BP9 concentration is consistent with the screening of radiation as the sole lethal agent. Computed values of biologically available light fluences are 5.0×10^{11} photons CFU^{-1} for high intensity, high power, pulsed EHD experiments and 6.6×10^8 photons CFU^{-1} for separate low power continuous UV experiments. The net availability of 3 orders of magnitude more photons during high intensity UV exposure suggests the possibility of a multiphotonic disinfection mechanism at play in the EHD process relative to low intensity case.

Introduction

Disinfection by electrohydraulic discharge (EHD) reactors can be an effective method for drinking water treatment. However, the lethal agents generated by EHDs remain to be identified, and their contributions to disinfection action quantified. EHDs generate hot, localized plasmas strongly emitting high intensity UV light, but also produce shockwaves, and generated hydroxyl radicals during water photodissociation. Optimization of this treatment process requires refinement of our knowledge about the relative importance of these factors on the effectiveness of the disinfection method.

Recent experiments have assessed the performance of EHD under relatively high-energy conditions (7 kJ per pulse) by varying initial cell concentrations and measuring the dose-response curves to infer the relative importance of each internal factor (*1*). The comparison between values of lethal dosages (LD) vs. initial cell concentrations in the EHD and in separate off-site experiments with low intensity UV light or ultrasonic exposure suggested that UV light inactivation is dominant over all other factors in the EHD (*2*).

Several attempts have been made by our group to study the direct effect of the high intensity UV emission in EHD reactors such as using opaque membranes or metal shields to block the UV emission, or adding small neutral density spheres or chemicals that attenuate light. However, due to the large currents (90 kAmps) that flow through our chamber and the potential damage induced by the original shockwave, we chose to use a soluble ultraviolet stabilizer as molecular screens.

The use of chemical sunscreens to mitigate UV effects is widespread in cosmetics and coatings. Many organisms are known to produce substances that absorb UV light such as carotenoids, flavonoids, scytonemin, mycosporine-like amino acids (MAAs), and melanin as a protection mechanism to lethal UV-radiation (*3*). Most of them are either specific (MAAs), unavailable commercially or insoluble in water as is the case with the carotenoids. The cosmetics and plastics industries use a wide variety of phenolic and non-phenolic compounds such as benzophenones, benzotriazoles, oxanilides, cyanoacrylates, and malonates to stabilize make-up mixtures and prevent polymer photodegradation (*4*). Of these examples, benzophenones (*5*) are the most stable and non-toxic compounds for our applications.

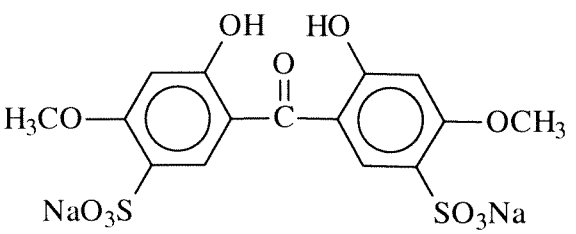

Benzophenone-9

2,2'-dihydroxy-4,4'-dimethoxybenzophenone-5,5'-disulfonic acid (BP9) is an o-hydroxybenzophenone with two sulfonic salt groups to facilitate dissolution. The calibration of UV absorption with initial concentration of BP9 sunscreen is linear over the range from 0 to 100 mg/L BP9 (*6*), and exposure of *E. coli* to 100 mg/L BP9 over a 42-hour period showed no decrease in viability; hence, various degrees of UV absorption can be achieved inside the reactor chamber by varying the initial concentrations of BP9.

The study that follows is a description of the findings regarding the role of UV emission in *E. coli* disinfection by electrohydraulic discharge reactors enabled by the use of BP9 sunscreen.

High-intensity UV Irradiation

Stepwise multiphoton absorption at UV light intensities higher than 10^6 W/cm^2 generated by picosecond and nanosecond laser irradiation produce nonlinear photoprocesses in nucleic acids (*7-9*). In our experiments the EHD reaches intensities as high as 3 x 10^6 W/cm^2, which leads us clear into the multiphotonic photochemistry regime.

In low-intensity, UV irradiation of nucleic acids, absorption to the first excited singlet and triplet states (S_1 and T_1 respectively) leads to formation of C_5-C_6 cyclobutyl dimers between neighboring pyridines weakening and distorting DNA strands, ultimately blocking DNA replication.

Non-conventional high-lying quasi-Rydberg S_N and T_N state photochemistries in thymine can occur at high intensity UV irradiation due to two photon absorption processes that lead to the formation of DNA-base radicals, ejection of a hydrated electron e_{aq}^-, or direct ionization (*10-12*). Oxidative damage incurred by the subsequent reactions between these highly energetic moeties and cellular material produces DNA single and double strand breaks (*7,13-15*).

The inactivation process displays similar kinetics to disinfection by pulsed radiolysis and ionizing radiation (*16,17*) and additional pathways of action have been

verified, i.e., formation of single and double strand DNA breaks (ssb, dsb), interstrand crosslinking, and protection by the cytoplasm (*13,15,18*).

Experimental Methods

The Pulsed Power Plasma Reactor System

The Caltech electrohydraulic discharge (EHD) reactor consists of two electrodes submerged in a 4-liter reaction vessel to which a 135 μF capacitor bank is discharged across the spark gap (*19-21*). A 300 ns rise time semiconductor switch is used to trigger the discharge and it is capable of generating a 20 μs pulse with a total energy of 25 kJ and 1 GW peak power. Figure 1 (Chapter 1) shows a schematic of the EHD reactor.

Under normal experimental conditions, measurements of the voltage across the electrodes can be as high as 5 kV with peak currents of 90 kA. The system is electrically analogous to an underdamped LRC circuit with a period of 50 μs. Following the rapid discharge of the capacitor bank, a fraction of the current leaks into the spark gap and heats the water surrounding the electrodes forming gas bubbles. These bubbles enable the formation of a plasma channel across the liquid medium. The plasma channel can reach temperatures in the range of 14 000 - 50 000 K and functions as a blackbody radiation source with a maximum emittance in the VUV spectrum (λ = 75 - 185 nm). The plasma channel consists of a highly ionized, high-pressure and high-temperature fluid. Once formed, the plasma channel tends to expand. The mechanical inertia of the surrounding water resists this expansion resulting in the development of very high pressures. The energy stored in the plasma channel is slowly dissipated (slow relative to the plasma formation process) as thermal radiation and mechanical work. At the detonation front, the high-pressure build up in the plasma is transmitted into the water interface and an intense compression wave (shock wave) is formed that travels ahead of the expanding gas bubble

at a speed several times faster than the speed of sound. Pressure jumps across the shock can be as high as ~ 5-20 kbars. When the shock wave reaches a free surface, the stress-free condition at the interface instantly transforms the compression wave into a tension (or rarefaction) wave and it is reflected back into the liquid medium. This rarefaction wave induces cavitation as it travels back through the water. The shock waves, rarefaction waves, and gas bubble expansion sustain a highly turbulent mixing environment until all pressures are equalized.

In a typical experiment, a 135 μF capacitor bank storing E_{CB} = 7 kJ at V_{CB} = 10.2 kV is discharged through a 4 mm electrode gap into 3.0 L of a 0.01 M phosphate-buffered (pH = 7.4) saline (PBS) solution within 40 μs. The peak current of these pulses is ~ 90 kA. The buffered PBS solution functions as a proper electrical conductive medium for the discharge to flow across the immersed electrodes, and provides a medium in which suspended *E. coli* communities remain in stasis. Upon charging the electrodes, local ohmic heating creates vapor microbubbles within the gap through which the EHD's occur. The energy utilized for vaporization is estimated at 5 kJ/pulse and the energy effectively delivered per pulse is about E_{PC} = 2 kJ.

We tested mixing conditions in the reactor during and between pulses by following the dispersal of small volumes of colored solutions (1 mL 0.01 M MnO_4K) injected in the gap region. Without pulsing, the colored solute is slowly homogenized by diffusion/convection throughout the reactor in about 2 hours. In contrast, a single pulse suffices to produce a uniformly colored solution. Assuming that in the latter case mixing is driven by pressure waves generated by the discharge, that these waves travel at the

speed of sound (1500 m/s), and that they travel back and forth across the reactor 10 times before dissipating, we estimate that mixing takes about 0.6 ms. Since the shortest time interval between consecutive discharges is 10 seconds, the reaction chamber can be assumed to be thoroughly mixed before each discharge. At typical pulse repetition and sampling rates, a 50 consecutive discharge experiment amounts to 2 ms plasma exposure time, but takes 1 hour to complete.

Bacterial Cultures and Procedures

Escherichia coli type-strain ATCC 25922 was used throughout the experiment. Stock cultures were maintained on LB agar slants in the dark at 5°C, and at -20°C in LB broth with 60 % glycerol added as cryoprotectant. Prior to each experiment, *E. coli* stock was inoculated into sterilized LB broth (1 % tryptone, 0.5 % yeast extract, and 1 % salt), and grown in the dark for 12 hours at 37°C, while shaken at 225 rpm. Cells from the exponential growth-phase were separated by centrifugation, washed once and resuspended in 0.01 M PBS (10X: 24.72 g Na_2HPO_4, 3.60 g $NaH_2PO_4 \cdot H_2O$, 170.0 g NaCl, pH = 7.4). Resuspended samples were appropriately diluted, then equilibrated in corresponding reactors for 5 min, and finally sterilized by EHD treatment. Sample aliquots, drawn at regular intervals, were held for less than 1 hour at room temperature, prior to incubation and counting.

Heterotrophic plate counts were performed to quantify the culturable bacteria present in each sample using Standard Method 9215C (*22*). The samples taken at known intervals during an EHD experiment were thoroughly mixed and diluted in sterile 0.01 M

phosphate-buffered saline (PBS), and 0.1 mL of appropriate dilutions were spread onto LB agar plates. The plates were counted following 12-15 hours incubation in the dark at 37 °C.

Benzophenone-9

Sunscreen *2,2'-dihydroxy-4,4'-dimethoxybenzophenone-5,5'-disulfonic acid* (BP9) was obtained from BASF Corp. under the trade name UVINUL DS-49 SG1. Stock solutions of Benzophenone-9 were prepared with MilliQ UVplus water at concentrations of 50 g/L BP9 and stored in dark containers kept constant at 5 °C. During an experiment, appropriate amounts of sunscreen solutions were added to the reactor to yield final concentrations ranging from 1 to 100 mg/L BP9.

We tested the degree of sensitivity of *E. coli* to BP9 sunscreen, by exposing concentrations of 3 x 10^9 CFU/mL to 5 g/L BP9 (50 times the maximum sunscreen concentration used throughout the experiment) for over 42 hours in 0.01 M PBS with no LB medium. The lack of change in viability observed during this induction period is an indication that *E. coli* is not sensitive to BP9.

Statistical Analyses

Plotted data that have error bars associated with them are shown as the mean ± the largest variance of triplicate samples. The relationships between the sunscreen concentrations and inactivation percentages by the electrohydraulic discharge process were determined using SigmaPlot (version 5.0) and Microsoft Excel (version 5.0). Data

used for the slopes of the rectified disinfection curves were computed by transforming the abscissa into logarithmic base 10 units and the ordinate into log*it* units using the mapping,

$$\log it(y_i) = \log_{10}\left(\frac{y_i}{100 - y_i}\right) \qquad (1)$$

The resulting linearized data sets were analyzed using SigmaPlot by the least-squares fit method of linear regression with associated standard errors for both y-intercepts and slopes. The relationships between the sunscreen concentrations and the slopes of each inactivation curve were then obtained from the regression analysis via the appropriate inverse transformations.

The values of lethal dosages for 50 % viability reduction, denoted by LD_{50}, were obtained by setting P_n to 0.5 and solving Eqn. 2 for n given y_o and m for each sunscreen concentration.

Results and Discussion

Dose-response Curves

Figure 2 shows the total viable *E. coli* concentration, expressed as CFU/mL for seven different concentrations of sunscreen BP9 (i.e., 0, 1, 5, 20, 40, 60, 100 mg/L respectively). For each case, the inoculated cultures were treated by 50 consecutive electrohydraulic discharges (EHDs) at 7 kJ/discharge, 25 °C, pH 7.4 and electrode gap length of 0.4 cm. The expression:

$$\log\left(\frac{P_n}{100-P_n}\right) = y_o - \frac{m}{2.303}\log n \qquad (2)$$

was used to fit all the data, where $P_n = 100 \times CFU_n/CFU_{o*}$ is the percentual survival probability, n is the number of electrohydraulic discharges, and y_o and m are regression constants. CFU_{o*} is a constant that normalizes the data and adjusts the values of P_n so that they fall in the range $0 \leq P_n \leq 100$. The relation between n and P_n is non-linear; however, if they are expressed in the form described by Eqn. 2, all the curves can be rectified accordingly. Table 1 summarizes the constants for each sunscreen concentration.

A general monotonic increase in the slopes of the rectified data is observed as the substrate concentration increases with a corresponding increase in the LD_{50}, suggesting that the viability of the microbes is directly dependent on the EHD emission of UV radiation. At 100 mg/L BP9, the extent of the UV absorbed by the sunscreen is total, no decrease in viability is observed in the reactor after 50 consecutive discharges. Furthermore, this behavior is an indication that mechanical damage and hydroxyl radical

attack, even though present in the process (*2*), do not contribute in a manner that is substantial to the decrease in the total viability observed.

The slopes of the rectified curves are most sensitive in the lower range of sunscreen concentrations, BP9 < 20mg/L, where a small perturbation in the substrate yields a significant change on the rates of disinfection. Beyond 20mg/L BP9, the slopes are grouped closely together and nearly horizontal, and the substrate effect on the slopes is barely noticeable.

The variance of the viability at 60 mg/L was very large so the data was not used in the calculations. At 100 mg/L, the slope is nearly horizontal, so in computing the inverse of the slopes, the propagation of error is significantly magnified; however, the variance is acceptable.

Figure 3 plots the dependent sunscreen concentration variable, versus the slope of the rectified disinfection curves. The solid line represents the results of our single photon model fit to the data as described below.

Modeling the Experiments

We will assume that our reactor can be analyzed as a sphere of R_{max} = 8.95 cm, corresponding to a total volume of 3000 cm^3, and that the electrical discharges across the electrode gap at its center effectively deliver about 2 kJ within 40 μs. This corresponds 50 MW released by a spherical hot spot of $A = 4\pi R_0^2 = 0.5$ cm^2 (R_0 = 0.2 cm, corresponds to half the electrode gap), i.e., to a energy flux of $J = 9.95 \times 10^{11}$ W m^{-2}. If

we assume that the emittance of the radiating volume is about 0.8, Stefan-Boltzmann's equation:

$$J=\sigma T^4 \qquad (3)$$

with $\sigma = 5.67 \times 10^{-8}$ W m^{-2} K^{-4}, leads to estimated temperatures of about T = 50 kK, in good accord with previous estimates (*23,24*). The radiation emitted by the discharge at λ < 180 nm is absorbed in a few mm by water and, therefore, does not propagate into the reactor, whereas that at λ > 300 nm is deemed to be inactive towards DNA damage. The fraction of actinic radiation flux can be calculated by integration of Planck's spectral distribution function for a blackbody at 50 000 K:

$$J_{\text{actinic}} = \frac{8\pi hc \int_{180nm}^{300nm} \frac{d\lambda}{\lambda^5[\exp(hc/\lambda kT)-1]}}{\sigma T^4} = 0.033 \qquad (4)$$

or $J_{actinic}$ = 3.3 MW cm^{-2} = 3.8×10^{24} photons (λ = 230 nm) cm^{-2} s^{-1}, which amounts to the emission of about 0.26 mEinsteins per pulse. If ε_λ (CFU^{-1} cm^2) and β_λ (L mg^{-1} cm^{-1}) are the spectral extinction coefficients of *E. coli* suspensions, and sunscreen solutions, respectively, and γ_λ is the spectral actinic efficiency for the induction of thymine dimers normalized to $\gamma_{180\,nm} = 1$, then the actinic radiation at λ absorbed by the *E. coli* population per unit volume per s within a spherical shell of thickness dR at a distance R from the discharge is given by:

$$I_{\lambda,R} = J_{\lambda,R_0}\left(\frac{R_0}{R}\right)^2 e^{-(\varepsilon_\lambda[\text{E.coli}]+\beta_\lambda[\text{SS}])R}\varepsilon_\lambda[\text{E.coli}]\gamma_\lambda 4\pi R^2 dR \qquad (5)$$

which upon integration over $\{R_0 \sim 0, R_{max}\}$ and summation over λ yields:

$$I = A \sum_{180nm}^{300nm} J_{\lambda R_0} \varepsilon_\lambda [E.coli] \gamma_\lambda \frac{1 - e^{-(\varepsilon_\lambda [E.coli] + \beta_\lambda [SS]) R_{max}}}{\varepsilon_\lambda [E.coli] + \beta_\lambda [SS]} \quad (6)$$

where [E.coli] and [SS] denote the concentrations of bacteria and sunscreen, respectively. A is a normalization factor that is obtained by identifying the sterilization slope in the absence of sunscreen with I ([SS] = 0). Application of Eqn. 6 to the dataset of Table 1 and using the measured spectral data (blackbody, *E. coli* and sunscreen) in Fig. 4 lead to the calculated slopes as function of sunscreen concentration shown in Fig. 3. This satisfactory agreement with experimental results supports the present analysis of the sterilization process by electrohydraulic discharges.

Discussion

A conservative estimate of the lethal fluence can be obtained from the photon flux = 3.3 MW cm^{-2} = 3.83 × 10^{24} photons cm^{-2} s^{-1} (λ = 230 nm) computed in the previous chapter, multiplied by the absorption cross-section of the cells. If we assume that in the biphotonic process occurring at high UV intensities, a second photon is always absorbed after the first one (*25*), the average absorption cross-section of the cells from 180 to 300 nm can be computed as the blackbody spectrum (ϕ_λ) weighted average:

$$\langle \sigma_{cell} \rangle = \frac{\int_{180}^{300} \phi_\lambda \varepsilon_\lambda d\lambda}{\int_{180}^{300} \phi_\lambda d\lambda} = 1.30 \text{ x } 10^{-9} \text{ cm}^2 \text{ CFU}^{-1} \quad (7)$$

Therefore, each cell absorbs 3.83 x 10^{24} photons cm^{-2} s^{-1} × $\langle \sigma_{cell} \rangle$ = 5.0 x 10^{15} photons CFU^{-1} s^{-1}, i.e., a photon is available every 0.2 femtoseconds. The lethal dose is computed as the lethal fluence attained within the time of exposure required to reach LD_{50}, i.e., 2.5 EHDs × 40 μs per EHD = 100 μs. Hence, cells see on average 5.0 x 10^{15} photons CFU^{-1} s^{-1} × 10^{-4} s = 5.0 x 10^{11} photons CFU^{-1} to reach LD_{50} = 2.5 EHDs.

For DNA bases, photon fluences higher than 3 x 10^{17} photons cm^{-2}, two-quantum events, in which virtually all T_1 absorb a second photon and are promoted to T_N, occur with unitary probability (*12,26*). Thus, the assumption invoked in Eqn. 7 above holds true since the computed value of UV intensity (3.83 x 10^{20} photons cm^{-2} per pulse) exceeds the threshold fluence.

In contrast, continuous exposure to 254 nm, 15W germicidal lamps, the photon flux 4.5 mW cm^{-2} = 5.75 x 10^{15} photons cm^{-2} s^{-1} (λ = 254 nm) multiplied by the absorption cross-section at 254 nm σ_{cell} = 1.13 x 10^{-9} cm^2 CFU^{-1} leads to 6.5 x 10^6 photons CFU^{-1} s^{-1}, i.e., a photon is available to a cell every 150 nanoseconds. Using the average time to reach LD_{50} = 102 s (or 1.7 min at 7 x 10^7 CFU mL^{-1}) gives a lethal dose of 6.6 x 10^8 photons CFU^{-1}, λ = 254 nm that cells see on average to reach 50% inactivation.

Comparing the light fluences between the high and low intensity experiments (5.0 x 10^{11} photons CFU^{-1} vs. 6.6 x 10^8 photons CFU^{-1} respectively) gives an indication of the relative efficiencies of both processes. At high intensity UV exposure (EHD), the cells require 3-orders of magnitude more photons to reach the same level of disinfection as the low intensity case. The net availability of more photons during high intensity UV

exposure suggests the possibility of a different disinfection mechanism at play relative to the low intensity case.

The lifetime of the lowest singlet excited state S_1 is 1–10 ps and the lowest triplet excited state T_1 is 1 μs respectively (*17,26*). Current calculations showed that on average, one photon is available every 0.2 fs during high intensity UV irradiation while one photon is available every 150 ns for low intensity UV exposure. In the latter case, the photochemistry of both singlet and triplet states is a single-quantum process as the pumping is not fast enough to allow for a second photon to be absorbed. Biphotonic events in the high intensity case can result by promotion to high-lying, quasi-Rydberg states from both $S_1 \rightarrow S_N$ and $T_1 \rightarrow T_N$. The energy deposited exceeds the ionization energy of DNA bases, leading to ionization and production of single DNA base photoproducts (*11*).

A decrease in the formation of thymidine dimers ensues as the S_1 and T_1 states are depleted by the absorption of a second photon (*26*). At intensities higher than 10^6 W cm^{-2}, the *uvr* and *rec* cell repair systems are also observed to have a decrease in activity (*27*) and a corresponding increase in single strand break and double strand break is usually observed (*13-15*).

It is clear that in the case of high intensity UV irradiation, the mechanism of disinfection is irreversible (via DNA ssb and dsb) so cells that do not survive the EHD process are in fact dead. Under low intensity UV irradiation, formation of DNA bipirimidines stops DNA replication engaging their repair mechanisms and cells remain viable until the system is either overwhelmed or the repair mechanism itself has been

damaged. However, a more detailed study needs to be performed to verify this conjecture.

Conclusions

High intensity UV emission is the principal disinfection mechanism in the EHD process. The use of BP9 sunscreen provided a mechanism to vary the intensity of UV emission and measure the amount of non-radiative viability in the reactor. In the absence of the UV component of disinfection, the dose-response curve was nearly horizontal, suggesting that other mechanisms like mechanical rupture and oxidative attack is minimal relative to the amount of high intensity UV damage. Empiric modeling of the disinfection process (Eqn. 6) accounted for the blackbody spectrum of the plasma, the absorption spectrum of water, *E. coli* and the sunscreen, as well as the Beer's law effect in a spherically symmetric frame and gave a satisfactory agreement with experimental data.

The discussions on high intensity UV inactivation indicate that the mechanism of disinfection is more akin to two-photon absorption processes in DNA pyridines that account for the lethal fluence and lethal dose difference between UV irradiation in EHD reactors and the previously investigated low intensity UV irradiation.

References Cited

(1) Ching, W.-K.; Sun, H. J.; Nealson, K. H.; Hoffmann, M. R. *Proceedings of the 1999 American Society for Microbiology*, Chicago, IL, 1999.

(2) Ching, W.-K.; Colussi, A. J.; Sun, H. J.; Nealson, K. H.; Hoffmann, M. R. *Environ. Sci. Technol.*, submitted for publication, 2001.

(3) Cockell, C. S.; Knowland, J. *Biol. Rev.* **1999**, *74*, 311.

(4) Kroschwitz, J. I. *Kirk-Othmer Encyclopedia of Chemical Technology*; 4th ed.; Kroschwitz, J. I., Ed.; Wiley: New York, 1991; Vol 17, pp 726.

(5) Kroschwitz, J. I. *Kirk-Othmer Encyclopedia of Chemical Technology*; 4th ed.; Kroschwitz, J. I., Ed.; Wiley: New York, 1991; Vol 7, pp 598.

(6) Ching, W.-K. , California Institute of Technology, Pasadena, CA. Unpublished work, 2000.

(7) Gorner, H. *J. Photochem. Photobiol. B: Biology* **1994**, *26*, 117.

(8) Nikogosyan, D. N.; Letokhov, V. S. *Riv. Nuovo Cimento* **1983**, *6*, 1.

(9) Nikogosyan, D. N.; Angelov, D. A.; Oraevsky, A. A. *Photochem. Photobiol.* **1982**, *35*, 627.

(10) Goez, M.; Zubarev, V. *Chem. Phys.* **2000**, *256*, 107.

(11) Reuther, A.; Nikogosyan, D. N.; Laubereau, A. *J. Phys. Chem.* **1996**, *100*, 5570.

(12) Oraevsky, A. A.; Nikogosyan, D. N. *Chem. Phys.* **1985**, *100*, 429.

(13) Schulte-Frohlinde, D.; Simic, M. G.; Gorner, H. *Photochem. Photobiol.* **1990**, *52*, 1137.

(14) Bothe, E.; Gorner, H.; Opitz, J.; Schulte-Frohlinde, D.; Siddiqi, A.; Malgorzata, W. *Photochem. Photobiol.* **1990**, *52*, 949.

(15) Masnyk, T. W.; Minton, K. W. *Photochem. Photobiol.* **1991**, *54*, 99.

(16) Schulte-Frohlinde, D.; Bothe, E. *Pulse radiolysis of nucleic acids in aqueous solutions*; CRC Press: Boca Raton, FL, 1991.

(17) Angelov, D.; Berger, M.; Cadet, J.; Getoff, N.; Keskinova, E.; Solar, S. *Radiat. Phys. Chem.* **1991**, *37*, 717.

(18) Kochevar, I. E.; Walsh, A. A.; Green, H. A.; Sherwood, M.; Shih, A. G.; Sutherland, B. M. *Cancer Res.* **1991**, *51*, 288.

(19) Willberg, D. M.; Lang, P. S.; Hochemer, R. H.; Kratel, A.; Hoffmann, M. R. *Environ. Sci. Technol.* **1996**, *30*, 2526.

(20) Willberg, D. M.; Lang, P. S.; Hochemer, R. H.; Kratel, A.; Hoffmann, M. R. *Chemtech* **1996**, *26(4)*, 53.

(21) Lang, P. S.; Ching, W.-K.; Willberg, D. M.; Hoffmann, M. R. *Environ. Sci. Technol.* **1998**, *32*, 3142.

(22 Clesceri, L. S.; Greenberg, A. E.; Trussell, R. R. *Standard Methods for the Examination of Water and Wastewater*; 17th ed.; Clesceri, L. S.; Greenberg, A. E.; Trussell, R. R., Ed.; APHA, AWWA, and WPCF: Washington, D.C., 1989.

(23) Kratel, A. W. H. "Pulsed Power Discharges in Water," Ph.D. Thesis, California Institute of Technology, 1996.

(24) Robinson, J. W.; Ham, M.; Balaster, A. N. *J. Appl. Phys.* **1973**, *44*, 72.

(25) Angelov, D.; Spassky, A.; Berger, M.; Cadet, J. *J. Am. Chem. Soc.* **1997**, *119*, 11373.

(26) Masnyk, T. W.; Nguyen, H. T.; Minton, K. W. *J. Biol. Chem.* **1989**, *264*, 2482.

(27) Nikogosyan, D. N.; Oraevsky, A. A.; Zavilgelsky, G. B. *Photobiochem. Photobiophys.* **1986**, *10*, 189.

BP9 [mg/L]	Co [10^6 CFU/mL]	y-intercept	m/2.303 (r^2)	2.303/m	LD_{50} [EHD]
0	26.75 ± 0.45	1.90 ± 0.31	-2.04 ± 0.11 (r^2 = 0.970)	-0.49 ± 0.03	2.53
1	18.96 ± 2.14	0.76 ± 0.36	-1.53 ± 0.11 (r^2 = 0.985)	-0.66 ± 0.05	1.65
5	22.0 ± 0.60	2.09 ± 0.26	-1.46 ± 0.08 (r^2 = 0.992)	-0.68 ± 0.04	4.16
20	19.0	3.17 ± 0.43	-1.02 ± 0.13 (r^2 = 0.953)	-0.98 ± 0.13	22.49
40	20.40 ± 1.60	4.05 ± 0.86	-1.05 ± 0.26 (r^2 = 0.843)	-0.95 ± 0.24	47.78
60	24.70 ± 13.30	5.73 ± 0.90	-1.47 ± 0.27 (r^2 = 0.906)	-	49.9
100	48.0 ± 1.0	0.17 ± 0.20	-0.12 ± 0.07 (r^2 = 0.228)	-	-

Table 1. Initial conditions and regression results of rectified dose-response curves for *Escherichia coli* disinfection by 50 consecutive EHDs with varying concentrations of added BP9 sunscreen. E_{CB} = 7 kJ, spark gap = 4 mm, pH = 7.4, and pulse rate = 0.1 Hz.

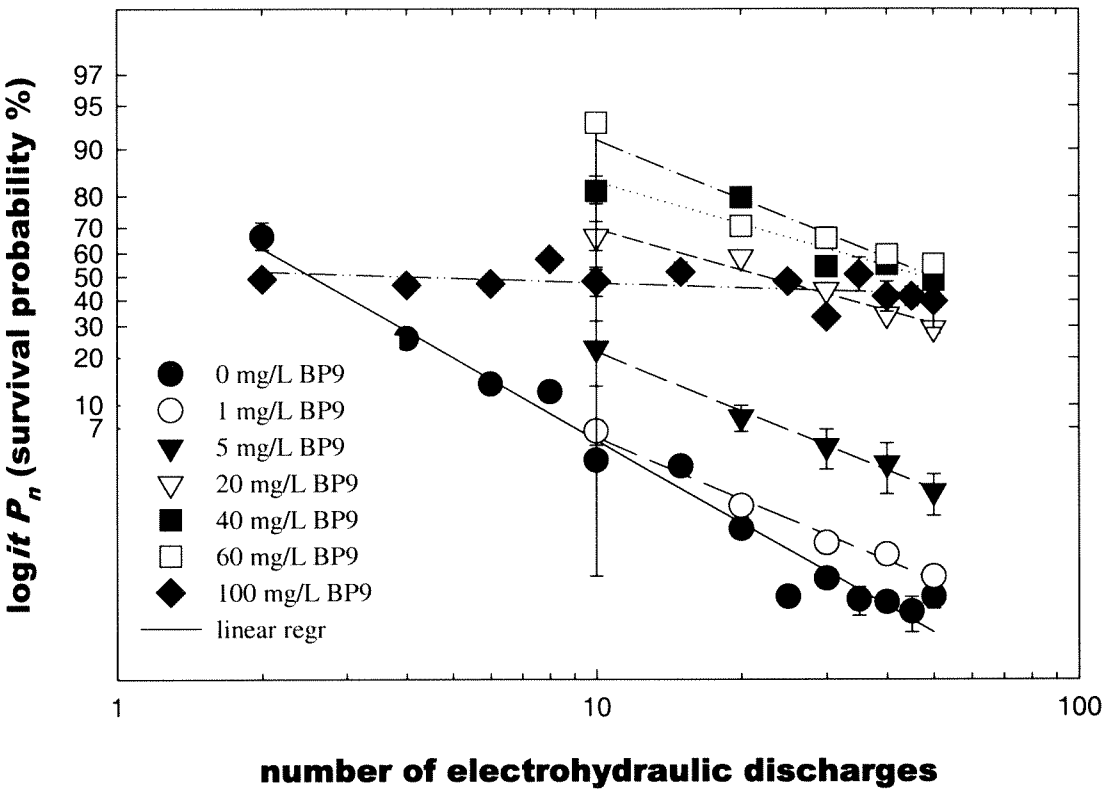

Figure 2. Total viable *E. coli* concentration, expressed as % viability at seven different concentrations of sunscreen BP9 added (0, 1, 5, 20, 40, 60, 100 mg/L). Each case was subject to 50 consecutive electrohydraulic discharges. Discharges are characterized by E_{CB} = 7 kJ, spark gap = 4 mm, and pulse rate = 0.1 Hz.

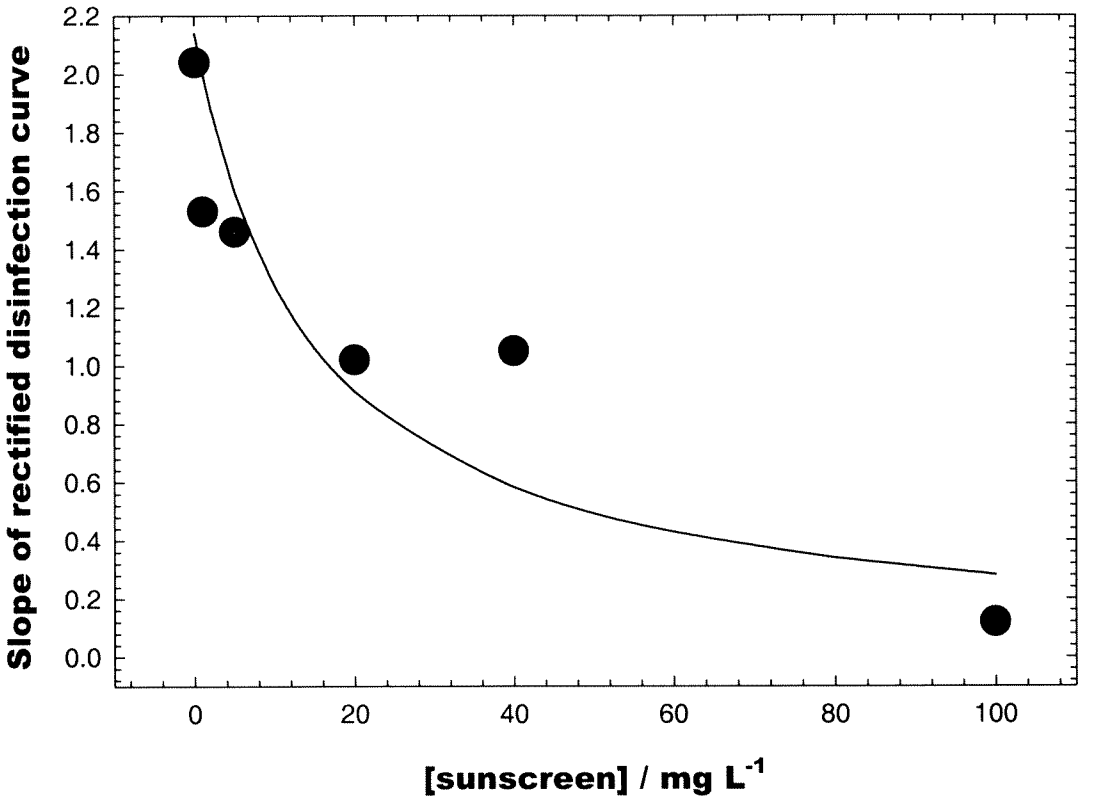

Figure 3. BP9 sunscreen concentration dependence on slope of rectified disinfection curve. Solid line represents single-photon model fit to data (Equation 6).

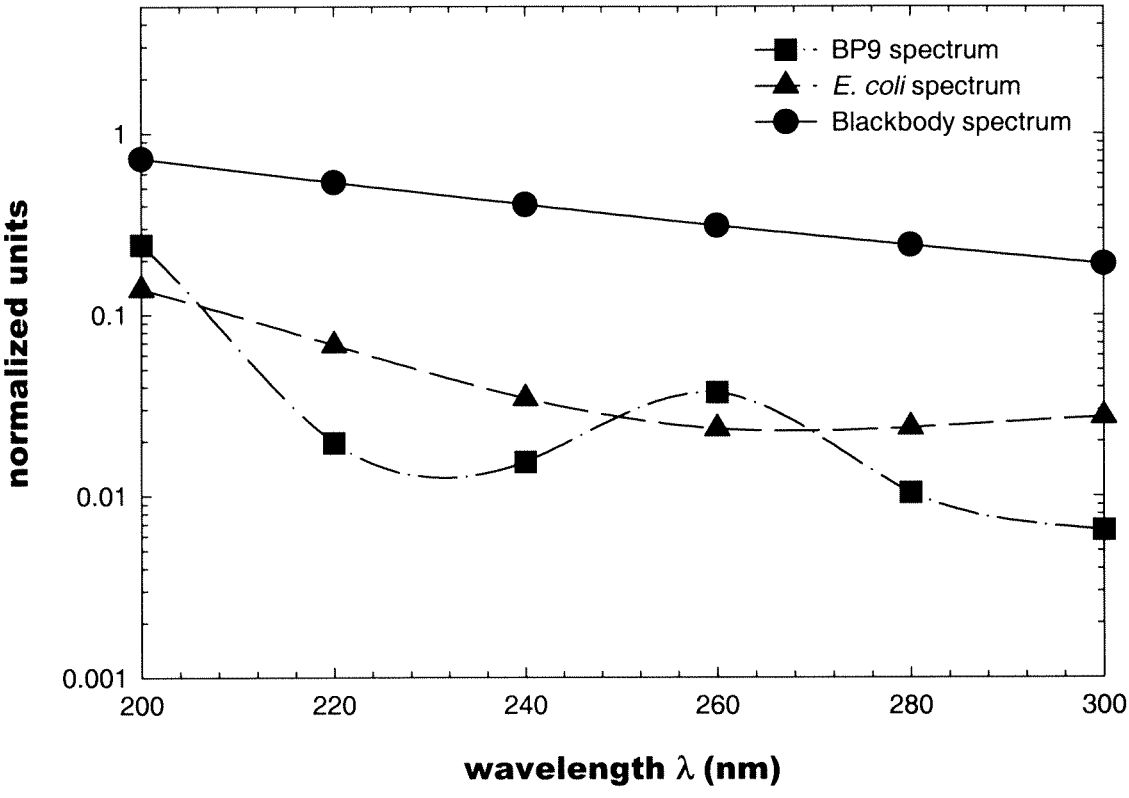

Figure 4. Normalized spectrum of 50 000 K blackbody (solid circles) at λ_{max} = 100 nm. Measured absorbance of *E. coli* (solid triangles) $\varepsilon_{254\ nm}$ = 1.13 x 10^9 mL CFU^{-1} cm^{-1}, and BP9 sunscreen (solid squares) $\langle\varepsilon\rangle_{180\text{-}300}$ = 0.06 L mg^{-1} cm^{-1}.

Chapter V

EHD Selective Pressure Experiments

Chapter V. EHD Selective Pressure Experiments

Introduction

Bacteria develop mechanisms of resistance in response to selective pressures from their environment. Known pathways of resistance have been heavily investigated in the past based on single modes of action such as antibiotic (*1-4*) and chemical inhibition (*5-9*), UV and radiation damage to cell material (*10-16*), thermal destruction (*17*), mechanical rupture (*18,19*), and oxidative attack (*20-25*). Only recently has there been an interest in studying combinatorial modes of resistance that has led to studies in combinatorial genetics and gene shuffling (*26-28*).

In the case of pulsed-power disinfection of *E. coli*, the three main modes of action are high intensity UV light damage, mechanical rupture of the cellular membrane, and hydroxyl radical attack. Low intensity UV light absorption leads to thymidine dimerization with four main mechanisms of repair, (i.e., photoreactivation, excision, recombination, and SOS systems) and resistant strains with gene deletions in *phr*, *polA*, *uvrABC*, *recABC*, and *umuDC* or combinations of them are well known. Very little is known in regards to resistance to mechanical rupture whereas resistance to oxidative damage has been observed in experiments involving hydrogen peroxide treatment (*22*), ozone sparging (*24*), and indirect ultrasonic cavitation (*25*). However, the study of resistance to the combination of all three mechanisms has not yet been done.

To resolve the overall behavior of the disinfection kinetics in electrohydraulic discharge treatments, a culture sample of *Escherichia coli* ATCC 25922 was subjected to

at 11 continuous cycles of growth and death under the same EHD conditions (E_{CB} = 7 kJ, pH = 7.0, gap length = 4 mm) in order to detect mutations of the initial culture.

Selective pressure experiments in the EHD reactor consisted of subjecting a sample of *E. coli* to repeated cycles of 50 consecutive discharges each that lowered the viability to 10 % of the initial value. At the end of each cycle, the cells were grown overnight until the initial viability was reached to start a new cycle. The pulsed nature of the discharge process, and the rapid decrease in viability, did not allow for constant selective pressure to be applied throughout the experiment. This partial EHD selective pressure also selected for the fastest and aggressively growing mutants as slow growing strains may be out competed during the quiescent growth periods without EHD.

Method of Approach

A sterile 100 mL flask with liquid LB medium was inoculated with frozen *Escherichia coli* ATCC 25922 and grown at 37 °C overnight in the dark, shaken at 225 rpm. The fully grown *E. coli* culture was centrifuged, washed and resuspended in 0.01M PBS solution and added to 3 L of 0.01M PBS in the EHD chamber to reach a final concentration of $\sim 10^7$ CFU/mL. The cell suspensions were then treated to 50 consecutive electrohydraulic discharges (EHDs) with E_{CB} = 7 kJ/pulse, at pH = 7.0 and spark gap = 4 mm. At the end of each EHD treatment, 1 mL of treated culture is used to inoculate a 100 mL flask of sterile liquid LB medium and grown overnight under the same growth conditions. The treatment process is repeated on the fully grown suspension until a total of at least 10 treatment cycles of 50 discharges each have been subjected to growth and death. During select cycles, aliquot samples were taken at intervals of 0, 10, 30, and 50 EHDs to obtain the dose-response curve from which values of LD_{50} could be obtained. Each sample in turn was diluted, plated in LB-agar solid medium, incubated overnight at 37 °C and counted accordingly.

GN2 Microplate™ Assay

Metabolic fingerprinting tests were performed on *E. coli* samples at 0, 4, 8, and 11 cycles to monitor changes in biochemistry and possibly detect propagation of other bacterial contamination. GN2 MicroPlate™ (Biolog, Hayward, CA) panels with 95 different carbon sources were inoculated with 150 µL *E. coli* samples at each given cycle

and assayed colorimetrically at 490 nm. Table 1 gives a detailed description of each carbon source and its corresponding position on the panel array.

Results and Discussion

Figure 1 shows the dose-response curves of *E. coli* after 0, 6, and 11 cycles of 50 consecutive EHDs each. After 11 cycles, the sample culture has been subjected to a total of 550 consecutive discharges which amounts to a total plasma exposure time of 13.2 ms. The entire experiment lasted 13 days. All three cycles show typical disinfection kinetics with a tailing component. Figure 2 shows the same curves in rectified coordinates, i.e., log*it*(% Viability) vs. log(EHDs). Cycle 6, however, shows a large variance, reflected in the low statistical correlation coefficient $r^2 = 0.586$.

Using the rectified data, a linearized regression analysis was applied to each curve. Table 2 shows the regression results on each of the three selected cycles. An increase in the degree of UV sensitivity in the sample would effect a decrease in the slope of the dose-response curve and a corresponding decrease in the values of LD_{50}. However, the LD_{50} values as reported in Table 2 remain constant as a function of increasing number of cycles, suggesting that there is no observed increase in sensitivity and thus no apparent effect during long-term exposures to EHD.

GN2 MicroPlates™ were used to test for growth activity under 96 metabolic carbon sources as a function of increasing selective pressure. Four assays were applied to *E. coli* samples at cycles 0, 4, 8, and 11, which corresponds to 50, 200, 400, and 550 total applied EHDs respectively. Figures 3 and 4 show the resulting assays for cycles 0 and 8 after 18 hours of incubation at 37 °C. Cycles 4 and 11 were saturated with the amount of dye produced in each channel so these two cases were not used in our discussion of the results.

Colorimetric measurements on each assay were done at 490 nm, and normalized relative to channel A1 (water blank). Tables 3 - 6 show the result of each assay. All wells with $\Delta OD_{490\,nm} \geq 0.100$ were labeled positive.

Tables 3 and 5 and Figures 3 and 4 indicate that *E. coli* is present in both cases, since they have the same metabolic fingerprint. The exception was found in well G10 with L-threonine as a carbon source whereby cycle 8 showed a positive well and cycle 0 showed a negative well.

However, 94 matched pairs of a possible 95 (since A1 well contains only water) give greater than 98 % metabolic similarity between cycle 0 and cycle 8. This clearly indicates that the organism present in cycle 0 is the same as the organism present in cycle 8. Furthermore, these results found no evidence of bacterial contamination that could have been propagated through the 13-day experiment.

Mutagenicity

The lack of permanent mutagenicity shown in the constant LD_{50} values in Table 2 indicate that the overall mechanisms of repair (if present) must be error free. Masnyk et al. (*29*) indicated that thymidine dimerization is bypassed in favor of biphotonic DNA base ionization pathways during high intensity UV irradiation that leads to DNA oxidative damage (by ionized base products) and single strand breaks (ssb). In this case, the *uvr* and *rec* repair systems were found to be the main mechanisms of repair associated with DNA UV damage and ssb (*30*), both of which are known to be error free.

The possibility also exists that the induction time (less than 10 cycles) may not be enough to incite mutagenic effects during partial EHD selective pressure experiments. However, it is well known that very short time exposures (~ few seconds) using low intensity UV lamps are sufficient to incite mutagenic effects on *E. c*oli populations so 550 total EHD exposures of 50 μs each of high intensity UV irradiation seem to be more than adequate.

Conclusion

No net kinetic change in the dose-response curves was observed as a result of 11 successive cycles of 50 consecutive EHDs each. The values of LD_{50} throughout the partial selective pressure experiments remained constant during the combination of the three biocidal agents (high intensity UV, shockwave, and hydroxyl radical), suggesting a lack of a global indicator of mutagenic effect to long term exposure to the EHD process. A more detailed study needs to be conducted to assess the genetic and enzymatic changes that individual cells can sustain during this treatment.

References Cited

(1) Anderson, R. M. *Nature Medicine* **1999**, *5*, 147.

(2) Travis, J. *Science* **1994**, *264*, 360.

(3) Levy, S. B. *The Antibiotic Paradox*; Plenum Press: New York, 1992.

(4) Tomasz, A. *New England J. Med.* **1994**, *330*, 1247.

(5) Webb, R. B.; Hass, B. S. *Mutat. Res.* **1984**, *137*, 1.

(6) Bower, C. K.; Daeschel, M. A. *Int. J. Food Microbiol.* **1999**, *50*, 33.

(7) Zelibor, J. L. J.; Doughten, M. W.; Grimes, D. J.; Colwell, R. R. *Appl. Environ. Microbiol.* **1987**, *53*, 2929.

(8) Osterblad, M.; Leistevuo, J.; Leistevuo, T.; Jarvinen, H.; Pyy, L.; Tenuvuo, J.; Huovinen, P. *Antimicrob. Agents Chemother.* **1995**, *39*, 2499.

(9) Isken, S.; de Bont, J. A. *Extremophiles* **1998**, *2*, 229.

(10) Arrage, A. A.; Phelps, T. J.; Benoit, R. E.; White, D. C. *Appl. Environ. Microbiol.* **1993**, *59*, 3545.

(11) Xue, Y.; Nicholson, W. L. *Appl. Environ. Microbiol.* **1996**, *62*, 2221.

(12) Minton, K. W. *Mol. Microbiol.* **1994**, *13*, 9.

(13) Minton, K. W. *Mutat. Res.* **1996**, *363*, 1.

(14) Battista, J. R. *Annu. Rev. Microbiol.* **1997**, *51*, 203.

(15) Mattimore, V.; Battista, J. R. *J. Bacteriol.* **1996**, *178*, 633.

(16) Wang, P.; Schellhorn, H. E. *Can. J. Microbiol.* **1995**, *41*, 170.

(17) Peak, M. J.; Robb, F. T.; Peak, J. G. *J. Bacteriol.* **1995**, *177*, 6316.

(18) Sieradzki, K.; Tomasz, A. *J. Bacteriol.* **1999**, *181*, 7566.

(19) Tuomanen, E.; Markiewicz, Z.; Tomasz, A. *J. Bacteriol.* **1988**, *170*, 1373.

(20) Ishikawa, T.; Ohta, Y.; Takeda, T.; Shigeoka, S.; Nishikimi, M. *FEBS Lett.* **1998**, *426*, 221.

(21) Demple, B.; Halbrook, J. *Nature* **1983**, *304*, 466.

(22) Asad, N. R.; Asad, L. M.; Silva, A. B.; Felzenszwalb, I.; Leitao, A. C. *Acta Biochim. Pol.* **1998**, *45*, 677.

(23) Dukan, S.; Touati, D. *J. Bacteriol.* **1996**, *178*, 6145.

(24) L'Herault, P.; Chung, Y. S. *Mol. Gen. Genet.* **1984**, *197*, 472.

(25) Miller, D. L.; Thomas, R. M.; Frazier, M. E. *Ultrasound Med. Biol.* **1991**, *17*.

(26) Shapiro, J. A. *Genetica* **1992**, *86*, 99.

(27) Courvalin, P. *Res. Microbiol.* **1999**, *150*, 367.

(28) Joiner, M. C.; Lambin, P.; Marples, B. *C. R. Acad. Sci. III* **1999**, *322*, 167.

(29) Masnyk, T. W.; Nguyen, H. T.; Minton, K. W. *J. Biol. Chem.* **1989**, *264*, 2482.

(30) Nikogosyan, D. N.; Oraevsky, A. A.; Zavilgelsky, G. B. *Photobiochem. Photobiophys.* **1986**, *10*, 189.

A1 water	A2 α-cyclodextrin	A3 dextrin	A4 glycogen	A5 tween 40	A6 tween 80	A7 N-acetyl-D-galactosamine	A8 N-acetyl-D-glucosamine	A9 adonitol	A10 L-arabinose	A11 D-arabitol	A12 cellobiose
B1 i-erythritol	B2 D-fructose	B3 L-fucose	B4 D-galactose	B5 gentiobiose	B6 α-D-glucose	B7 m-inositol	B8 α-D-lactose	B9 lactulose	B10 maltose	B11 D-mannitol	B12 D-mannose
C1 D-melibiose	C2 β-methyl D-glucoside	C3 D-psicose	C4 D-raffinose	C5 L-rhamnose	C6 D-sorbitol	C7 sucrose	C8 D-trehalose	C9 turanose	C10 xylitol	C11 methyl pyruvate	C12 mono-methyl succinate
D1 acetic acid	D2 cis-aconitic acid	D3 citric acid	D4 formic acid	D5 D-galactonic acid lactone	D6 D-galacturonic acid	D7 D-gluconic acid	D8 D-glucosaminic acid	D9 D-glucuronic acid	D10 α-hydroxy butyric acid	D11 β-hydroxy butyric acid	D12 γ-hydroxy butyric acid
E1 p-hydroxy phenylacetic acid	E2 itaconic acid	E3 α-ketobutyric acid	E4 α-ketoglutaric acid	E5 α-ketovaleric acid	E6 D,L-lactic acid	E7 malonic acid	E8 propionic acid	E9 quinic acid	E10 D-saccharic acid	E11 sebacic acid	E12 succinic acid
F1 bromo succinic acid	F2 succinamic acid	F3 glucoronamide	F4 alaninamide	F5 D-alanine	F6 L-alanine	F7 L-alanyl-glycine	F8 L-asparagine	F9 L-aspartic acid	F10 L-glutamic acid	F11 glycil-L-aspartic acid	F12 glycyl-L-glutamic acid
G1 L-histidine	G2 hydroxy L-proline	G3 L-leucine	G4 L-ornithine	G5 L-phenylalanine	G6 L-proline	G7 L-pyroglutamic acid	G8 D-serine	G9 L-serine	G10 L-threonine	G11 D,L-carnitine	G12 γ-amino butyric acid
H1 urocanic acid	H2 inosine	H3 uridine	H4 thymidine	H5 phenyl ethylamine	H6 putrescine	H7 2-aminoethanol	H8 2,3-butanediol	H9 glycerol	H10 D,L-α-glycerol phosphate	H11 glucose-1-phosphate	H12 glucose-6-phosphate

Table 1. Biolog GN2 MicroPlate™ test panel. All carbon sources contain tetrazolium violet used as a redox dye for colorimetric identification at 490 nm. Each bacterial sample was suspended in GN/GP-IF medium.

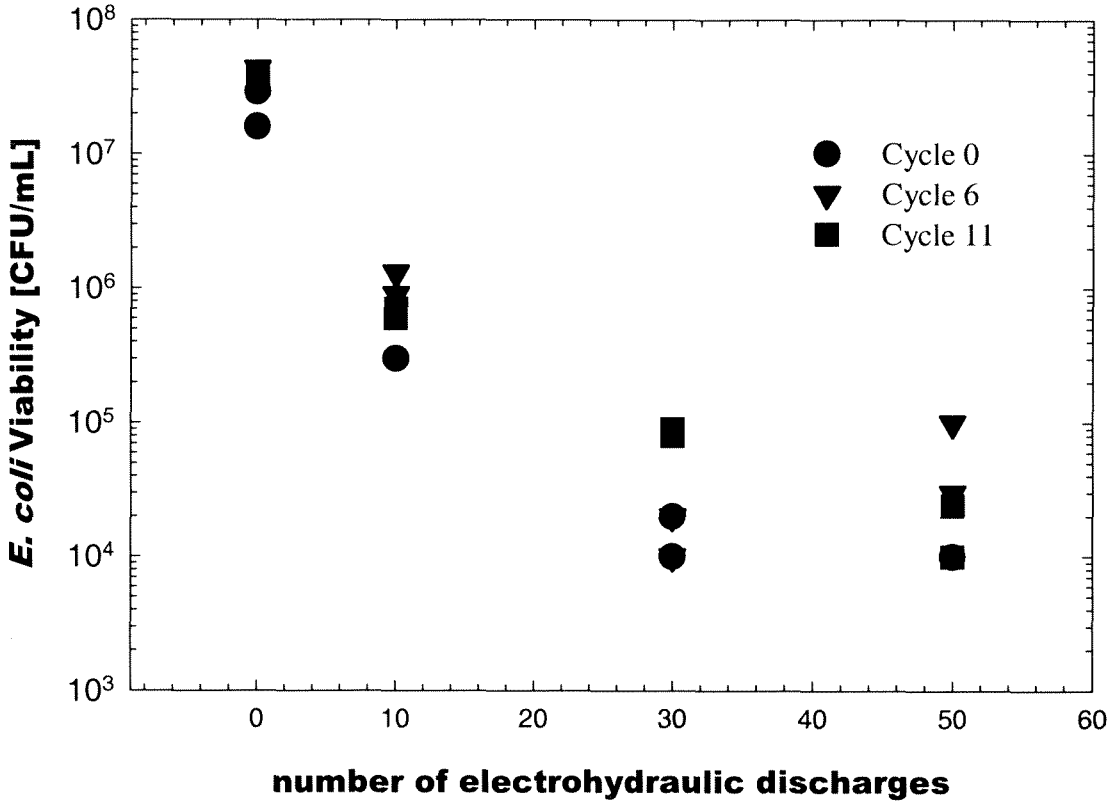

Figure 1. EHD selective pressure experiments of *E. coli* suspensions in 0.01 M PBS at pH = 7.4, subject to 50 EHDs per cycle for a total of 11 cycles. Discharges are characterized by E_{CB} = 7 kJ, spark gap = 4 mm. Cycle 0 represents the kinetics of *E. coli* subject to 50 EHDs. Cycle 6 represents the kinetics after a total of 6 cycles each of 50 EHDs (= 300 EHDs total). Cycle 11 represents the kinetics after a total of 11 cycles each of 50 EHDs (= 550 EHDs total).

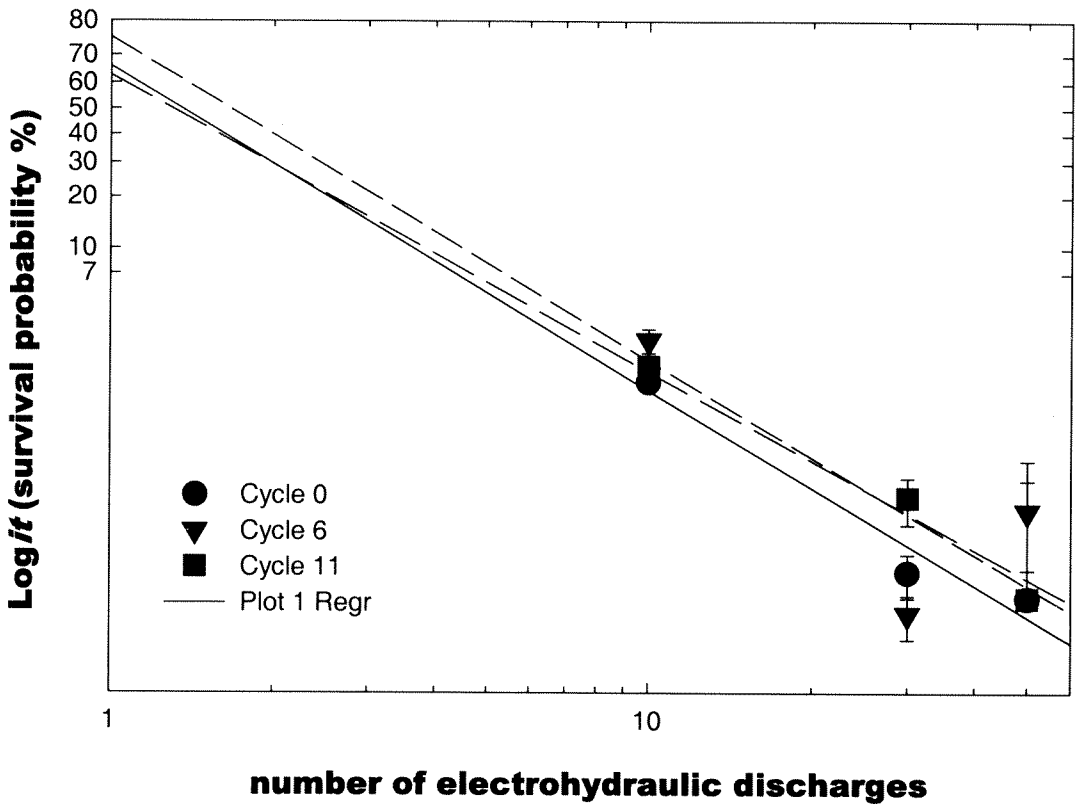

Figure 2. Rectified log*it* plot of the data in Fig. 1. Cycle 0 represents the kinetics of E. coli subject to 50 EHDs. Cycle 6 represents the kinetics after a total of 6 cycles each of 50 EHDs (= 300 EHDs total). Cycle 11 represents the kinetics after a total of 11 cycles each of 50 EHDs (= 550 EHDs total). The plotted lines are regression fits to the data.

Data 01/01/2001	Cycle 0	Cycle 6	Cycle 11
C_o [CFU/mL]	2.25E+07	4.30E+07	3.80E+07
y-intercept	0.67 ± 1.53	0.53 ± 5.59	1.13 ± 0.97
slope	-5.11 ± 1.07	-4.67 ± 3.93	-5.09 ± 0.68
r^2	0.958	0.586	0.983
LD_{50}	0.22	0.24	0.27

Table 2. Linear regression results of cycles 0, 6, and 11 of rectified data for EHD selective pressure experiments. Cycle 0 represents the kinetics of *E. coli* subject to 50 EHDs. Cycle 6 represents the kinetics after a total of 6 cycles each of 50 EHDs (= 300 EHDs total). Cycle 11 represents the kinetics after a total of 11 cycles each of 50 EHDs (= 550 EHDs total). The plotted lines are regression fits to the data.

Cycle 0 Selective Pressure Test Panel Result

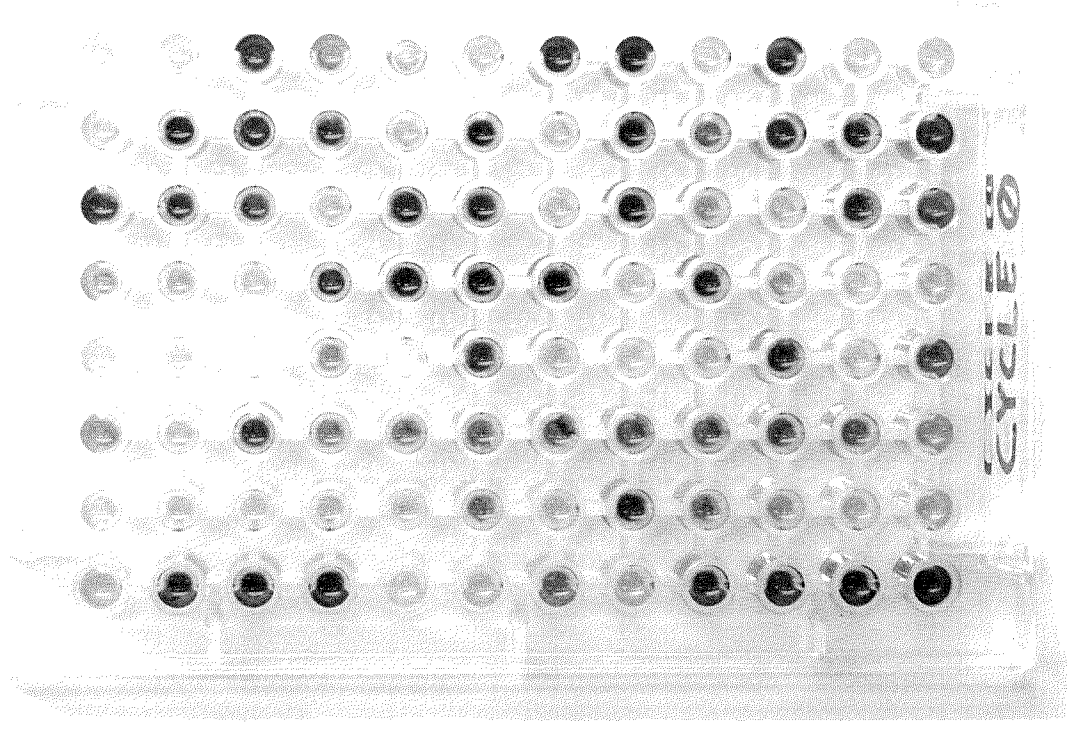

Figure 3. Image of metabolic fingerprint results for *E. coli* at cycle 0 using Biolog GN2 MicroPlate™ test panel.

Absorbance of blank slot A1 = 0.865 measured at 490 nm.

Cycle 8 Selective Pressure Test Panel Result

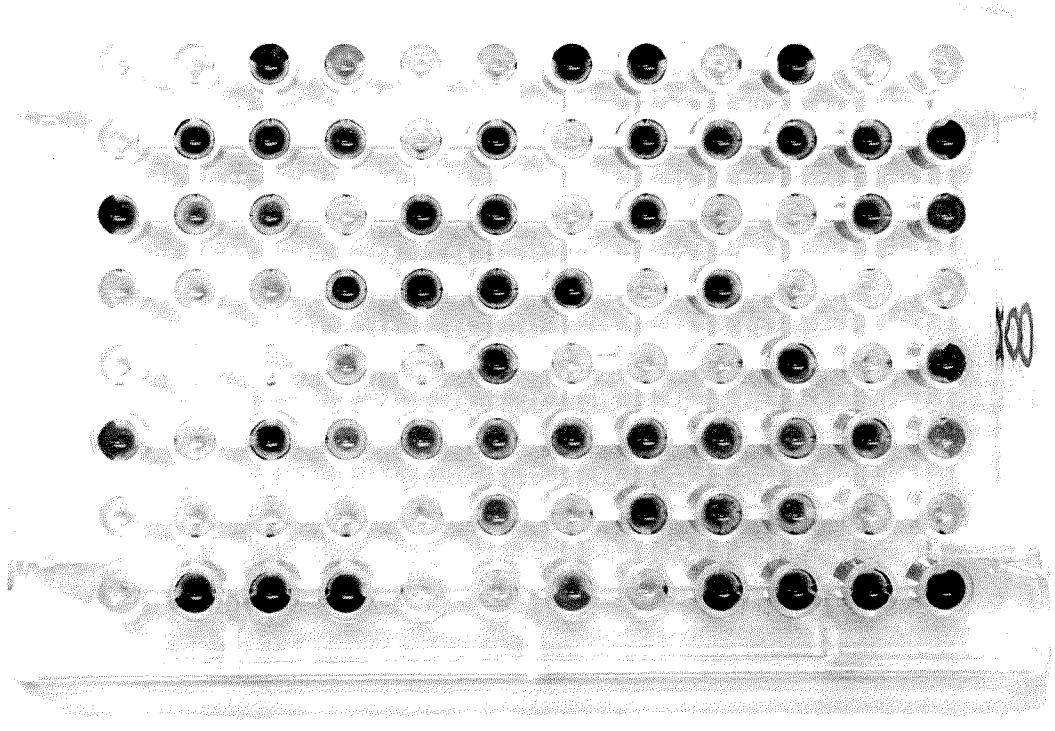

Figure 4. Image of metabolic fingerprint results for *E. coli* at cycle 8 (= 400 EHDs) using Biolog GN2 MicroPlate™ test panel. Absorbance of blank slot A1 = 0.667 measured at 490 nm.

Cycle 0 Selective Pressure Test Panel Result

	1	2	3	4	5	6	7	8	9	10	11	12
A	blank	0.019	0.479	0.247	-0.093	-0.041	0.717	0.954	-0.020	0.904	-0.096	-0.123
B	-0.069	0.875	0.467	0.851	-0.077	1.018	0.029	1.083	0.384	0.437	0.890	0.752
C	0.740	0.566	0.420	0.033	0.607	0.937	0.020	0.992	0.137	-0.048	0.829	0.334
D	0.027	0.014	-0.128	0.314	0.539	0.832	1.091	-0.140	0.894	-0.032	-0.127	-0.107
E	-0.146	-0.192	-0.523	0.179	-0.449	0.539	-0.054	-0.161	-0.055	0.421	-0.141	0.598
F	0.112	-0.133	0.390	0.167	0.097	0.341	2.070	0.124	0.181	0.265	0.267	-0.038
G	-0.206	-0.209	-0.227	-0.172	-0.225	0.207	-0.131	0.435	0.265	-0.030	-0.180	-0.076
H	-0.178	0.464	0.455	0.485	-0.281	-0.192	0.222	-0.193	0.551	0.357	0.769	0.823

Table 3. Metabolic fingerprint results for *E. coli* at cycle 0 using Biolog GN2 MicroPlate™ test panel. Absorbance of blank slot A1 = 0.865 measured at 490 nm. Grey boxes indicate positive (+) measurement of metabolic function, using $\Delta\ OD_{490} > 0.100$.

Cycle 4 Selective Pressure Test Panel Result (saturated)

	1	2	3	4	5	6	7	8	9	10	11	12
A	blank	-0.078	-0.016	0.211	-0.012	0.005	0.679	0.881	0.091	0.621	-0.037	-0.259
B	-0.179	0.345	0.110	0.496	-0.233	0.337	0.141	0.571	0.015	0.418	0.309	0.808
C	0.514	0.260	0.407	-0.048	0.152	0.447	0.250	0.581	0.075	0.128	0.472	0.277
D	0.182	0.242	0.100	-0.022	0.315	0.687	0.494	0.188	0.644	-0.156	0.181	0.140
E	-0.007	0.035	-0.623	0.407	-0.638	0.188	0.053	-0.125	0.255	0.086	0.097	0.071
F	0.098	-0.022	0.109	0.066	0.187	0.112	0.285	-0.071	0.403	0.182	0.361	-0.363
G	0.027	0.055	0.051	-0.021	0.201	0.139	-0.049	0.142	-0.294	0.095	0.130	0.081
H	0.052	0.131	0.516	0.424	-0.171	-0.073	0.517	0.011	0.512	0.333	0.674	0.307

Table 4. Metabolic fingerprint results for *E. coli* at cycle 4 (= 200 total EHDs) using Biolog GN2 MicroPlate™ test panel. Absorbance of blank slot A1 = 1.217 measured at 490 nm. Grey boxes indicate positive (+) measurement of metabolic function, using $\Delta\ OD_{490} > 0.100$.

Cycle 8 Selective Pressure Test Panel Result

1	2	3	4	5	6	7	8	9	10	11	12
blank	0.011	0.759	0.283	-0.056	0.019	0.920	1.225	0.049	1.265	-0.035	-0.067
-0.067	1.071	0.853	1.082	-0.021	1.129	0.008	1.285	0.784	0.846	1.157	1.197
0.917	0.281	0.534	-0.031	0.896	1.018	0.027	1.116	0.124	-0.051	0.813	0.598
0.072	0.071	0.063	0.514	0.882	0.879	1.314	-0.030	0.888	-0.050	-0.059	-0.065
-0.103	-0.185	-0.276	0.127	-0.252	0.604	-0.142	-0.026	-0.106	0.870	-0.094	0.797
0.376	-0.091	0.679	0.150	0.251	0.390	0.345	0.286	0.405	0.267	0.514	0.075
-0.060	-0.119	-0.174	-0.089	-0.167	0.301	-0.094	0.603	0.261	0.136	-0.098	-0.132
-0.161	0.669	0.685	0.584	-0.241	-0.136	0.342	-0.091	0.768	0.496	0.905	1.116

Table 5. Metabolic fingerprint results for *E. coli* at cycle 8 (= 400 total EHDs) using Biolog GN2 MicroPlate™ test panel. Absorbance of blank slot A1 = 0.667 measured at 490 nm. Grey boxes indicate positive (+) measurement of metabolic function, using $\Delta\ OD_{490} > 0.100$.

Cycle 11 Selective Pressure Test Panel Result (saturated)

	1	2	3	4	5	6	7	8	9	10	11	12
A	blank	0.066	0.291	0.347	0.083	0.067	0.418	0.599	0.140	0.788	0.124	0.098
B	0.044	0.728	0.440	0.537	0.116	0.684	0.165	0.804	0.391	0.547	0.700	0.489
C	0.586	0.271	0.469	0.154	0.500	0.606	0.167	0.627	0.260	0.124	0.586	0.163
D	0.372	0.243	0.248	0.114	0.516	0.662	0.843	0.098	0.679	0.033	-0.010	0.160
E	-0.011	0.026	-0.393	0.325	-0.342	0.265	0.129	0.118	0.074	0.258	0.008	0.252
F	0.214	0.043	0.165	0.217	0.130	0.253	0.155	-0.005	0.181	0.302	0.213	0.056
G	0.038	0.063	-0.098	0.059	0.147	0.204	0.086	0.331	0.145	0.262	-0.051	0.031
H	-0.016	0.326	0.272	0.529	-0.090	0.050	0.395	0.156	0.524	0.412	0.656	0.726

Table 6. Metabolic fingerprint results for *E. coli* at cycle 11 (= 550 total EHDs) using Biolog GN2 MicroPlate™ test panel. Absorbance of blank slot A1 = 1.056 measured at 490 nm. Grey boxes indicate positive (+) measurement of metabolic function, using $\Delta\ OD_{490} > 0.100$.

Chapter VI

Discussion and Conclusions

Chapter VI. Discussion and Conclusions

Disinfection Kinetics

The disinfection by pulsed plasma discharges has been demonstrated. The inactivation kinetics of *Escherichia coli* suspensions follows a non-linear dose-response behavior that is not associated with inhomogeneous mixing conditions inside the reactor. A log*it* function was used to rectify the data to obtain values of LD_{50}. The rates of inactivation were limited to 2-log reduction (or 99 % reduction) at high concentrations of *E. coli* (10^7 CFU mL^{-1}) subject to 50 consecutive EHD discharges.

The tailing behavior in the dose-response curves is not an artifact but a phenomenon intrinsic to the process of disinfection by electrohydraulic discharges (Chap. 3). This is substantiated by the values of LD_{50} in EHD disinfection that are constant over a 3-orders of magnitude variation in initial cell concentration (Fig. 4, Chap. 3). The tailing behavior is also not associated with increased absorptivity of treated *E. coli* suspensions as shown by absorbance measurements of raw (unfiltered) samples after 0, 60 and 100 consecutive EHDs that remain unchanged over the range of 200 to 400 nm (Fig. 1). Furthermore, this tailing behavior occurs in both high (10^7 CFU mL^{-1}) and low (10^3 CFU mL^{-1}) concentrations of *E. coli* with different intrinsic rates of disinfection (Fig. 2).

The LD_{50} dependence on initial cell concentrations for UV and EHD treated samples (Fig. 4, 5 in Chap. 3) show a constant value over 3-orders of magnitude followed by a sharp increase in LD_{50}. This behavior is attributed to the non-linear relationship

between the absorbance and the *E. coli* cell concentration. This dependence is not observed in experiments involving ultrasonic irradiation (Fig. 6, Chap. 3), since the process is light independent. Figure 3 shows the absorbance at 600 nm (OD_{600}) as a function of increasingly denser *E. coli* suspensions. The absorbance measurements are nearly zero and sharply increase beyond 10^8 CFU mL^{-1} as observed in the UV and EHD experiments.

High Intensity UV Disinfection

Results from Chap. 4 suggest that the UV mechanism of disinfection is linked to biphotonic absorptions of high-intensity UV irradiation by DNA thymine. This high intensity multiphotonic process is known to produce less thymidine dimer photoproducts and more single and double strand breaks (*1,2*).

Varying concentrations of benzophenone-9 (BP9) were used as chemical sunscreens to disable the UV component of disinfection in the EHD reactor. No loss of viability was observed in fully saturated solutions of *E. coli* with BP9 attesting that UV is the principal disinfection agent in the electrohydraulic discharge process. Furthermore, there is no indication that mechanical damage is involved in the overall process of inactivation by EHD.

Vitalism vs. Mechanism

Background

The majority of the discussions on the kinetics of disinfection, since the discovery of the *microorganism law of logarithmic order of destruction* (*3-5*), focus on two principal views on the order of death: *vitalism* and *mechanism* (*6,7*).

The tenet of *vitalism* is that individuals (or cells) in a population are not identical (*8*); therefore, in a homogeneous population of microorganisms, resistance to a disinfectant varies in different individuals. It follows that the survival times should be normally distributed as the majority of these individuals possess an average degree of resistance while a minority possess a greater or a lesser degree of resistance. Typically, survival curves of this type exhibit sigmoidal or concave upward behavior.

According to the *mechanistic* theory, there is a similarity in resistance among all individuals in a homogeneous population and the process of inactivation is a stepwise time process analogous to chemical reactions (*8*). At a given time, a portion of the population participates in the disinfection reaction so the reactions are first order or n^{th} order composed of a series of single step reactions. Survival curves of this type are usually logarithmic. The tailing phenomenon, in this case, is a feature bound to the mechanism of destruction, a change in the resistance during the process or a deviation from linearity.

In Chap. 5, (Figs. 1, 2) no change in the dose-response curves is observed in the presence of EHD selective pressures after 11 cycles of 50 consecutive EHDs each. If the

vitalistic conception of inactivation is ascribed to these results, then an increasing degree of resistance should be observed; every time the *E. coli* suspension is subject to an EHD event, the less resistant cells die out, so the population frequency distribution must skew towards the more resistant individuals. This increase in resistance was not observed; therefore, the assumption of the *vitalistic* conception does not apply here.

The results of this work suggest that a *mechanistic* process must be occurring. However, the details of such a mechanism is not known. More careful studies on the direct effect of high intensity UV irradiation on *E. coli* must be performed in order to obtain a greater understanding of the EHD dose-response curves.

Metabolic fingerprinting assays were used to detect bacterial contaminants propagated through the 13-day experiment. The study found no evidence of contamination. In addition, a 98 % metabolic homology of carbon consumption activities is reported between initial and final cultures.

Recommendations for Future Research

Combined Ozone/EHD Disinfection Experiments

Combined EHD/ozone disinfection experiments are based on the introduction of an additional variable (ozone) which, in the presence of high intensity UV irradiation, produce high concentrations of hydroxyl radicals. The kinetics of disinfection are further complicated by the fact that ozone itself is a disinfectant, so both reactants, and products in addition to the EHD, now play significant roles. In addition, the synergistic effects between ozone and EHD can be studied as observed in the chemical degradation of environmental contaminants (*9*).

Figures 4 and 5 show the kinetic simulation of dissolved ozone, hydroxyl radical concentrations, and viability during a combined EHD/ozone experiment. The following is a step by step description of the set-up.

Using a 3-L test solution in the EHD reactor chamber that has been sparged with ozone prior to the onset of the electrohydraulic discharge treatment, the solution is allowed to reach a steady state aqueous-phase concentration of ozone in the chamber. The characteristic time t_{dis} for ozone to reach a steady state is in the order of minutes and can be measured directly in the reaction chamber using a spectrophotometer.

The fully sparged solution is then inoculated with *E. coli* at a fixed initial cell concentration, when the experiment starts. At this point, the only disinfection effect is due to ozone. The ozone treatment is allowed to proceed for a finite time t_{oz} whereby no

electrohydraulic discharges are imposed. The dose-response curve during this pre-discharge phase would be expected to follow an exponential decay of the form (*10*),

$$\log\left(\frac{N}{N_0}\right) = -k^*_{oz}t \qquad (1a)$$

$$k^*_{oz} = k_i c_0 \qquad (1b)$$

where N_0 is the viability at time zero, N is the viability of *E. coli* at time t, k_i is the second-order disinfection rate constant, c_0 is the constant dissolved ozone concentration, k^*_{oz} is the pseudo first-order constant, and t is the contact time.

At the start of the electrohydraulic discharge treatment, a fraction of the initial aqueous-phase concentration of ozone is effectively converted into hydroxyl radicals by exposure to plasma-generated VUV light. The light is emitted by the plasma channel in the form of a blackbody spectrum centered at 180 nm (*11,12*). The absorption spectrum of ozone has a maximum at 260 nm, which favors the photodissociation pathway that leads to the production of singlet oxygen $O(^1D)$. An 85 - 90 % yield of $O(^1D)$ is usually expected to be converted from ozone with the remaining amount being carried over to the production of triplet oxygen $O(^3P)$ (*13*). The $O(^3P)$ pathway is enhanced at high temperatures so an increased reaction of the triplet oxygen and water in the vicinity of the plasma channel would be observed; however, this reaction is slow and eventually leads to hydroxyl radical formation. Measured first-order rate constants in liquid and gas for molecular oxygen k_{3P} and k_{1D} (*14-18*) are shown in the table below.

Table 1. Rates of Ozone Decomposition.

Reaction	$Rate_{liquid}$ [$M^{-1}s^{-1}$] 300 K	$Rate_{gas}$ [$M^{-1}s^{-1}$] 300 K
$O_3 \rightarrow O_2 + O(^3P)$, thermal	1.6×10^{-6}	2.3×10^{-5}
$O(^3P) + H_2O \rightarrow 2OH\bullet$, thermal	-	$2 - 4 \times 10^{-3}$
$O(^1D) + H_2O \rightarrow 2OH\bullet$, photolysis	9.4×10^{7}	$1 - 2 \times 10^{11}$

In general, the rates of $O(^3P)$ reaction are much slower than the rates of $O(^1D)$. Knowing the percent yield of $O(^3P)$ production from ozone photodissociation and the limiting rate of reaction with water, then ozone can be assumed to be predominantly converted into $O(^1D)$ in the electrohydraulic discharge reactor, i.e.,

$$O_3 + h\nu \rightarrow O_2 + O(^1D) , \ \lambda < 300 \text{ nm} \qquad (2a)$$

$$O(^1D) + H_2O \rightarrow 2OH\bullet \qquad (2b)$$

With the onset of the first electrohydraulic discharge, a fraction of the dissolved ozone is photodissociated into hydroxyl radicals in the presence of water. The size of this fraction dictates the kinetics of the disinfection process following an EHD event. If a small percent of the dissolved ozone is converted into hydroxyl radicals, then the rate of dissolution is slow, since the background ozone concentration is near steady state, and the variation of dissolved ozone is small (Fig. 4). For large percentages of hydroxyl radical conversion, the rate of ozone dissolution is fast and the variation of ozone is large. The kinetics of ozone disinfection (Eqns. 1a,b) assume a constant excess dissolved concentration of ozone. Large fluctuations in hydroxyl radical concentrations produce nonlinear disinfection kinetics that are dependent on the instantaneous background dissolved ozone concentrations (Fig. 5).

The rate of disinfection during an EHD episode k^*_{ehd} is a lumped parameter that depends on the rate of hydroxyl radical disinfection k^*_{OH} and the disinfection rates of UV and ozone, i.e.,

$$k^*_{ehd} = f(k^*_{OH}, k'_{UV}, k'_{oz}) \qquad (3)$$

where k'_{oz} and k'_{UV} are the coupled intrinsic rates of disinfection during an EHD. The higher reactivity of the hydroxyl radical species and the enhancement of hydroxyl radical production due to EHD suggests that k^*_{ehd} will be faster than k^*_{oz} from the pre-discharge phase of the experiment (Fig. 5). The size of this increase in inactivation rate is unknown and will limit the number of EHDs that can be imposed on the experiment. This increase can be measured by tracking the difference between the viability before and after an EHD. The time t_{ehd} can be set to allow for several sampling points between consecutive electrohydraulic discharges.

In summary, there are several variables that are key for this investigation of the kinetics of *E. coli* disinfection in the combined EHD/ozone experiment:

(i) Measurement of the ozone dissolution time

(ii) Measurement of the ozone disinfection rate constant

(iii) Measurement of the amount of ozone loss following a single electrohydraulic discharge.

Ozone Dissolution Experiment

Using an HDPE sparging disc with an array of 11 concentric 0.030 in. diameter holes, a mixture of O_3/O_2 can be flowed through the reactor at fixed flow rates. The rate of ozone

dissolution can be computed from the characteristic time for the solution to reach a steady state under different O_3/O_2 mixtures and ozonator settings. Ozone measurements can be made by addition of iodide into the sample aliquots and measuring triiodide formation spectrophotometrically as a function of time. Iodide oxidation is given stoichiometrically by the reaction,

$$3I^- + O_3 + 2H^+ \rightarrow I_3^- + O_2 + H_2O \qquad (4)$$

Ozone Disinfection Rate Constant

After a mixture of O_3/O_2 at a constant flow rate is allowed to reach a steady state, the solution can be inoculated with *E. coli* at a fixed initial cell concentration. Viability measurements can be made from sample aliquots taken out of the reactor at fixed time intervals into vials containing sodium sulfite to stunt further ozone disinfection. Each sample aliquot is diluted and plated in triplicate on agar media and incubated in the dark at 37 °C.

The oxidation of sulfite by ozone follows the reaction,

$$\tfrac{1}{2}O_3 + \tfrac{1}{2}SO_3^{2-} \rightarrow \tfrac{1}{2}O_2 + \tfrac{1}{2}SO_4^{2-} \quad , \quad \Delta G^\circ = -211 \text{ kJ/mol} \qquad (5)$$

Possible interactions in solution with *E. coli* must be investigated by performing independent growth/inhibition experiments with added sulfite and sulfate ions at experimentally determined concentrations.

Hydroxyl Radical Production in the EHD

Assuming the ozone reactions (Eqns. 2a,b) go to completion and assuming the quantum yield Φ for $O(^1D)$ production in ozone photolysis is known (*19*), then the rate of ozone loss is proportional to the stoichiometric rate of hydroxyl radical production times the quantum yield,

$$-\frac{d}{dt}[O_3] = \frac{\Phi}{2}\frac{d}{dt}[OH\bullet] \qquad (6)$$

If the ozone concentration is known as a function of time, by virtue of the previous equation, then the rate of hydroxyl radical formation can be approximated by

$$\frac{\Delta[OH\bullet]}{\Delta t} \cong -2\Phi\frac{\Delta[O_3]}{\Delta t} \qquad (7)$$

where the approximation becomes more exact in the limit $\Delta t \rightarrow 0$.

Combined Peroxydisulfate/EHD Disinfection Experiments

Sulfate radical production by flash photolysis of peroxydisulfate is not a novel technique (*20,21*). Peroxydisulfate absorbs light with a maximum at 248 nm leading to photodissociation into sulfate radicals $\bullet SO_4^-$. The peroxydisulfate photodissociation proceeds stoichiometrically according to the reaction,

$$S_2O_8^{2-} + h\nu \rightarrow 2 \bullet SO_4^- \qquad (8)$$

The sulfate radical is a very strong one-electron oxydizing agent with a redox potential ~ 2.5 – 3.0 Volts (*22*), similar to •OH. Using peroxydisulfate-sulfate radical pair as a disinfection agent might provide an alternative to ozone-hydroxyl radical disinfection that forgoes the complex kinetics of ozone depletion described previously. Both radical species are equally reactive; however, in the latter case, ozone (the reactant) is also a disinfection agent whereas peroxydisulfate is not.

A similar peroxydisulfate depletion mechanism is expected as in the case of ozone (Fig. 5) and the amount of sulfate radicals produced is dependent on the concentration of peroxydisulfate ion present in solution (*23*). Since the kinetics of disinfection are not affected by the initial concentration of the reactant (Fig. 6), there is no need to measure the amount of peroxydisulfate loss following an electrohydraulic discharge.

The fate of the sulfate radical depends highly on the chemical species present in the reactor. The relatively high redox potential (~ 2.5 – 3.0 V) makes this radical a very strong oxidant. The typical sulfate radical decay kinetics can be described by the following reactions (*24*),

$$\bullet SO_4^- + \bullet SO_4^- \rightarrow S_2O_8^{2-} \quad (9a)$$

$$\bullet SO_4^- + H_2O \rightarrow \bullet OH + HSO_4^- \quad (9b)$$

$$\bullet SO_4^- + S_2O_8^{2-} \rightarrow SO_4^{2-} + S_2O_8^- \quad (9c)$$

In the context of water disinfection, only the sulfate radical $\bullet SO_4^-$ and the hydroxyl radical •OH affect the viability of the bacteria (Fig. 6). For this reason, measuring bacterial disinfection under these circumstances can only be a direct result of a sulfate/hydroxyl radical competition mechanism.

References Cited

(1) Masnyk, T. W.; Nguyen, H. T.; Minton, K. W. *J. Biol. Chem.* **1989**, *264*, 2482.

(2) Nikogosyan, D. N.; Oraevsky, A. A.; Zavilgelsky, G. B. *Photobiochem. Photobiophys.* **1986**, *10*, 189.

(3) Chick, H. *J. Hygiene* **1908**, *8*, 92.

(4) Watson, H. E. *J. Hygiene* **1908**, *8*, 536.

(5) Madsen, T.; Nyman, M. *Z. Hygiene Infektionskranheiten* **1907**, *57*, 388.

(6) Cerf, O. *J. Appl. Bacteriol.* **1977**, *42*, 1.

(7) Hiatt, C. W. *Bacteriol. Rev.* **1964**, *28*, 150.

(8) Lee, R. E.; Gilbert, C. A. *J. Phys, Chem.* **1918**, *22*, 348.

(9) Destaillats, H.; Colussi, A. J.; Joseph, J. M.; Hoffmann, M. R. *J. Phys. Chem. A* **2000**, *104*, 8930.

(10) Hunt, N.; Marinas, B. *Wat. Res.* **1997**, *31*, 1355.

(11) Willberg, D. M.; Lang, P. S.; Hochemer, R. H.; Kratel, A.; Hoffmann, M. R. *Environ. Sci. Technol.* **1996**, *30*, 2526.

(12) Lang, P. S.; Ching, W.-K.; Willberg, D. M.; Hoffmann, M. R. *Environ. Sci. Technol.* **1998**, *32*, 3142.

(13) Geiser, J. D.; Dylewski, S. M.; Mueller, J. A.; Wilson, R. J.; Toumi, R.; Houston, P. L. *J. Chem. Phys.* **2000**, *112*, 1279.

(14) Sehested, K.; Corfitzen, H.; Holcman, J.; Hart, E. J. *J. Phys. Chem.* **1992**, *96*, 1005.

(15) Zehavi, D.; Rabani, J. *J. Phys. Chem.* **1971**, *75*, 1738.

(16) Tsang, W.; Hampson, R. F. *J. Phys. Chem. Ref. Data* **1986**, *15*, 1087.

(17) Ahlheim, M.; Gunther, R. *Combust. Flame* **1979**, *35*, 117.

(18) Streit, G. E.; Howard, C. J.; Schmeltekopf, A. L.; Davidson, J. A.; Schiff, H. I. *J. Chem. Phys.* **1976**, *65*, 4761.

(19) Wayne, R. P. *Atmos Environ* **1987**, *21*, 1683.

(20) Hayon, E.; McGarvey, J. J. *J. Phys. Chem.* **1967**, *71*, 1472.

(21) Kraljic, I. *Int. J. Radiat. Chem.* **1970**, *2*, 59.

(22) Neta, P.; Huie, R. E.; Ross, A. B. *J. Phys. Chem. Ref. Data* **1988**, *17*, 1027.

(23) Bao, Z.-C.; Barker, J. R. *J. Phys. Chem.* **1996**, *100*, 9780.

(24) McElroy, W. J.; Waygood, S. J. *J. Chem. Soc. Faraday Trans.* **1990**, *86*, 2557.

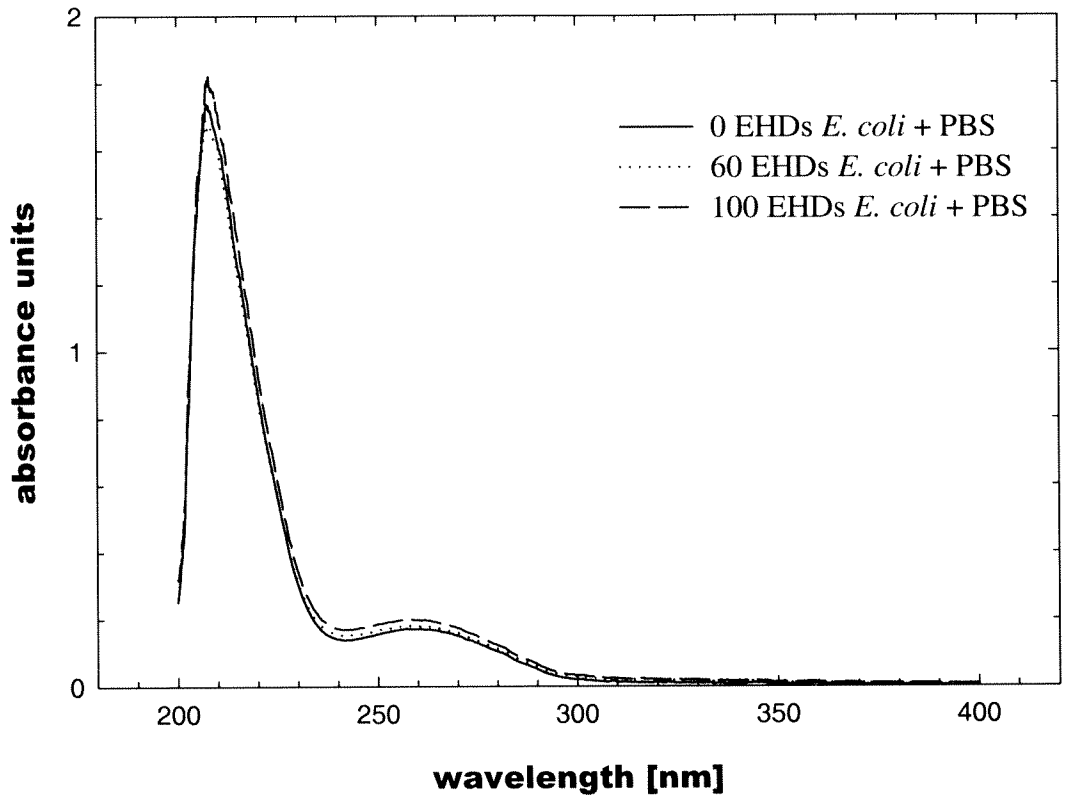

Figure 1. Absorbance measurements of 1/100th dilutions of EHD generated samples with *E. coli* in 0.01M PBS at 0 EHDs (solid line), 60 EHDs (dotted line), and 100 EHDs (dashed line).

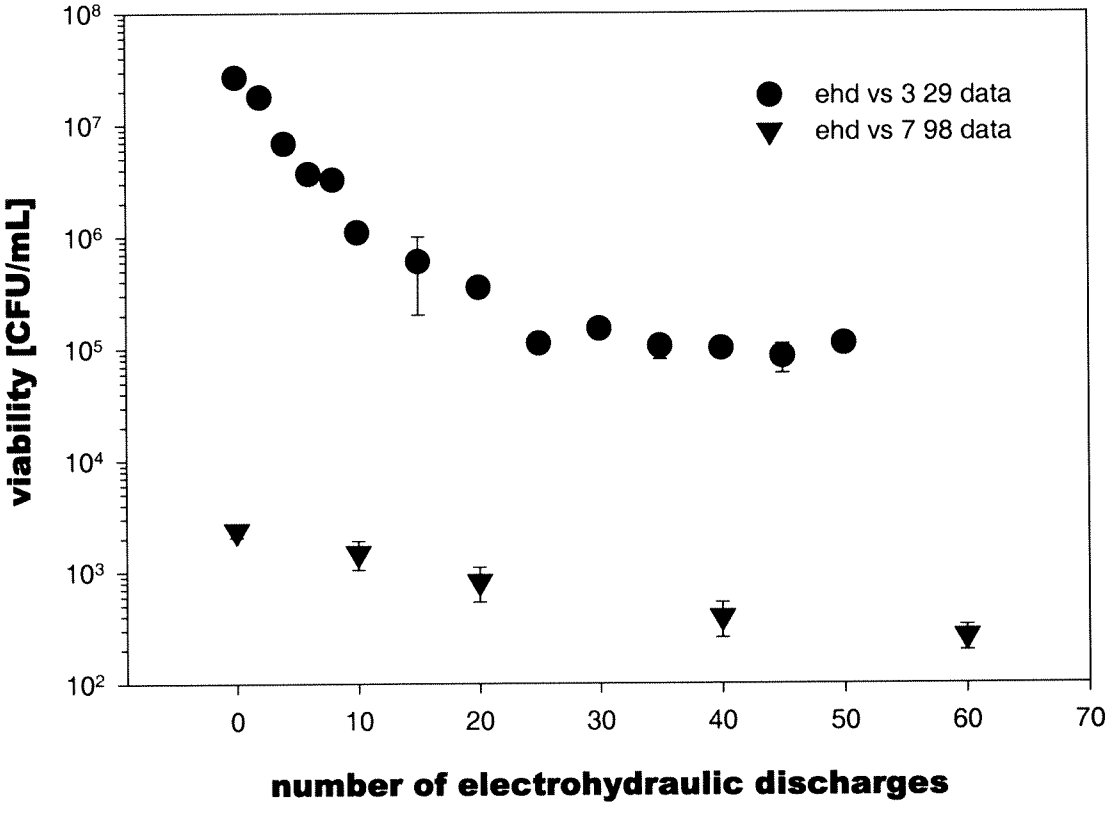

Figure 2. Full-scale EHD disinfection experiments of *E. coli* suspensions of 3 x 10^7 CFU mL^{-1} (solid circles) and 2 x 10^3 CFU mL^{-1} (solid triangles) in 0.01 M PBS at pH = 7.4. Discharges are characterized by E_{CB} = 7 kJ, spark gap = 4 mm, and pulse rate = 0.1 Hz.

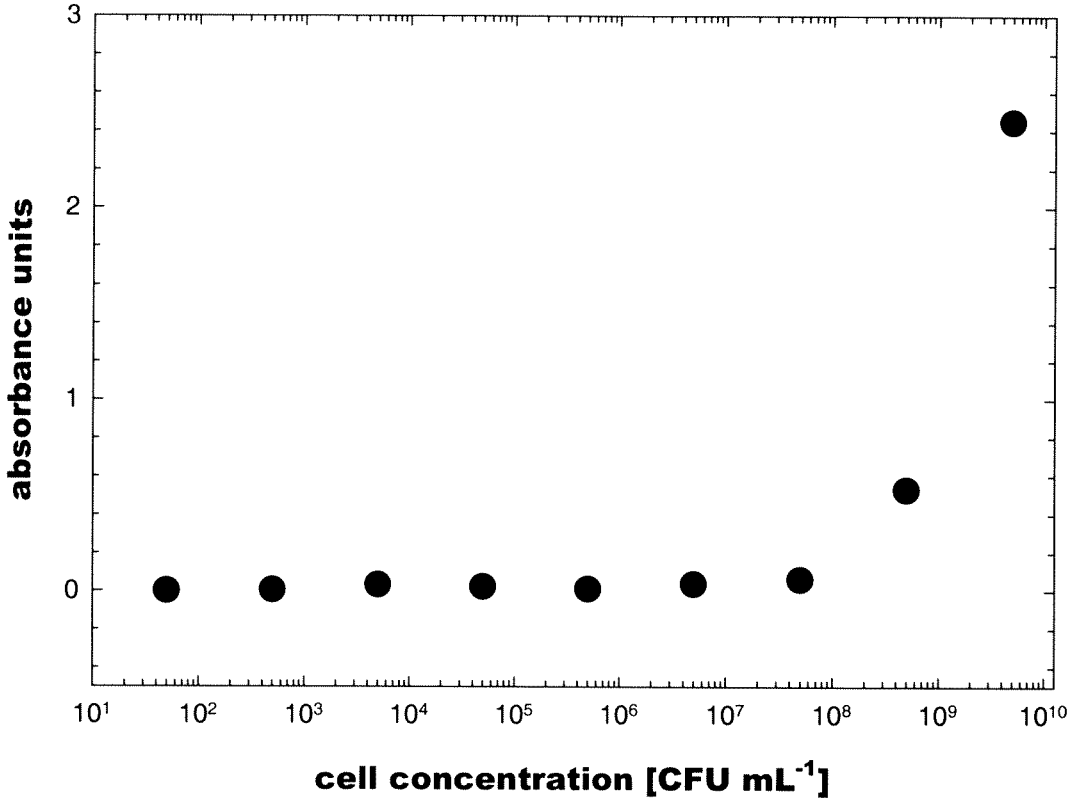

Figure 3. Absorbance measurements of *E. coli* concentrations at 600 nm (OD_{600}).

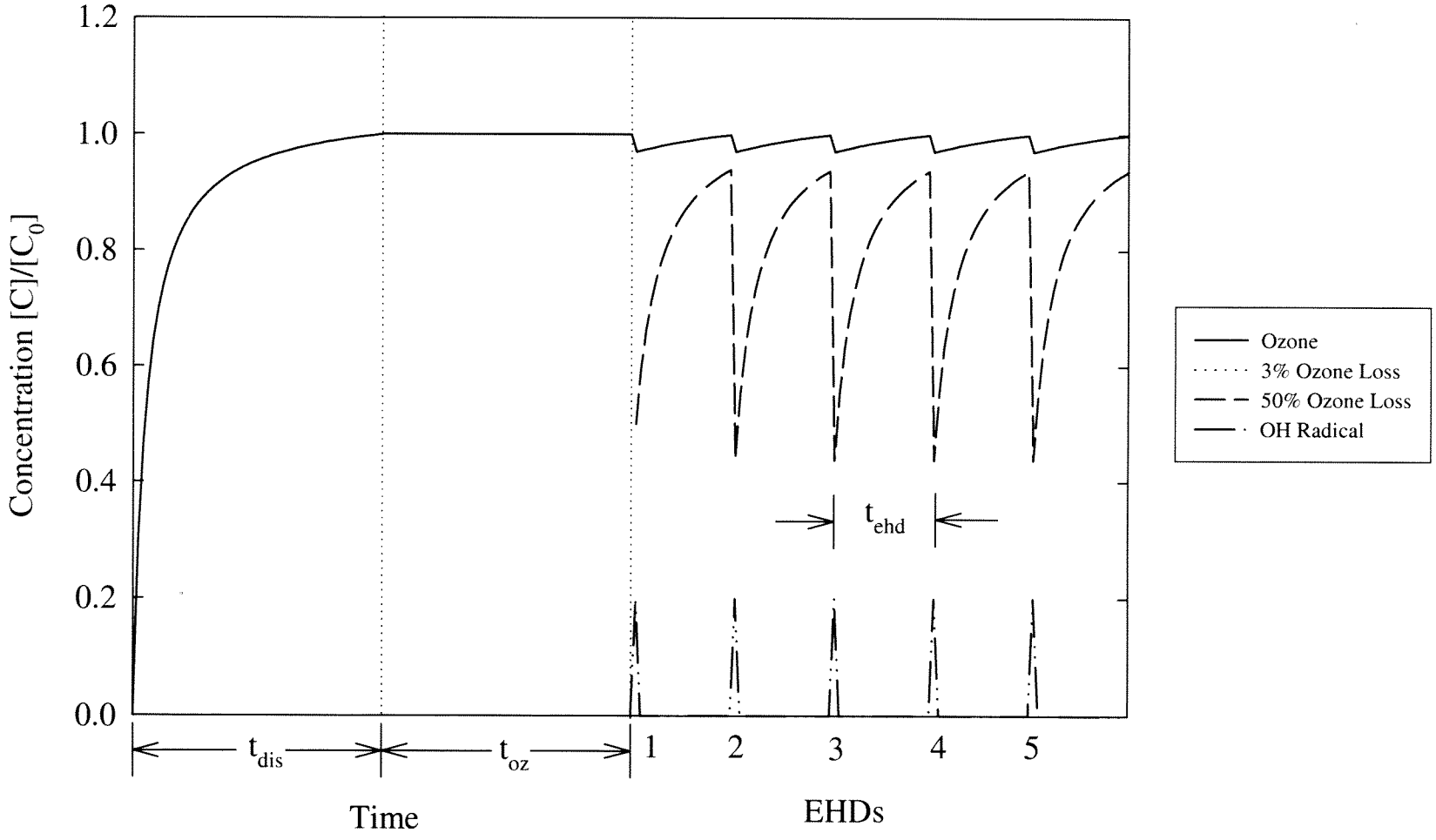

Figure 4. Kinetic simulation of ozone and hydroxyl radical concentrations in a combined EHD/Ozone experiment.

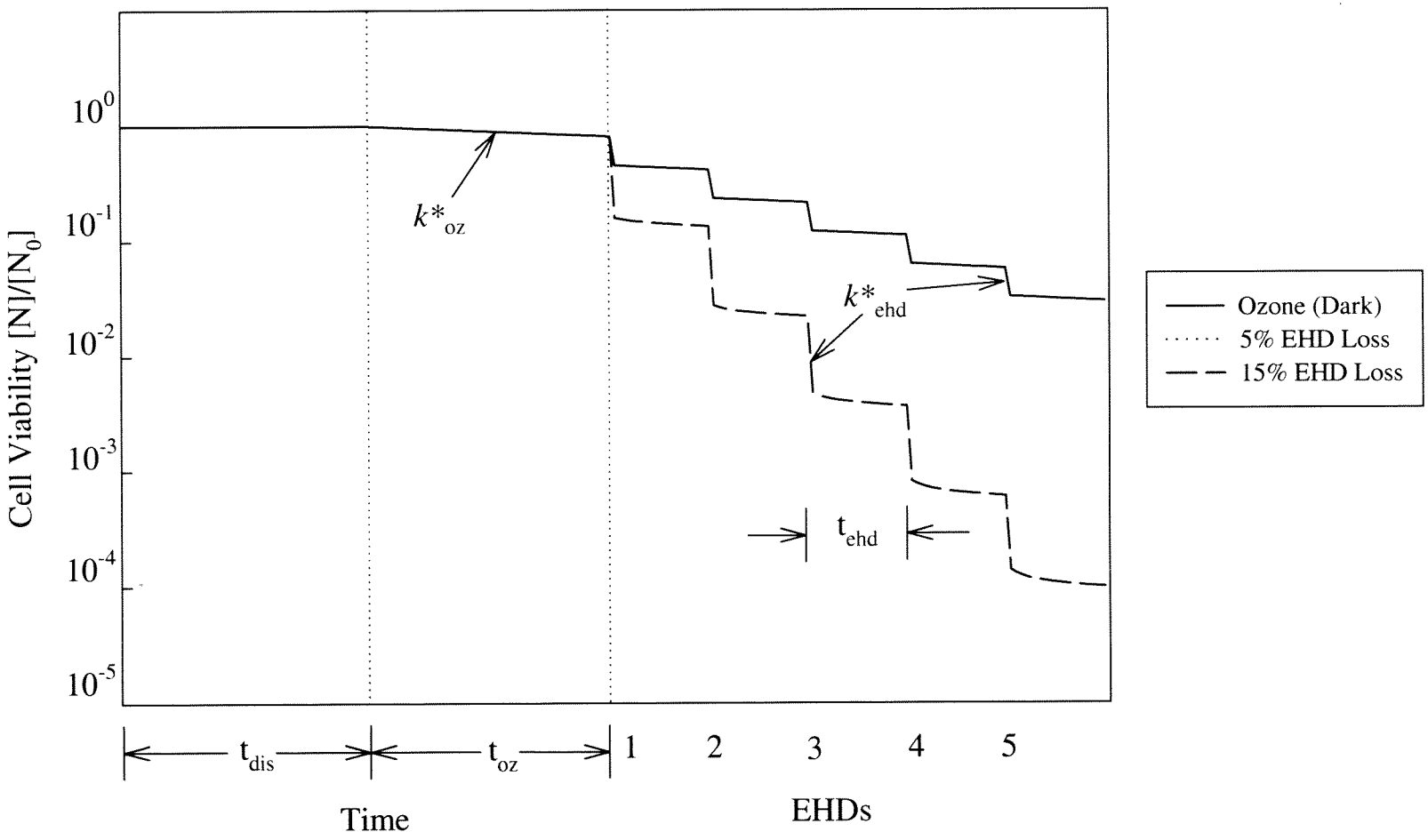

Figure 5. Kinetic simulation of cell viability in a combined EHD/ozone reactor.

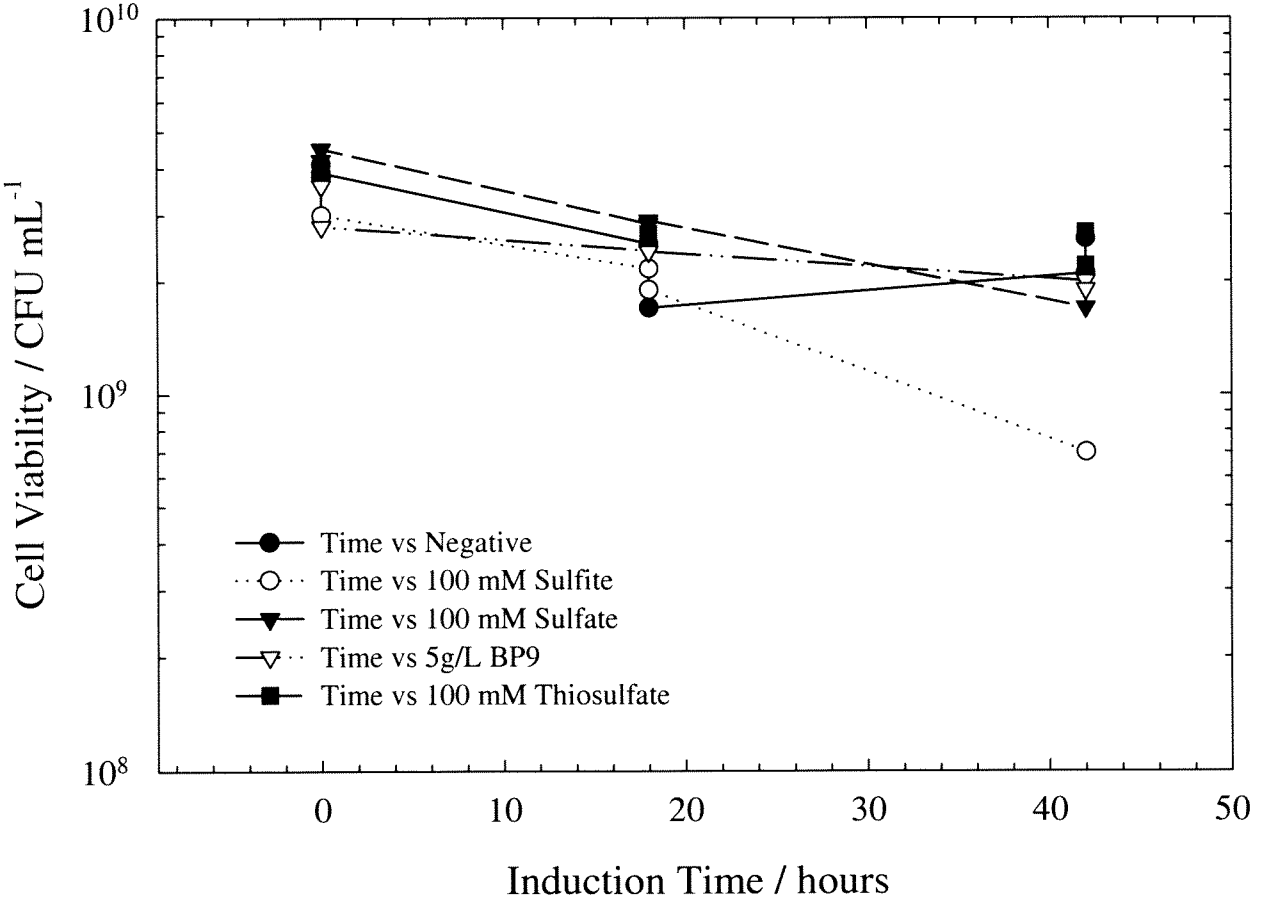

Figure 6. *E. coli* sensitivity experiments with sulfite, sulfate, thiosulfate and benzophenone-9 in 0.01 M PBS at 25 °C over a 42-hour time period. Initial cell concentration was 4 x 10^9 CFU mL^{-1}. All experiments and incubations were done in the dark.

Appendix

EHDs	12/99 Data	11/98 Data	12/99 Data
0	46000000	28100000	860000
1			
2	28000000	15800000	380000
3			
4	11300000	9500000	103000
5			
6	9200000	5200000	9000
8	4600000	3700000	
10	3800000	2790000	
15	1700000	1510000	
20	1030000	1330000	1200
25	740000	854000	
30		694000	
35	400000	604000	
40	250000	473000	
45	360000	546000	
50		490000	

EHDs	3/29/00 A	3/29 B	3/29 Mean	3/29 Variance	3/29 %error
0	2.72E+07	2.63E+07	26750000	450000	1.68
1					
2	1.92E+07	1.64E+07	17800000	1400000	7.87
3					
4	6.40E+06	7.30E+06	6850000	450000	6.57
5					
6	4.00E+06	3.30E+06	3650000	350000	9.59
8	3.60E+06	2.90E+06	3250000	350000	10.77
10	1.00E+06	1.20E+06	1100000	100000	9.09
15	1.00E+06	2.00E+05	600000	400000	66.67
20	3.60E+05	3.40E+05	350000	10000	2.86
25	1.00E+05	1.20E+05	110000	10000	9.09
30	1.70E+05	1.30E+05	150000	20000	13.33
35	1.30E+05	8.00E+04	105000	25000	23.81
40	1.10E+05	9.00E+04	100000	10000	10.00
45	1.10E+05	6.00E+04	85000	25000	29.41
50	1.30E+05	9.00E+04	110000	20000	18.18

Table A1. Raw data for EHD disinfection experiments on 11/98, 12/99 and 3/29/00. Disinfection of *E. coli* suspensions (3 L) in 0.01 M PBS at pH = 7.4 by 50 consecutive electrohydraulic discharges. E_{CB} = 7 kJ, spark gap = 4 mm, and pulse rate = 0.1 Hz.

EHDs	10/98 Data A	10/98 Data B	10/28 Data C	10/28 Mean	10/28 Variance	10/28 %error
0	1.44E+09	1.52E+09	1.41E+09	1456666666.67	63333333.33	4.35
1	1.14E+09		1.29E+09	1215000000.00	75000000.00	6.17
2	1.41E+09		1.65E+09	1530000000.00	120000000.00	7.84
3	6.30E+08	6.70E+08	7.30E+08	676666666.67	53333333.33	7.88
4	6.80E+08		5.20E+08	600000000.00	80000000.00	13.33
5	4.20E+08	3.20E+08	3.50E+08	363333333.33	56666666.67	15.60
6						
8						
10	2.80E+06	2.20E+06	3.60E+06	2866666.67	733333.33	25.58
15						
20	4.30E+04	3.50E+04	3.50E+04	37666.67	5333.33	14.16
25						
30	4.00E+02	7.00E+02	6.00E+02	566.67	166.67	29.41

EHDs	7/98 A	7/98 B	7/98 C	7/98 D	7/28 Mean	7/28 Variance	7/28 %error
0	2100	2070	2700	2600	2367.5	332.5	14.04
1							
2							
3							
4							
5							
6							
8							
10	1140	1250	1900	1600	1472.5	427.5	29.03
15							
20	550	620	1100	1000	817.5	282.5	34.56
25							
30							
35							
40	350	530	300		393.3	136.7	34.75
45							
50							
60	220	330	300	200	262.5	67.5	25.71
80	180	130		200	170	40	23.53
100	140	140	100		126.7	26.7	21.05

Table A2. Raw data for EHD disinfection experiments on 7/98 and 10/98.

Disinfection of *E. coli* suspensions (3 L) in 0.01 M PBS at pH = 7.4 by 50 consecutive electrohydraulic discharges. E_{CB} = 7 kJ, spark gap = 4 mm, and pulse rate = 0.1 Hz.

EHD	C1	C1 Mean	C1 Var	C1 error%	C1 %	C1 var%
0	17500000	15866667	1766667	11.13	100.00	11.13
0	16000000					
0	14100000					
2	8600000	7333333	1266667	17.27	46.22	7.98
2	6800000					
2	6600000					

EHD	C2	C2 Mean	C2 var	C2 error%	C2 %	C2 var %
0	9800000	9400000	400000	4.255319	100	4.255319
0	9000000					
0						
2	4950000	3883333	1066667	27.46781	41.31206	11.34752
2	3800000					
2	2900000					

EHD	C3	C3 mean	C3 Var	C3 error%	C3 %	C3 var%
0	5590000	4496667	1093333	24.31	100.00	24.31
0	4200000					
0	3700000					
2	1330000	1293333	53333.33	4.12	28.76	1.19
2	1310000					
2	1240000					

Table A3. Raw data of EHD disinfection rate dependence on initial cell concentration of 3.0-L volumes of *E. coli* subject to 2 consecutive discharges. E_{CB} = 7 kJ, pH = 7.4 in 0.01 M PBS. $C_1 = 1.7 \times 10^7$ CFU mL^{-1}; $C_2 = 9.4 \times 10^6$ CFU mL^{-1}; $C_3 = 5.5 \times 10^6$ CFU mL^{-1}.

EHD	C4	C4 mean	C4 var	C4 error%	C4 %	C4 var %
0	1370000	1306667	66666.67	5.10	100.00	5.10
0	1310000					
0	1240000					
2	204000	180333.3	23666.67	13.12	13.80	1.81
2	165000					
2	172000					

EHD	C5	C5 mean	C5 var	C5 error%	C5 %	C5 var %
0	690000	665000	25000	3.76	100.00	3.76
0	640000					
0						
2	32000	24000	8000	33.33	3.61	1.20
2	19000					
2	21000					

EHD	C6	C6 mean	C6 var	C6 error%	C6 %	C6 var %
0	94000	84500	9500	11.24	100.00	11.24
0	75000					
0						
2	10400	7833.333	2566.667	32.77	9.27	3.04
2	6500					
2	6600					

Table A4. Raw data of EHD disinfection rate dependence on initial cell concentration of 3.0-L volumes of *E. coli* subject to 2 consecutive discharges. E_{CB} = 7 kJ, pH = 7.4 in 0.01 M PBS. $C_4 = 1.3 \times 10^6$ CFU mL^{-1}; $C_5 = 6.6 \times 10^5$ CFU mL^{-1}; $C_6 = 9.4 \times 10^4$ CFU mL^{-1}.

US	C1	C1 mean	C1 var	C1 %err
0	1.32E+10	13200000000	0	0.00
0				
1				
1				
2	1.33E+10	13300000000	0	0.00
2				
3	1.23E+10	12300000000	0	0.00
3				
4	4.8E+09	4800000000	0	0.00
4				
5	2.3E+09	2300000000	0	0.00
5				
7	1.3E+09	1300000000	0	0.00
10	1E+09	1000000000	0	0.00

US	C2	C2 mean	C2 var	C2 %err
0	7.58E+09	7.69E+09	1.1E+08	1.43
0	7.8E+09			
1	2.4E+09	2.25E+09	1.5E+08	6.67
1	2.1E+09			
2	1.2E+09	1.3E+09	1E+08	7.69
2	1.4E+09			
3	4.2E+09	1.4E+09	0	0.00
3				
4	1.4E+09	1.4E+09	0	0.00
4				
5	8E+08	8E+08	0	0.00
5				
7				
10				

Table A5. Raw data of US disinfection rate dependence on initial cell concentration of 100-mL volumes of *E. coli* subject to 5 minutes of ultrasonic irradiation (C_1 was subject to 10 minutes) at pH = 7.4 in 0.01M PBS. $C_1 = 1.8 \times 10^{10}$ CFU mL^{-1}; $C_2 = 4.7 \times 10^9$ CFU mL^{-1}.

US	C3	C3 mean	C3 var	C3 % err
0	1.4E+08	1.49E+08	8500000	5.72
0	1.57E+08			
1	1.62E+08	1.65E+08	3000000	1.82
1	1.68E+08			
2	1.19E+08	1.19E+08	0	0.00
2				
3	74000000	74000000	0	0.00
3				
4	87000000	87000000	0	0.00
4				
5	1.06E+08	1.06E+08	0	0.00
5				
7				
10				

US	C4	C4 mean	C4 var	C4 %err
0	1.1E+08	1.19E+08	9000000	7.56
0	1.28E+08			
1	1.15E+08	1.02E+08	13000000	12.75
1	89000000			
2	58300000	62650000	4350000	6.94
2	67000000			
3	74500000	70250000	4250000	6.05
3	66000000			
4	41000000	41000000	0	0.00
4				
5	50000000	50000000	0	0.00
5				
7				
10				

Table A6. Raw data of US disinfection rate dependence on initial cell concentration of 100-mL volumes of *E. coli* subject to 5 minutes of ultrasonic irradiation at pH = 7.4 in 0.01M PBS. $C_3 = 1.6 \times 10^8$ CFU mL^{-1}; $C_4 = 1.1 \times 10^8$ CFU mL^{-1}.

US	C5	C5 mean	C5 var	C5 % err
0	12000000	11650000	350000	3.00
0	11300000			
1	11000000	12100000	1100000	9.09
1	13200000			
2	10400000	10850000	450000	4.15
2	11300000			
3	9500000	9550000	50000	0.52
3	9600000			
4	8500000	9050000	550000	6.08
4	9600000			
5	9400000	9200000	200000	2.17
5	9000000			
7				
10				

US	C6	C6 mean	C6 var	C6 %err
0	1180000	1200000	20000	1.67
0	1220000			
1	1150000	1060000	90000	8.49
1	970000			
2	860000	880000	20000	2.27
2	900000			
3	960000	970000	10000	1.03
3	980000			
4	970000	955000	15000	1.57
4	940000			
5	810000	810000	0	0.00
5	810000			
7				
10				

Table A7. Raw data of US disinfection rate dependence on initial cell concentration of 100-mL volumes of *E. coli* subject to 5 minutes of ultrasonic irradiation at pH = 7.4 in 0.01M PBS. $C_5 = 1.2 \times 10^7$ CFU mL^{-1}; $C_6 = 1.1 \times 10^6$ CFU mL^{-1}.

UV	C1	C1 mean	C1 var	C1 %err
0	1440000000	1.46E+09	63333333	4.35
0	1520000000			
0	1410000000			
1	1290000000	9.67E+08	4.97E+08	51.38
1	470000000			
1	1140000000			
2	1.41E+09	1.53E+09	1.2E+08	7.84
2	1.65E+09			
2				
3	7.30E+08	6.77E+08	53333333	7.88
3	6.70E+08			
3	6.30E+08			
4	6.80E+08	6E+08	80000000	13.33
4	5.20E+08			

UV	C2	C2 mean	C2 var	C2 %err
0	9.3E+08	8.33E+08	96666667	11.60
0	8.3E+08			
0	7.4E+08			
1	4.3E+08	4.93E+08	63333333	12.84
1	5.1E+08			
1	5.4E+08			
2	3.20E+08	3E+08	20000000	6.67
2	2.80E+08			
2				
3	1.47E+08	1.38E+08	17666667	12.83
3	1.20E+08			
3	1.46E+08			
4	1.77E+07	17650000	50000	0.28
4	1.76E+07			

Table A8. Raw data of UV disinfection rate dependence on initial cell concentration of 100-mL volumes of *E. coli* subject to 1 minute of ultraviolet irradiation at pH = 7.4 in 0.01M PBS. $C_1 = 2.2 \times 10^9$ CFU mL^{-1}; $C_2 = 1.1 \times 10^9$ CFU mL^{-1}.

UV	C3	C3 mean	C3 var	C3 % err
0	1.3E+08	1.24E+08	10333333	8.31
0	1.14E+08			
0	1.29E+08			
1	860000	563333.3	296666.7	52.66
1	390000			
1	440000			
2	8.00E+03	6000	2000	33.33
2	4.00E+03			
2				
3	2.40E+03	2066.667	333.3333	16.13
3	2.00E+03			
3	1.80E+03			
4	2.80E+03	3100	300	9.68
4	3.40E+03			

UV	C4	C4 mean	C4 var	C4 %err
0	62000000	65000000	3000000	4.62
0	68000000			
0				
1	8000	4000	4000	100.00
1	2000			
1	2000			
2	1.50E+03	1500	0	0.00
2	1.50E+03			
2				
3	1.10E+03	1200	200	16.67
3	1.10E+03			
3	1.40E+03			
4	1.59E+03	1560	30	1.92
4	1.53E+03			

Table A9. Raw data of UV disinfection rate dependence on initial cell concentration of 100-mL volumes of *E. coli* subject to 1 minute of ultraviolet irradiation at pH = 7.4 in 0.01M PBS. $C_3 = 2.3 \times 10^7$ CFU mL^{-1}; $C_4 = 6.4 \times 10^5$ CFU mL^{-1}.

UV	C5	C5 mean	C5 var	C5 % err
0	10200000	11100000	900000	8.108108
0	11300000			
0	11800000			
1	400	400	0	0
1	400			
1	400			
2	1.60E+02	170	10	5.882353
2	1.80E+02			
2				
3	2.10E+02	170	40	23.52941
3	1.40E+02			
3	1.60E+02			
4	2.20E+02	225	5	2.222222
4	2.30E+02			

UV	C6	C6 mean	C6 var	C6 %err
0	840000	866666.7	83333.33	9.62
0	950000			
0	810000			
1	100	63.33333	36.66667	57.89
1	40			
1	50			
2	1.00E+02	115	15	13.04
2	1.30E+02			
2				
3	4.00E+01	33.33333	6.666667	20.00
3	3.00E+01			
3	3.00E+01			
4	2.00E+01	20	0	0.00
4	2.00E+01			

Table A10. Raw data of UV disinfection rate dependence on initial cell concentration of 100-mL volumes of *E. coli* subject to 1 minute of ultraviolet irradiation at pH = 7.4 in 0.01M PBS. $C_5 = 2.5 \times 10^5$ CFU mL^{-1}; $C_6 = 3.2 \times 10^4$ CFU mL^{-1}.

EHD	Co	LD_{50}
	1.59E+07	39.64
	9.70E+06	96.55
	9.40E+06	33.50
	5.57E+06	54.45
	4.50E+06	22.66
	2.12E+06	17.24
	1.31E+06	13.09
	1.19E+06	19.26
	9.73E+05	15.87
	6.65E+05	7.43
	3.33E+05	8.78
	2.10E+05	12.64
	1.42E+05	7.47
	1.83E+04	13.96
	1.75E+03	8.71

UV	Co	LD50
	1.46E+09	47.74
	8.33E+08	36.33
	1.24E+08	3.19
	65000000	1.71
	11100000	1.46
	866666.7	1.32

US	Co mean	LD50
	1.32E+10	69.35
	7.69E+09	57.06
	1.49E+08	149.39
	1.19E+08	86.33
	11650000	241.56
	1200000	205.98

Table A11. Raw data for LD_{50} dependence on initial cell concentration on electrohydraulic discharge process (EHD), ultraviolet irradiation (UV), and ultrasonic irradiation (US). Units of LD_{50}(EHD) are in number of EHDs, LD_{50}(UV) are in minutes of UV exposure, and LD_{50}(US) are in minutes of US irradiation.

26-Aug	Vol [mL]	OD_{600}	Time [min]	Abs 420	Abs 550	β-gal Activity
0S	*1*	0.063	*127.17*	*0.313*	*0.041*	*30.10*
0C	*1*	0.063	*23.63*	*0.561*	*0.046*	*322.61*
0T	*1*	0.063	*10.72*	*0.799*	*0.051*	***1050.55***
0S	1	0.063	130.33	0.245	0.044	*20.35*
0C	1	0.063	20.05	0.427	0.049	*271.04*
0T	1	0.063	9.58	0.687	0.024	***1068.48***
10S	1	0.11806				
10C	1	0.11806	20.07	0.715	0.057	*259.96*
10T	1	0.11806	13.00	0.772	0.118	***368.48***
20S	1	0.14523	84.68	0.348	0.068	*18.64*
20C	1	0.14523	21.65	0.909	0.205	*174.92*
20T	1	0.14523	16.18	0.743	0.092	***247.52***
30S	1	0.13597	35.22	0.502	0.041	*89.85*
30C	1	0.13597	29.27	0.538	0.044	*116.00*
30T	1	0.13597	15.67	0.613	0.060	***238.49***

EHD	Super	Cell	Super+Cell	% Super	% Cell
0	0.00	322.61	322.61	0.00	100.00
10	0.00	259.96	259.96	0.00	100.00
20	18.64	174.92	193.56	9.63	90.37
30	89.85	116.00	205.84	43.65	56.35

Table A12. Raw data for β-D-galactosidase experiments on 8/26/98. *E. coli* suspension (3 L) in 0.01 M PBS at pH = 7.4 subject to 30 consecutive electrohydraulic discharges. E_{CB} = 7 kJ, spark gap = 4 mm, and pulse rate = 0.1 Hz.

EHDs	0 mg/L	mean	error	% C/Co	% error
0	27200000	26750000	450000	100.00	1.68
0	26300000				
0					
2	19200000	17800000	1400000	66.54	7.87
2	16400000				
4	6400000	6850000	450000	25.61	6.57
4	7300000				
6	3300000	3650000	350000	13.64	9.59
6	4000000				
8	3600000	3250000	350000	12.15	10.77
8	2900000				
10	1000000	1100000	100000	4.11	9.09
10	1200000				
10					
15	1000000	1000000	0	3.74	0.00
15					
20	360000	350000	10000	1.31	2.86
20	340000				
20					
25	100000	110000	10000	0.41	9.09
25	120000				
30	170000	150000	20000	0.56	13.33
30	130000				
30					
35	130000	105000	25000	0.39	23.81
35	80000				
40	110000	100000	10000	0.37	10.00
40	90000				
40					
45	110000	85000	25000	0.32	29.41
45	60000				
50	130000	110000	20000	0.41	18.18
50	90000				
50					

Table B1. Raw data for sunscreen experiments. [BP9] = 0 mg/L.

EHDs	1 mg/L	mean	error	% C/Co	% error
0	17000000	18960000	2140000	100.00	11.29
0	21100000				
0	18800000				
2					
2					
4					
4					
6					
6					
8					
8					
10	1000000	1250000	250000	6.59	20.00
10	1500000				
10					
15					
15					
20	400000	366000	66000	1.93	18.03
20	400000				
20	300000				
25					
25					
30	200000	195000	5000	1.03	2.56
30	190000				
30					
35					
35					
40	160000	160000	0	0.84	0.00
40					
40					
45					
45					
50	100000	110000	10000	0.58	9.09
50	110000				
50	120000				

Table B2. Raw data for sunscreen experiments. [BP9] = 1 mg/L.

EHDs	5 mg/L	mean	error	% C/Co	% error
0	22000000	22000000	600000	100.00	2.73
0	21400000				
0	22600000				
2					
2					
4					
4					
6					
6					
8					
8					
10	7000000	4960000	2040000	22.55	41.13
10	4100000				
10	3800000				
15					
15					
20	2000000	1816000	366000	8.25	20.15
20	2000000				
20	1450000				
25					
25					
30	1500000	1140000	360000	5.18	31.58
30	900000				
30	1020000				
35					
35					
40	800000	860000	340000	3.91	39.53
40	1200000				
40	600000				
45					
45					
50	500000	540000	180000	2.45	33.33
50	400000				
50	720000				

Table B3. Raw data for sunscreen experiments. [BP9] = 5 mg/L.

EHDs	20 mg/L	mean	error	% C/Co	% error
0 0 0	19000000	19000000	0	100.00	0.00
2 2					
4 4					
6 6					
8 8					
10 10 10	11600000 13700000	12650000	1050000	66.58	8.30
15 15					
20 20 20	11000000 11200000	11100000	100000	58.42	0.90
25 25					
30 30 30	8110000 8720000	8415000	305000	44.29	3.62
35 35					
40 40 40	6390000 6580000	6485000	95000	34.13	1.46
45 45					
50 50 50	5190000 5870000	5530000	340000	29.11	6.15

Table B4. Raw data for sunscreen experiments. [BP9] = 20 mg/L.

EHDs	40 mg/L	mean	error	% C/Co	% error
0	22000000	20400000	1600000	100.00	7.84
0	19000000				
0	20200000				
2					
2					
4					
4					
6					
6					
8					
8					
10	17200000	16600000	600000	81.37	3.61
10	16000000				
10					
15					
15					
20	16500000	16250000	250000	79.66	1.54
20	16000000				
20					
25					
25					
30	11100000	11100000	0	54.41	0.00
30					
30					
35					
35					
40	11300000	11300000	0	55.39	0.00
40					
40					
45					
45					
50	9900000	9900000	0	48.53	0.00
50					
50					

Table B5. Raw data for sunscreen experiments. [BP9] = 40 mg/L.

EHDs	60 mg/L	mean	error	% C/Co	% error
0	38000000	24700000	13300000	100.00	53.85
0	16000000				
0	20100000				
2					
2					
4					
4					
6					
6					
8					
8					
10	33000000	23060000	9940000	93.36	43.10
10	19000000				
10	17200000				
15					
15					
20	18100000	17400000	700000	70.45	4.02
20	16700000				
20					
25					
25					
30	15300000	16300000	1000000	65.99	6.13
30	17300000				
30					
35					
35					
40	14400000	14650000	250000	59.31	1.71
40	14900000				
40					
45					
45					
50	13600000	13650000	50000	55.26	0.37
50	13700000				
50					

Table B6. Raw data for sunscreen experiments. [BP9] = 60 mg/L.

EHDs	100 mg/L	mean	error	% C/Co	% error
0	49000000	48000000	1000000	100.00	2.08
0	47000000				
0					
2	23000000	23500000	500000	48.96	2.13
2	24000000				
4	22100000	22250000	150000	46.35	0.67
4	22400000				
6	23000000	22500000	500000	46.88	2.22
6	22000000				
8	29000000	27500000	1500000	57.29	5.45
8	26000000				
10	26000000	23000000	3000000	47.92	13.04
10	20000000				
10					
15	23000000	25000000	2000000	52.08	8.00
15	27000000				
20					
20					
20					
25	23000000	23000000	0	47.92	0.00
25					
30	16000000	16000000	0	33.33	0.00
30					
30					
35	21000000	24500000	3500000	51.04	14.29
35	28000000				
40	23000000	20000000	3000000	41.67	15.00
40	17000000				
40					
45	22000000	20000000	2000000	41.67	10.00
45	18000000				
50	24000000	19000000	5000000	39.58	26.32
50	14000000				
50					

Table B7. Raw data for sunscreen experiments. [BP9] = 100 mg/L.

EHD	cycle 0	0 mean	0 var	0 % error	0 % mean	0 % var
0	16000000.00	22500000.00	6500000.00	28.8889	100.0000	28.8889
0	29000000.00					
10	300000.00	300000.00	0.00	0.0000	1.3333	0.0000
10	300000.00					
30	10000.00	15000.00	5000.00	33.3333	0.0667	0.0222
30	20000.00					
30						
50	10000.00	10000.00	0.00	0.0000	0.0444	0.0000
50						
50						

EHD	cycle 6	6 mean	6 var	6 % error	6 % mean	6% var
0	43000000.00	43000000.00	0.00	0.0000	100.0000	0.0000
0	43000000.00					
10	1300000.00	1100000.00	200000.00	18.1818	2.5581	0.4651
10	900000.00					
30	10000.00	15000.00	5000.00	33.3333	0.0349	0.0116
30	20000.00					
30						
50	100000.00	76666.67	46666.67	60.8696	0.1783	0.1085
50	30000.00					
50	100000.00					

EHD	cycle 11	11 mean	11 var	11% error	11% mean	11% var
0	38000000.00	38000000.00	0.00	0.0000	100.0000	0.0000
0	38000000.00					
10	600000.00	650000.00	50000.00	7.6923	1.7105	0.1316
10	700000.00					
30	90000.00	83333.33	6666.67	8.0000	0.2193	0.0175
30	80000.00					
30	80000.00					
50	10000.00	17000.00	7000.00	41.1765	0.0447	0.0184
50	24000.00					
50						

Table C1. Raw data from 1/1/2001 for EHD selective pressure experiments in Ch. 5.